공학박사학위논문

Fatty acid double layer coated iron-based nanoparticles with stable mobility and selective reactivity to hydrophobic contaminants in subsurface

지방산 이중 코팅을 통한 지중 내 안정적인 이동성과 소수성 오염물질의 선택적 반응성을 가진 철 나노입자 개발

2017 년 12 월

서울대학교 대학원
건설환경공학부
우 희 수

Abstract

Injection of reactive iron-based nanoparticles (Fe NPs) to the DNAP sources in the subsurface is one of the emerging efficient technologies as an alternative to predominant treatment technologies. The small size of reactive nanomaterials (e.g., 10 ~ 100 nm) can offer the potential of being derivable in the contaminated subsurface, and thus, potentially eliminate the need for excavation. However, due to their high surface energy, Fe NPs tend to rapidly agglomerate in water forming micro to millimeter scale aggregates or flocs, which weaken their mobility in groundwater. Moreover, commonly encountered groundwater solutes such as anions, cations, and dissolved organic matters can affect the reactivity of Fe NPs negatively.

In this study, fatty acid double layer mimic lipid bilayer, a constituent of cell membrane, was used as a stabilizer of Fe NPs to achieve stable mobility and selective reactivity toward chlorinated hydrocarbons and the method for coating the fatty acid double layer onto the surface of Fe NP was developed. Fatty acid double layer coated Fe NPs (PO-OFe) were prepared through two sequential steps: 1) primary hydrophobic layer preparation via thermal decomposition method with oleic acid; 2) secondary hydrophilic layer by potassium oleate. The mas of coated fatty acid was approximately 50% of total particle mass, and zeta potential of PO-OFe has reached the vast extent of – 115 mV, indicated that aqueous stability and superior mobility of PO-OFe could be obtained by electrostatic and steric repulsive forces induced from the fatty acid double layer.

PO-OFe remained stable in the aqueous phase in sedimentation test although unmodified Fe NPs were deposited on the bottom of the test cell only in 2 h, indicating

fatty acid double layer prohibit nanoparticle from agglomeration. Consistent with the sedimentation teste results, no deposition was detected in 1-D column tests, the mobility of which is even better than that of CMC-Fe which are the modified Fe NPs by one of the mostly used modifications for Fe NP stabilization in remediation application. Due to non-polar zone in a fatty acid double layer onto the surface of PO-OFe, hydrophilic dissolved groundwater solutes, as well as a reducible contaminant (nitrate), rarely affected the reactivity of PO-OFe toward carbon tetrachloride, a model chlorinated solvent, at an insignificant level, suggesting that PO-OFe have selective reactivity. Nitrate that is well known as a reducible hydrophilic contaminant by zero valent iron was not transformed by the contact with PO-OFe and the reaction rate of PO-OFe was slower than those of unmodified or CMC modified Fe NPs. These are attributable to the presence of non-polar zone in a fatty acid double layer that can block hydrophilic molecules from permeation through the layer and require hydrophobic contaminants to be diffused through the layer onto the surface of Fe NPs.

The selective reactivity will keep the fatty acid double layer coated iron nanoparticles reactive. Therefore, the higher longevity of PO-OFe can be expected especially in the geochemical condition of high concentration of groundwater solutes. Remedial action using the reactants with the longevity and high mobility can offer the chance to clean-up the site where as-used technologies cannot be economically applied. Fatty acid double layer coated Fe NPs may be a suitable remediation alternative for these sites.

Keyword : Fatty acid, Fe nanoparticle, Stabilization, Mobility, Selective reactivity, Subsurface remediation, Chlorinated solvents, Dechlorination

Student Number : 2008-21041

Table of Contents

List of Figures

List of Tables

List of Abbreviations

CF	Chloroform
CMC	Carboxymethyl cellulose
CMC-Fe	CMC modified Fe NPs via pre-agglomeration modification
CT	Carbon tetrachloride
DCE	Dichloroethylene
DCM	Dichloromethane
DDW	N_2 purged deionized water
DLVO	Derjaguin-Landau-Verwey-Overbeek
DNAPL	Dense non-aqueous phase liquid
DOC	Dissolved organic matter
DW	Deionized water
Fe NP	Iron nanoparticle
HA	Humic acid
HPO-OFe	PO-OFe stabilized in high concentration of PO
IC	Ion chromatography
LPO-OFe	PO-OFe stabilized in minimum concentration of PO
MC	Micelle concentration
M-Fe	Commercial ZVI NPs
MSDS	Material safety data sheet
NOM	Natural organic matter
OFe	Oleic acid (fatty acid) coated Fe NPs
PCBs	Polychlorinated biphenyls
PCE	Tetrachloroethylene

PO	Potassium oleate
PoCMC-Fe	CMC modified Fe NPs via post-agglomeration modification
PO-OFe	Oleic acid and potassium oleate double layer coated Fe NPs
PoOl-Fe	PO modified Fe NPs via post-agglomeration modification
PRB	Permeable reactive barrier
PV	Pore volume
SO	Sodium oleate
TCE	Trichloroethylene
TEM	Transmission electron microscopy
TGA	Thermogravimetric analysis
TOC	Total organic carbon
VC	Vinyl chloride
XDLVO	Extended DLVO
XRD	X-ray diffraction
ZVI	Zero valent iron
ZVI NP	Zero valent iron nanoparticle

Chapter 1. Introduction

Chlorinated solvents, such as trichloroethylene (TCE), tetrachloroethylene (PCE), carbon tetrachloride (CT), are one of the mostly found contaminants in subsurface as a result of their widespread use in various industrial processes and improper storage, disposal, transit, and handling methods (Frascari et al., 2015). Approximately 80% of all Superfund sites with subsurface contamination and more than 3,000 Department of Defense sites in the US are contaminated by chlorinated solvents (SERDP and ESTCP, 2004). In Korea, there are insufficient studies on the exact usage and the current contamination condition of chlorinated solvents. Considering the domestic industrial structure, of which main components are semiconductors, electricity, electronics, and automobile industries, and the consumption of the chemical substances related with chlorinated solvents, it can be estimated that subsurface contamination in Korea by chlorinated solvents is not negligible.

The analysis of the major chlorinated solvents' material safety data sheets (MSDS) indicates that they are classified as known or suspected human carcinogens. It is obvious that the exposure to TCE or PCE can cause malfunction of the nervous system, damage in major organ including liver and lung, and even death (ASTDR, 2017). Considering the contamination frequency in the subsurface and the toxicity, US EPA has regulated chlorinated solvents as 'Top Priority Pollutants.' The Ministry of Environment in Korea is also categorizing and regulating them as a group of 'Specific Substance Harmful to Water Quality' mainly because they are harmful to animals and plants and potentially causes cancer.

Unique properties of chlorinated solvents make its remediation so severe while cleaning up the contaminated site by chlorinated solvents are the top priority. They have 1) a density greater than water, 2) low solubility (hydrophobic), and 3) persistent. They mitigate below the water table in subsurface until they reach to bedrock or impermeable layer forming dense non-aqueous phase liquid (DNAPL) sources. Due to its low solubility and persistent, the dissolution from a DNAPL source may persist for several decades and act as a constant groundwater contamination source presenting soluble phase of the solvents (Karn et al., 2009). Although the concentration of dissolved chlorinated solvents is very low, living organism including human can be exposed to an unacceptable environmental and health risk for their high toxicity.

The conventional and most widely used method to clean up the groundwater contaminated with chlorinated solvents are a pump and treat method and zero-valent iron (ZVI) permeable reactive barriers (PRB) (Smith and Burns, 2002; Vogan et al., 1999). During the operation of pump and treat systems, the contaminated groundwater is pumped out and treated at the surface followed by recharging the treated water back into the subsurface or discharging it. Although this approach is useful for some simple sites, it is expensive and has failed to clean up DNAPL contaminated groundwater (McKinney and Lin, 1996). With the continuous pump and treat operation, the dissolved chlorinated solvents may be removed, but the concentrations can be rebounded in the groundwater once the pumping is stopped, mainly due to the presence of a DNAP source (Council, 1994; Keely and Boulding, 1989). The PRB technology using micro-sized (granular) ZVI are simple and cost-effective at the sites with shallow depths and relatively low contaminants concentrations. However, barrier installation cost increase in deeper aquifers and higher contaminants concentrations (Gavaskar et al., 1998). Above all, its major drawback is that it cannot directly remediate the DNAPL source in the subsurface (i.e., passive remediation technology).

Injection of reactive nanomaterials to the DNAP sources in the subsurface is one of the emerging efficient technologies as an alternative to predominant treatment technologies such as pump and treat and PRB. The small size of reactive nanomaterials (e.g., 10 ~ 100 nm) can offer the potential of being derivable in the contaminated subsurface, and thus, potentially eliminate the need for excavation. The limitation induced by the site topography and facility operations in remediation practices at the site where applying ex-situ remediation technologies also make the use of reactive nanomaterials more effective (Zhang, 2003). Among reactive nanomaterials, iron-based nanoparticles (Fe NPs) have been considered as a promising reactive nanomaterial for environmental applications, due to several advantages; 1) relative low toxicity, 2) abundance in nature, related with low production cost, 3) high reductive reactivity (mainly using ZVI as a bulk-reducing agent) (Cundy et al., 2008; Huber, 2005). Numerous laboratory and field studies have reported the possibility for ZVI NPs to be successfully used for remediation of the sites contaminated by chlorinated solvents showing good performances in treating target contaminants (Bardos et al., 2015; Elliott and Zhang, 2001; Lien and Zhang, 1999; Matheson and Tratnyek, 1994; Wang and Zhang, 1997).

However, due to their high surface energy, Fe NPs tend to rapidly agglomerate in water forming micro to millimeter scale aggregates or flocs, which weaken their mobility in groundwater. Moreover, commonly encountered groundwater solutes such as anions, cations, and dissolved organic matters can affect the reactivity of Fe NPs negatively (*i.e.,* decrease in the reactivity). Considering the primary purpose of using reactive nanomaterials for subsurface remediation as an alternative to prevailing remediation technologies, they should be 'stable' in delivering to the source and contaminants plume in the subsurface. Injected particles need to flow along the groundwater, and the

reactivity of them should be maintained until they contact with the sources and plume of the chlorinated solvents.

To prevent particle aggregation and facilitate the efficient delivery, researchers have investigated various surface modification methods for Fe NPs. However, attempts to develop modification methods that preserve the reactivity of Fe NPs from groundwater solutes and simultaneously satisfy the sufficient mobility have not been reported. So, the overall objective of this research to develop a new modification method of Fe NPs that presents the stable mobility and the selective reactivity to chlorinated solvents for subsurface remediation. The specific studies were conducted in the following chapters (chapter 3, 4, 5).

In chapter 3, the idea and concept of the modification method that preserves the reactivity of Fe NPs from groundwater solutes and simultaneously satisfy the sufficient mobility was presented. The preparation process of newly developed Fe NPs (PO-OFe) was also explained. The difference in physio-chemical characteristics of Fe NPs was analyzed according to the various Fe NPs synthesis methods.

In chapter 4, the mobility of PO-OFe was evaluated using filtration theory. Sedimentation test and 1-D column transport experiments with varying pore water velocity were conducted. Significant characteristics related to nanoparticle mobility in porous media such as hydrodynamic diameter, zeta potential were measured and used as key factors to identify the mobility increase mechanisms of fatty acid double layer coating.

In chapter 5, the reactivity of PO-OFe to both a hydrophobic and a hydrophilic, ionic contaminant was evaluated through batch type experiments. Dissolved groundwater solutes that commonly encountered in field groundwater were prepared at the concentration relevant to field groundwater concentrations. The effect of dissolved groundwater solutes on the reactivity of PO-OFe to a hydrophobic contaminant was also evaluated to verify the selective permeability of the fatty acid double layer and of which mechanisms were analyzed.

Chapter 2. Background

2.1 Reductive dechlorination of chlorinated hydrocarbons by Fe NPs

The transformation of chlorinated hydrocarbons including biotic and abiotic transformations can be divided into two general classes (Vogel et al., 1987): 1) oxidations and reductions and 2) substitutions and dehydrohalogenations. Among above transformation reactions, substitutions and dehydrohalogenations doesn't require the external electron transfer. Oxidations and reductions require the external electron transfer, which can be occurred through the surface reaction between chlorinated hydrocarbons and transition metals (e.g., iron). Chlorines attached to carbons can be substituted with hydroxide ions or other nucleophilic groups through substitution reaction (Smith and Burns, 2002). Substitution of chlorinated hydrocarbons in water (especially hydrolysis) leads to the production of alcohols or other less toxic compounds (Zhang, 2003). If these alcohols are halogenated, then subsequent hydrolysis to acids or diols can occur. Chlorinated alkenes in water also can undergo elimination reactions that produce alkanes with no net change of the oxidation state of carbons (Matheson and Tratnyek, 1994).

Certain transition metals and metal complexes mediated transformation of chlorinated hydrocarbons can be occurred through oxidations and reductions, which require the external electron transfer (Vogel et al., 1987). In the environment for groundwater remediation application (anoxic condition), abiotic reduction reaction for chlorinated hydrocarbons should be occurred in the presence of the metals and metal

complexes (Matheson and Tratnyek, 1994). Most reductions by transition metal complexes involve the transfer of electrons and the formation of an alkyl radical. The alkyl radical that results from the electron transfer can undergo several reactions. The simplest reaction is that the radical undergoes a second electron transfer and protonation, which is predominant. Another involves the loss of a second halogen substituent from a carbon atom adjacent to the radical carbon to form an alkene. In the absence of a good proton donor such as hydrogen dimerization of the radical can be occurred (Vogel et al., 1987). Above transformation reactions with respect to halogenated (or chlorinated) hydrocarbons are summarized in Figure 2.1.

Among transition metals capable of reducing chlorinated hydrocarbons, iron has drawn the attention for the applicable reductants being used as a remediation agent for chlorinated hydrocarbons (Zhang, 2003). Elemental iron (zero valent iron, ZVI) oxidized to ferrous iron and releases two electrons following oxidation half reaction:

$$Fe^{0}_{(s)} \rightarrow Fe^{2+}_{(aq)} + 2e^{-}_{(aq)} \qquad (0.1)$$

These released electrons begin to lead to the transformation of chlorinated hydrocarbons in accordance with the electron transfer. For the reduction of chlorinated methanes such as carbon tetrachloride (CT), sequential dechlorination through hydrogenolysis take place in the presence of ZVI:

$$CCl_4 + 2e^- + H^+ \rightarrow CHCl_3 + Cl^- + 2e^- + H^+ \rightarrow CH_2Cl_2 + 2Cl^- \qquad (0.2)$$

With each successive dechlorination, the reaction proceeds more slowly.

Reactions	Examples
Substitution	
(a) hydrolysis	
$RX + H_2O \rightarrow ROH + HX$	$CH_3CH_2CH_2Br + H_20 \rightarrow CH_3CH_2CH_2OH + HBr$
(b) conjugation and other nucleophilic reactions	
$RX + N^- \rightarrow RN + X^-$	$CH_3CH_2Br + HS^- \rightarrow CH_3CH_2SH + Br^-$
Dehydrohalogenation	
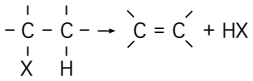	$CCl_3CH_3 \rightarrow CCl_2CH_2 + HCl$
Oxidation	
(a) α-hydroxylation	
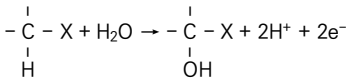	$CH_3CHCl_2 + H_2O \rightarrow CH_3CCl_2OH + 2H^+ + 2e^-$
(b) halosyl oxidation	
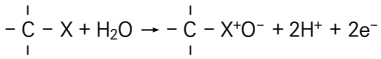	$CH_3CHCl_2 + H_2O \rightarrow CH_3CHClCl^+O^- + 2H^+ + 2e^-$
(c) epoxidation	
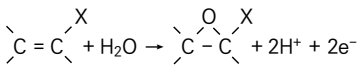	$CHClCCl_2 + H_2O \rightarrow CHClOCCl_2 + 2H^+ + 2e^-$
Reduction	
(a) hydrogenolysis	
$RX + H^+ + 2e^- \rightarrow RH + X^-$	$CCl4 + H^+ + 2e^- \rightarrow CHCl_3 + Cl^-$
(b) dihalo-elimination	
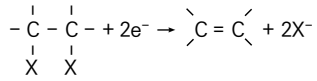	$CCl_3CCl_3 + 2e^- \rightarrow CCl_2CCl_2 + 2Cl^-$
(b) coupling	
$2RX + 2e^- \rightarrow R–R + 2X^-$	$2CCl_4 + 2e^- \rightarrow CCl_3CCl_3 + 2Cl^-$

Figure 2.1 Abiotic reactions of halogenated aliphatic compounds (modified from Vogel et al., 1987)

Tetrachloroethene (TCE) can be also reduced to ethane in accordance with the reaction illustrated in Figure 2.2. There are two main reduction pathways for the TCE dechlorination: 1) Beta-elimination pathway, in which TCE is transformed directly to ethane via the production of chloroacetylene and acetylene avoiding the formation of vinyl chloride (VC); and 2) Hydrogenolysis, which occurs one chlorine atom is transformed to hydrogen in each step, so that dichloroehtenes (including cis-1,2-DCE, trans-1,2-DCE, 1,1-DCE) and VC are generated from the degradation of TCE. Beta-elimination pathway is believed as a common pathway of TCE degradation with ZVI (Liu et al., 2005).

Prominent reductive mechanisms for degradation of chlorinated hydrocarbons with ZVI can be summarized by following reactions (McDowall, 2005):

$$Cl_2C=CCl_2+H^++2e^-\rightarrow Cl_2C=CClH+Cl^- \quad (0.3)$$

$$Cl_2C=CCl_2+2e^-\rightarrow ClC\equiv +2Cl^- \quad (0.4)$$

$$CCl_3H\rightarrow :CCl_2+HCl\rightarrow \text{variety of products} \quad (0.5)$$

$$RCl_2C-CClHR^{'}\rightarrow RClC=CClR^{'}+H^++Cl^- \quad (0.6)$$

$$RClC=CClR+H_2\rightarrow RHClC-CClHR \quad (0.7)$$

These are hydrogenolysis (reaction 2.3), beta-elimination (reaction 2.4) or alpha-elimination (reaction 2.5), dehydrohalogenations (reaction 2.6) and hydrogenation (reaction 2.7). Hydrogenolysis and beta-elimination reaction are the dominant reaction pathways.

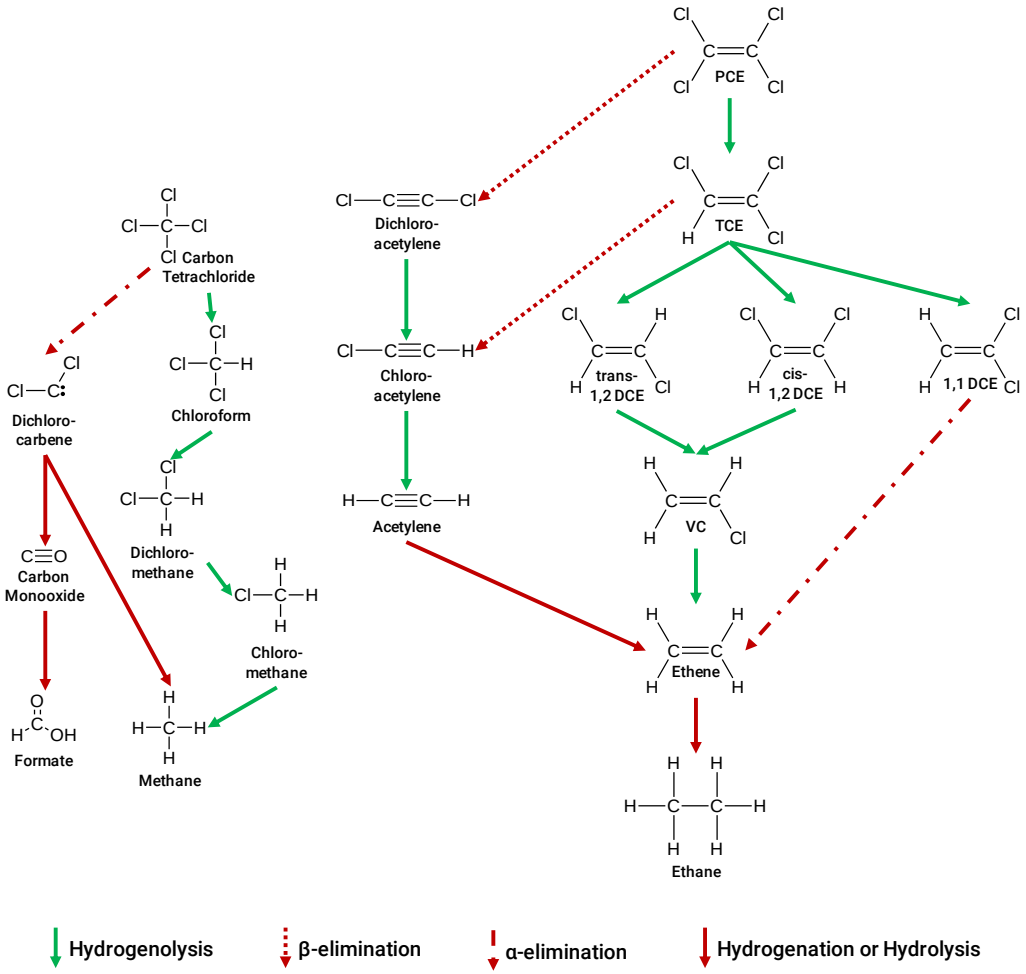

Figure 2.2 Reductive dechlorination pathways of chlorinated methanes, ethanes, and ethenes (Modified from Arnold and Roberts, 2000; Song and Carraway, 2006)

The greater reactivity can be expected using ZVI NPs, however, the degradation pathways of chlorinated hydrocarbons are not significantly changed. Several advantages can be obtained using ZVI NPs due to larger surface area, greater density of reactivity sites on the particle surfaces, and higher intrinsic reactivity of the reactive surface sites (Tratnyek and Johnson, 2006): 1) more rapid degradation of contaminants (e.g., chlorinated ethenes; 2) degradation of contaminants that do not undergo reductive dechlrorination with micro or macro-sized granular ZVI; 3) produce lesser toxic byproducts (e.g., production of vinyl chloride can be avoided with ZVI NPs).

Some papers have also reported that iron oxide particles or nanoscale iron oxide particles can be applied to degrade chlorinated hydrocarbons. Mixed-valence Fe(II)-Fe(III) oxides have proven to degrade CT or TCE (Danielsen and Hayes, 2004; Erbs et al., 1999; Lee and Batchelor, 2002; McCormick and Adriaens, 2004). Evidence from the literatures suggested that iron oxide particles promote formation of the relatively benign carbine products such as formate, the degradation pathway of which is different using ZVI particles. One of the Metasable Fe(II) oxide, FeO (wustite), have been reported to be used as a remediation reagent for nitrate reductive removal (Rakshit et al., 2005). Rakshit et al. (2005) suggested the degradation pathway for the removal of nitrate with wustite as following reaction:

$$12FeO_{(s)} + NO_3^- + H_2O + 2H^+ = 4Fe_3O_4 + NH_4^+ \quad (0.8)$$

Besides toxic chlorinated hydrocarbons such as CT and TCE, Fe NPs has been shown to able to degrade other compounds found at contaminated sites including pesticides (e.g., DDT), heavy metals (such as Hg, As, Ni), organic dyes (orange II). Common contaminants that can be degraded by Fe NPs are summarized in Figure 2.3 (Li et al., 2006b).

Chlorinated Methanes
- Carbon tetrachloride (CCl_4)
- Chloroform($CHCl_3$)
- Dichloromethane (CH_2Cl_2)
- Chloromethane (CH_3Cl)

Chlorinated Benzenes
- Hexachlorobenzene (C_6Cl_6)
- Pentachlorobenzene (C_6HCl_5)
- Tetrachlorobenzenes ($C_6H_2Cl_4$)
- Trichlorobenzenes ($C_6H_3Cl_3$)
- Dichlorobenzenes ($C_6H_4Cl_2$)
- Chlorobenzene (C_6H_5Cl)

Pesticides
- DDT ($C_{14}H_9Cl_5$)
- Lindane ($C_6H_6Cl_6$)

Organic Dyes
- Orange II ($C_{16}H_{11}N_2NaO_4S$)
- Chrysoidin ($C_{12}H_{13}ClN_4$)
- Tropaeolin O ($C_{12}H_9N_2NaO_5S$)

Heavy Metals
- Mercury (Hg^{2+})
- Nickel (Ni^{2+})
- Cadmium (Cd^{2+})
- Lead (Pb^{2+})
- Chromium (Cr(VI))
- Arsenic (As(III), As(V))

Trihalomethanes
- Bromoform ($CHBr_3$)
- Dibromochloromethane ($CHBr_2Cl$)
- Dichlorobromomethane ($CHBrCl_2$)

Chlorinated Ethenes
- Tetrachloroethene (C_2Cl_4)
- Trichloroethene (C_2HCl_3)
- cis-Dichloroethene ($C_2H_2Cl_2$)
- trans-Dichloroethene ($C_2H_2C_{l2}$)
- 1,1-Dichloroethene ($C_2H_2C_{l2}$)
- Vinyl Chloride (C_2H_3Cl)

Other Polychlorinated Hydrocarbons
- PCBs
- Chlorophenols
- 1,1,1-trichloroethane

Other Organic Contaminants
- N-nitrosodiumethylamine (NDMA) ($C_4H_{10}N_2O$)
- TNT ($C_7H_5N_3O_6$)

Inorganic Anions
- Perchlorate (ClO_4^-)
- Nitrate ($NO_3^{-)}$

Figure 2.3 Common contaminants that can be remediated by iron nanoparticles (Li et al., 2006b)

2.2 Synthesis of Fe NPs

The most conventional method to prepare ZVI NPs in laboratory is chemical reaction method. ZVI NPs are usually synthesized by reduction of ferrous or ferric salts using reduction agents (e.g., sodium borohydrides) (Elliott and Zhang, 2001; Lien and Zhang, 1999; Lien and Zhang, 2001; Ponder et al., 2000). Wang and Zhang (1997) synthesized ZVI NPs by mixing 1.6 M $NaBH_4$ and 1.0 M $FeCl_3 \cdot 6H_2O$ solutions according to the following reaction:

$$Fe\left(H_2O\right)_6^{3+} + 3BH_4^- + 3H_2O \rightarrow Fe^0 + 3B\left(OH\right)_3 + 10.5H_2 \quad (0.9)$$

This reaction is easy to adjust for making ZVI NPs with different physicochemical properties. The adding of surfactants or stabilizers in the synthesis route have been widely adopted to control the size and core-shell morphology of ZVI NPs (Carpenter et al., 2003; He et al., 2007; Sun et al., 2006).

Like the synthesis method for ZVI NPs chemical coprecipitation from an aqueous phase is a facile and conventional method to synthesize iron oxides NPs (Faraji et al., 2010; Korolev et al., 2002; Shen et al., 1999). Typical stoichiometry is the chemical coprecipitation is to react aqueous mixtures of ferric and ferrous salts with a ratio of 2:1. The mixture, then, are mixed with an alkaline solution at room temperature so that iron oxides NPs are produced. The reaction mechanism is shown in the following reaction (Zhou et al., 2016):

$$Fe^{2+} + 2Fe^{3+} + 8OH^- \rightarrow Fe_3O_4 + 4H_2O \quad (0.10)$$

More recently, highly crystalline and monodisperse Fe NPs have been generated using thermal decomposition methods similar to those used for semiconductor quantum dots (Yu et al., 2004). The synthesis of magnetite (Fe_3O_4) using thermal decomposition method is a common synthesis route. Iron acetylacetonate and iron oleate were commonly used as a starting material to form magnetite in a mixed solution of surfactnats and solvents such as oleic acid, oleylamine, and phenyl ether (Bronstein et al., 2007; Park et al., 2004; Sun et al., 2004; Zhang et al., 2006). Rockenberger et al. (1999) demonstrated that monodisperse γ-Fe_2O_3 could be obtained by thermal decomposition of an iron complex in octylamine. Hou et al. (2007) reported that monodisperse spherical wustite structure FeO nanocrystals were prepared by applying iron acetylacetonate as a precursor in oleic acid and oleylamine. ZVI NPs synthesis using thermal decomposition was also reported by Hyeon's group (Kim et al., 2007; Park et al., 2004). Iron oleate complex or iron stearate can be thermally decomposed and formed to crystalline ZVI NPs after decomposition process at high temperature (380 ℃).

There are various other Fe NPs synthesis methods reported. For example, a commercial iron nanoparticle product known as RNIP (Toda Kogyo Corp., Schaumberg, IL) have been widely used in groundwater remediation and ZVI NPs based researches synthesized by gas-phase reduction. RNIP was synthesized from the reduction of goethite and hematite particles with hydrogen gas at high temperature (e.g., 200-600 ℃) (Uegami et al., 2006). Li et al. (2009) reported a precision ball milling technique by which the starting iron materials were grinded into pieces with the diameter of less than 100 nm. Similarly, Golder Associates Inc. produced ZVI NPs in large quantities by the mechanical ball milling of macroscale ZVI (Crane and Scott, 2012).

2.3 Transport of Fe NPs in subsurface

2.3.1 Agglomeration of unmodified Fe NPs

The most important advantage of reducing the iron particle size from micro or macro to nano size (about 10 to 100 nm diameter) is the ability to directly inject nanoparticles directly into the contaminated subsurface. The injected Fe NPs are expected to be dispersed and transported to the source and contaminated plumes in subsurface. However, agglomeration of Fe NPs is a thermodynamically favorable, and it can take place in a several ways, mainly due to direct inter-particle interactions (He and Zhao, 2005; Hotze et al., 2010; Sun et al., 2007). The forces of inter-particle interactions with respect to Fe NPs include van der Waals forces, electrostatic double layer interactions, and magnetic dipolar interactions. Even in the absence of a magnetic field, magnetic interactions among Fe NPs are appreciable to affect the stability of the particles leading particles to aggregates (Phenrat et al., 2007). Moreover, van der Waals forces attracted each particle to be agglomerated. Without surface modification, chain-like aggregation of Fe NPs is commonly observed (Liu et al., 2005; Nurmi et al., 2005), and observation of sedimentation of Fe NPs is also common (Jiemvarangkul et al., 2011; Lin et al., 2009; Schrick et al., 2004; Sun et al., 2007; Tiraferri et al., 2008).

Because of rapid aggregation of Fe NPs, the mobility of unmodified Fe NPs has been observed to be limited in laboratory soil column experiments and filed scale tests. In numerous studies conducting column transport experiments with unmodified Fe NPs, unmodified Fe NPs cannot permeate the packed columns and were retained in the initial part of the column around solution influent port (He et al., 2007; Jiemvarangkul et al., 2011; Kanel et al., 2007; Raychoudhury et al., 2010; Schrick et al., 2004). Early pilot scale field trials reported by Elliott and Zhang (2001) have indicated limited ZVI NPs'

subsurface migration, with maximum transport distances of only a few meters in saturated sediments. This limited transport of unmodified ZVI NPs can be considered being positioned away from the application point. Typically, on the order of 10 m or more is needed for field application by direct push well injection systems (Henn and Waddill, 2006). Realizing the very limited and insufficient mobility and deliverability of unmodified ZVI NPs has been grown the need for development of effective stabilization techniques to make ZVI NPs more deliverable (Zhao et al., 2016).

2.3.2 Stabilization of Fe NPs by surface treatment and transport of stabilized Fe NPs in porous media

Stabilization of Fe NPs can be acquired through surface modification. In the surface modification method, stabilizer molecules are attached onto the Fe NP surface to create repulsion forces. A stabilizer enhances dispersion and stabilization of Fe NPs through (Zhao et al., 2016): 1) electrostatic stabilization, which creates an electrical double layer and presents electrical repulsive force; 2) steric stabilization, provide physical barrier when the layers of stabilizer molecules overlap; 3) network stabilization, facilitate formation of a viscous or gel network preventing particle aggregation (Fig. 2.4). Many polymers have been used to stabilize Fe NPs via the above stabilization mechanisms, the most successful of which are high molecular weight natural molecules or polyelectrolytes (Phenrat et al., 2008). Many of the commonly used polymers (e.g., CMC, PAA, PAP, and PV3A) are negatively charged, so that provide strong electrostatic repulsion since soil is usually negatively charged (Yan et al., 2013).

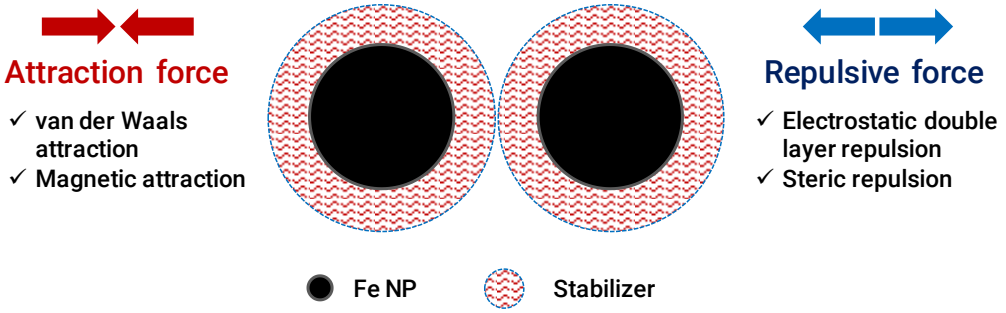

Figure 2.4 Schematic representation of surface modification stabilization (where surface coating facilitates particle repulsion)

There are two common ways for stabilization of Fe NPs: 1) pre-agglomeration modification, i.e., adding a stabilizer in the suspension during Fe NPs synthesis; and 2) post-agglomeration modification, where Fe NPs stabilization is performed following particle synthesis. For the latter, sonication treatment is often applied to break down the aggregates during or before the adding of stabilizer. Thermodynamically, the pre-agglomeration stabilization is more preferable to obtain smaller and stable particle, while break down the aggregates often need high energy and is not likely to be successful with sonication treatment or other pretreatments during the post-agglomeration stabilization (Zhao et al., 2016).

Natural biopolymers including guar gum have been used as a stabilizer that presents Fe NPs repulsive force from steric hindrance and polymer network, however, do not have charged functional groups to contribute to electrostatic repulsion (Tiraferri et al., 2008). Shear thining polymers like Xanthan gum are also effective to stabilize Fe NPs (Comba et al., 2011). These polymers are commonly used with the post-agglomeration modification. The gum solution creates gelling or networking between individual particles with a high viscosity at low shear rate, resulting in stabilization of Fe NPs

(Comba et al., 2011; Comba and Sethi, 2009). This approach has an advantage when Fe NPs at very high concentration are to be injected (Vecchia et al., 2009). However, the high viscosity of solution (about 1,000 cP at shear rates below $1s^{-1}$) induced by high concentration of added polymer called for the need cost-consuming injection methods due to large pressure required for injection.

Food-grade polysaccharides (e.g., starches, celluloses and chitosan) and/or their derivatives can act as effective stabilizers to yield stable Fe NPs applicable for the in situ injection remediation action (Zhao et al., 2016). These macromolecules possess some novel features, which may prove valuable for stabilizing Fe NPs. First, the macromolecules used as stabilizers for Fe NPs are consist of various functional groups, which may serve as an effective binder between Fe NPS and the molecule and a shield the coated Fe NPs from agglomeration (He and Zhao, 2005; He and Zhao, 2007; Kim et al., 2003). Second, they are lower cost than other stabilizers used so far (He et al., 2010). Third, these materials are environmentally friendly and biocompatible (He et al., 2009; He et al., 2007; Raychoudhury et al., 2010).

Among polysaccharides-based macromolecules, modified carboxymethyl cellulose (CMC) are commonly studied in environmental engineering field. Synthesis of CMC-modified ZVI NPs through pre-agglomeration modification was developed by researchers at Auburn University (He and Zhao, 2007). They employed a water soluble CMC during particle synthesis by which smaller size of particle can be obtained and the particle size can be controlled (He and Zhao, 2007; He et al., 2007). A water soluble CMC have been found that it can build a negative zeta potential onto the surface of particle because of the negatively charged carboxymethyl groups (pKa = 4.3), so that very stable Fe NPs can be synthesized. CMC-stabilized Fe NPs were also used as a form of bimetallic composite with Pd (CMC-FePd) to enhance the reactivity. He et al. (2007) found that CMC-FePd particles showed a 37 times faster TCE degradation rate than the

unmodified ZVI NPs. The primary reason for the enhanced reactivity of CMC-modified ZVI NPs is based on the superior stability.

Due to the superior stability and high reactivity, CMC-modified ZVI NPs have been considered most promising as a proper modified ZVI NPs for subsurface remediation, and has been extensively tested in laboratory studies (Tratnyek and Johnson, 2006). It has been demonstrated in transport experiments that CMC-modified ZVI NPs with pre-agglomeration modification showed good mobility due to electro-steric repulsion provided by CMC coating. He et al. (2009) demonstrated that a constant concentration plateau was reached at full breakthrough, ranging from 0.99 for glass beads to Field scale experiments for the soil. The Brownian diffusion was the predominant mechanism for particle removal in all cases, while gravitational sedimentation also played an important role. Xu and Zhao (2007) observed that the CMC-modified ZVI NPs are highly derivable in the soil column. 81% of influent CMC-modified ZVI NPs was detected at full breakthrough through a sandy loam soil packed 1-D column. They claimed that some stabilized ZVI NPs can be intercepted by the soil via filtration mechanisms and the particles become larger aggregates followed by oxidation.

Several field scale studies showing increased mobility of stabilized Fe NPs in porous medium have been reported. He et al. (2010) tested CMC-stabilized FePd for in situ destruction of chlorinated ethenes such as PCE, TCE and polychlorinated biphenyls (PCBs). Four test wells installed along the groundwater flow direction (spaced at 1.5 m), including one injection well (IW), one up-gradient monitoring well (MW-3) and two down-gradient monitoring wells (MW-1 and MW-2) (Fig. 2.5). Stabilized FePd NP suspension was prepared on-site right before the injection to preserve the maximum reactivity and then injected into the deep, unconfined aquifer. One month later after the injection, approximately 37.4% and 70.0% of the injected CMC-stabilized FePd was detected in MW-1, respectively, confirming the high mobility of the particle through the

aquifer. The study also reported that higher mobility of the particles was observed when the injection was performed under higher pressure. Bennett et al. (2010) pilot tested the transport and reactivity toward chlorinated ethenes of CMC-stabilized ZVI NPs through single well push-pull tests. They showed that about 30% of stabilized ZVI NPs were recovered, comparing the tracer, following a significant loss of mobility after a 13 h lag time, suggesting that groundwater recirculation and other methods may be need for stable delivery of ZVI NPs.

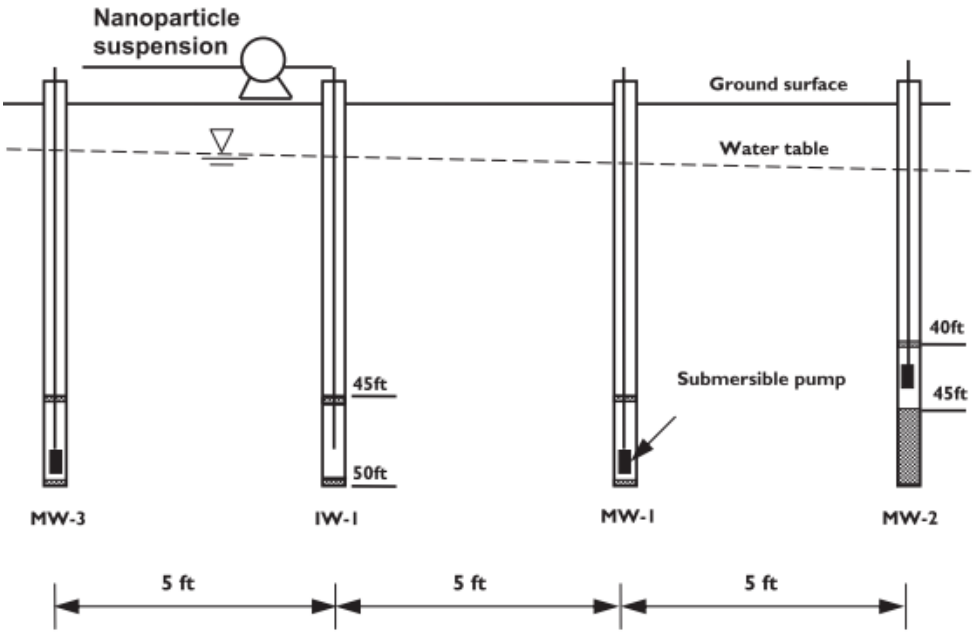

Figure 2.5 A sectional view of the aquifer at the testing site and schematic of the in situ injection of CMC-stabilized FePd NPs (He et al., 2010)

2.3.3 Quantification of particle mobility in porous media

The classical filtration theory (Tufenkji and Elimelech, 2004) is often applied to model the transport of stabilized ZVI NPs in porous media and evaluate the mobility quantitatively. Typically, the retention (or deposition) of nanoparticles in porous media is attributed to three mechanisms: 1) diffusion due to Brownian motion; 2) sedimentation due to gravity; 3) interception of the nanoparticles due to the exclusive particle size (Yao et al., 1971). In the filtration theory, the transport of nanoparticles to the surface of spherical collectors are expressed as the theoretical single collector efficiency, η_0 and the ratio of the rate of particle deposition on a collector to the rate of collisions with that collector is referred to as the attachment efficiency, α, when conditions are not favorable in particle attachment (Lecoanet et al., 2004).

A useful correlation equation for predicting single collector efficiency was developed by Tufenkji and Elimelech (2004), in which dimensionless parameters governing particle deposition and filtration are used for calculation of the efficiency factor like following equations:

$$\eta_0 = \eta_D + \eta_I + \eta_G \tag{0.11}$$

$$\eta_D = 2.4 A_S^{1/3} N_R^{-0.081} N_{Pe}^{-0.715} N_{vdW}^{0.052} \tag{0.12}$$

$$\eta_I = 0.55 A_S N_R^{1.55} N_{Pe}^{-0.125} N_{vdW}^{0.125} \tag{0.13}$$

$$\eta_G = 0.475 N_R^{-1.35} N_{Pe}^{-1.11} N_{vdW}^{0.053} N_{gr}^{1.11} \tag{0.14}$$

where η_D is the transport by diffusion, η_I is the transport by interception, and η_G is the transport due to gravity, A_S is the porosity-dependent parameter of Happel's model, N_R is the aspect ratio of particle size to collector size, N_{Pe} is the Peclet number, N_{vdW} is the van der Waals number, N_{gr} is the gravitational force number. The attachment

efficiency is usually determined by using column experiments since current theories are inadequate to predict the attachment efficiency:

$$\alpha = -\frac{2}{3}\frac{d_c}{(1-f)L\eta_0}\ln(C/C_0) \tag{0.15}$$

Here, L is the filter medium such as glass bead and sand packed length, C/C_0 is the column outlet normalized particle concentration at the steady plateau of breakthrough, f is the porosity of a porous medium, dc is the diameter of spherical collector, η_0 is the single collector efficiency determined from Eq. 2.11.

A number of studies have used the filtration theory to interpret results from column studies. One common method to compare the mobility of stabilized Fe NPs from experimental results is to compare the attachment efficiency coefficient calculated using Eq. 2.15. Reported attachment efficiency coefficients were summarized in Table 2.1.

Table 2.1 Reported attachment efficiency coefficients

Stabilizer	α	Reference
Polyelectrolyte	0.0003	He et al. (2009)
Polyelectrolyte	0.00045	Jeimvarangkul et al. (2011)
Polyelectrolyte	0.002	Raychoudhury et al. (2010)
Polyelectrolyte	0.002	He et al. (2009)
Carbon support	0.07	Schrick et al. (2004)
Surfactant	0.18	Kanel et al. (2007)
Polyelectrolyte	0.3	Raychoudhury et al. (2010)
Polyelectrolyte	0.32	Phenrat et al. (2009)
Polyelectrolyte	0.36	Schrick et al. (2004)

2.4 Impact of dissolved groundwater constituents on the reactivity of Fe NPs

2.4.1 Inorganic anions

Typical groundwater contains dissolved inorganic anions (e.g., HCO_3^-, SO_4^{2-}, NO_3^-, and HPO_4^{2-}) that can react with Fe NP surface and induce surface passivation (i.e., decrease in reactivity). The effect of inorganic anions of Fe NP reactivity to chlorinated solvents has been investigated in several studies. The effect of various anions on the reactivity of granular iron particles have been studied by several researches. There are three potential mechanisms for the effects (Agrawal et al., 2002; Johnson et al., 1998; Klausen et al., 2001; Schlicker et al., 2000; Su and Puls, 2004): 1) competition for reactive sites by iron reducible solutes (e.g., nitrate); 2) formation of passivating oxide layer blocking access to reactive sites; 3) dissolution of iron oxide layer increasing the reactivity of iron particles. These mechanisms can be also applied to analyze the effect of common anions on the reactivity of Fe NPs because the only physical difference between granular iron particles and Fe NPs is the size of particle.

Among typical dissolved inorganic anions, nitrate (NO_3^-) can be reduced by Fe NP and therefore strongly influence Fe NP reactivity. Liu et al. (2007) reported inhibition of TCE reduction by RNIP (commercial ZVI NP without surface treatment for stabilization) at high nitrate concentrations (≥ 3 mN). At low concentration, however, TCE reduction was not significantly affected. The decreased ZVI NP reactivity at high concentrations NO_3^- was attributed to competition between NO_3^- and TCE for reactive sites and electrons, and passivation of the ZVI NP surface due to formation of iron (hydr)oxides.

The effect of non-reducible anions such as Cl^-, HCO_3^-, SO_4^{2-}, and HPO_4^{2-} on RNIP reactivity was also explored by Liu et al. (2007). They decreased the TCE reduction rate

in increasing order of $Cl^- < SO_4^{2-} < HCO_3^- < HPO_4^{2-}$ which is consistent with their affinity to form complexes with iron oxides. This suggests the decreased TCE dehalogenation may be attributed to passivation of the ZVI NP surface by formation of Fe-anion complexes.

Lim and Zhu (2008) reported classified a loss in reactivity of Pd dopped ZVI NP for the 1,2,4-trichlorobenzene degradation in the presence of various anions. Based on the nature of inhibitory effect, they classified the anions as 1) adsorption-precipitation passivating species (phosphate, carbonate), 2) redox-active species (nitrate, nitrite, perchlorate), and catalyst poisons (sulfide, sulfite).

2.4.2 Natural organic matter (NOM)

Beside inorganic anions, groundwater naturally contains significant amount of natural organic matter (NOM). NOM is a generic term for the organic substances originated from decomposition of animal and plant bodies (Gschwend, 2016). NOM generally contains various types of functional groups such as carboxyl acid, hydroxyl, phenolic, amino, and quinines (Chen et al., 2011). Those complex organic molecules in NOM, especially carboxylic groups, were found to adsorb on the surface of Fe NPs, resulting in the change of surface characteristics of particles (Ramos-Tejada et al., 2003). By the adsorbed NOM, the mobility of Fe NPs in porous media can be enhanced (Johnson et al., 2009). NOM was also reported to serve as an electron-transfer mediator with the bulk solution (Tratnyek et al., 2011).

Effect of adsorbed NOM on the reactivity of Fe NPs can be categorized into two different hypotheses: 1) NOM can enhance electron transfer and thus Fe NP reactivity for pollutant degradation through electron shuttle effects (Tratnyek et al., 2011); 2) adsorbed NOM can block the reactive sites of Fe NPs forming surface complexes with iron and thus decreases ZVI reactivity (Chen et al., 2011; Zhang et al., 2011). The

enhanced dechlorination due to the presence of humic acid in ZVI system was observed for PCE dechlorination (Tratnyek et al., 2011). However, the increased reactivity of Fe NPs in the presence of NOM have not been reported. In contrast, several researches were reported the negative effect related with dechlorination of contaminants by the adsorption of NOM onto the surface of Fe NPs. Zhang et al. (2011) reported that TCE degradation kinetics decreased by 21 and 39% in the presence of 20 and 40 mg/L, respectively, of humic acid. Vindedahl et al. (2016) reported that the reductive degradation of 4-chloronitrobenzene by ferrous iron adsorbed onto the goethite nanoparticles was suppressed in case of the presence of humic acid.

Chapter 3. Concept and preparation of fatty acid double layer coated iron-based nanoparticles

3.1 Introduction

In addition to the high reactivity of iron-based nanoparticles (Fe NPs), which is attributed to its small particle size and large specific surface area, its broad usability has attracted the attention of researchers (Li et al., 2006a; Lien et al., 2006). It is possible to directly inject Fe NPs into the contaminant source area in the subsurface to remove the contaminant and contaminated plumes when Fe NPs are applied to the soil and groundwater remediation field. Compared with the typical ex-situ method, pump and treat method, the remediation method using Fe NP injection does not require groundwater pumping and an extended period of clean-up time, which can significantly reduce the cost of remediation (Cook, 2009; Karn et al., 2009; Müller and Nowack, 2010). Mainly, if the ex-situ method is difficult to apply due to infrastructures or buildings on the ground below which the source of contaminant is located, injection of reactive Fe NPs to the site to remediate contaminated groundwater can be the best alternative.

Fe NPs injected in subsurface must have sufficient ‘reactivity’ to reduce the concentration of contaminants below acceptable levels and adequate ‘mobility’ to remove plume and the dissolved part of contaminants in groundwater to successfully remediate the contaminated site. Significant research progress has been made in understanding the reactivity of Fe NPs. Studies on physicochemical characterization

(Nurmi et al., 2005; Sun et al., 2006), reaction rate (Matheson and Tratnyek, 1994; Stewart, 2005), reaction path (Lien and Zhang, 1999; Liu et al., 2005; Matheson and Tratnyek, 1994) , lifetime (Liu and Lowry, 2006; Sarathy et al., 2008), which can affect the reactivity, have been actively reported. The studies on mobility are based on investigation of the agglomeration and precipitation mechanism of nanoparticles (Hotze et al., 2010; Phenrat et al., 2008; Phenrat et al., 2007), evaluation of the adsorption and deposition on porous media (Sen and Khilar, 2006), and increase of mobility by surface coating (He et al., 2010; Jiemvarangkul et al., 2011; Kanel et al., 2007). Based on the results of the researches, Various stabilization methods have been proposed, confirming dispersion of nanoparticles in the aqueous phase and the mobility in porous media.

Because of geochemical cycles (dissolution and precipitation) of minerals in the subsurface, groundwater consists typically of various ions and dissolved organic matters such as NO_3^-, Cl^-, SO_4^{2-}, HCO_3^-, and HPO_4^{2-}, and natural organic matter (NOM) and these dissolved groundwater solutes can affect the reactivity, longevity, and the performance of Fe NPs. Several studies have reported that non-reducible ionic species decreased ZVI reactivity through the formation of a passivating oxide layer (Agrawal et al., 2002; Johnson et al., 1998; Su and Puls, 2004). Some similar effects of anionic species on the performances of bare ZVI NPs were experimentally observed (Feng et al., 2008; Liu et al., 2007). More recently, the effects of dissolved groundwater solutes on the reactivity of polyelectrolytes stabilized ZVI NPs have been reported (Phenrat et al., 2015). These results imply that these solutes cause the reactive site blocking due to the formation of Fe-anion complexes and the adsorption of NOM on the Fe NP surface, leading to an inhibitory effect on the reactivity of Fe NPs.

Although the effect of dissolved groundwater solutes on the reactivity of Fe NPs can reduce its applicability in the field, a strategy to stabilize Fe NPs both for adequate ‘mobility’ and selective ‘reactivity’ only to target contaminants have not been reported.

In this study, the idea for the strategy was developed and a new method for stabilizing Fe NPs have been developed based on the idea.

'Lipid bilayer membrane' inspired a newly developed method to stabilize Fe NPs. The lipid bilayer is flat sheets that form a continuous barrier around all cells and made of two layers of lipid molecules such as phospholipid (Fig. 3.1). The most important property of the lipid bilayer for this study is that it is a semipermeable structure, meaning that large molecules and small polar molecules cannot cross the bilayer. Only hydrophobic molecules can readily pass through the bilayer (Lodish et al., 2000). The contaminants of interest in this study are as categorized in chlorinated solvents, which are reducible by Fe NPs and hydrophobic. Therefore, if the lipid bilayer can cover the surface of Fe NP, dissolved groundwater solutes, especially anions, cannot pass through the layer. Thus passivation by the solutes cannot occur. On the other hand, hydrophobic contaminants such as TCE, PCE, and CT can easily pass through the lipid bilayer.

Oleic acid was used to form the lipid bilayer on the iron surface. Oleic acid is a fatty acid that is widely found in animals and plants, and the carboxylic acid at the end of its structure makes it possible to bind oleic acid to the metal surface. Also, oleic acid is widely used as a stabilizer for dispersing Fe NPs in a hydrophobic organic solvent (Zhang et al., 2006). Therefore, in this study, coating a fatty acid double layer on the iron surface was tried by forming stabilization layers in sequence. The particle coated with oleic acid is not dispersed in water due to the hydrophobic carbon chain of oleic acid. Therefore, as shown in Fig. 3.2, preparing a double layer was tried by using oleic acid and metal oleate, which has the same carbon chain as oleic acid but can be dispersed in water. In chapter 3, the preparation of fatty acid double layer coated Fe NPs was discussed and the formation of bilayer was confirmed by TEM, XRD and TGA analysis. In the following chapters, the mobility and reactivity of newly developed Fe NPs were evaluated.

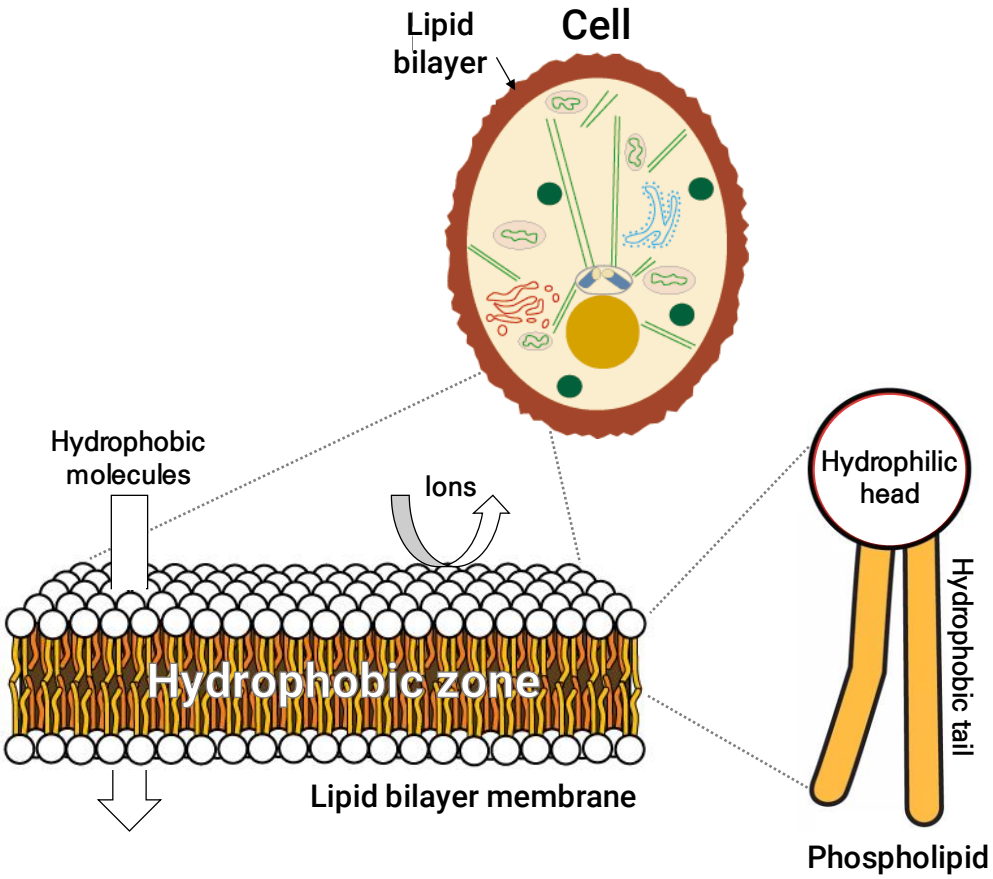

Figure 3.1 Schematic diagram of structures of lipid bilayer

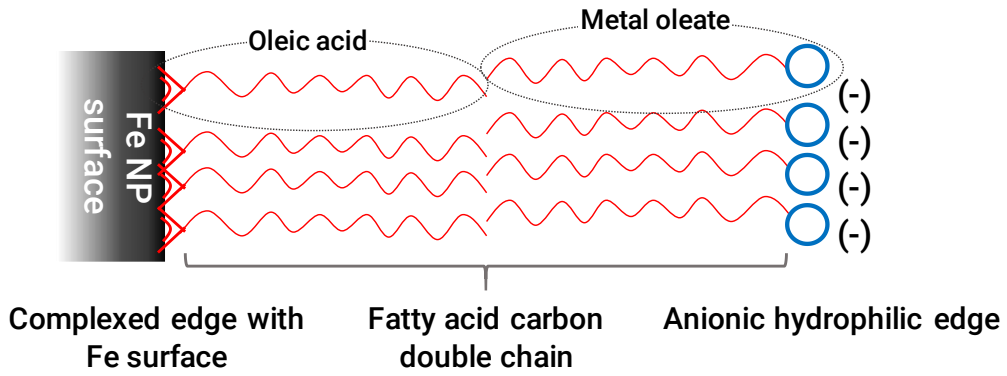

Figure 3.2 Schematic diagram of fatty acid double layer coating on Fe NP surface

3.2 Materials and methods

3.2.1 Chemicals

Ferrous sulfate Following chemicals were purchased from Sigma-Aldrich (St. Louis) and used as received without further purification: ferrous sulfate heptahydrate (ACS reagent), sodium borohydride (98%), sodium carboxymethyl cellulose (CMC, average molecular weight = 90k), potassium oleate (technical grade, 87%), oleic acid (technical grade, 90%), acetone (HPLC grade), ethanol (ACS reagent), n-hexane (GC grade). Toluene (GC grade, JT Baker), potassium hydroxide (extra pure, 85%, Daejung), ferrous stearate (9% Fe, Strem) were also used as received without further purification. Deionized water produced from Milli-Q (Millipore) was used as standard aqueous matrix, and N_2 purged deionized water (DDW) was also used to minimize surface passivation of Fe NPs by the aqueous matrix.

3.2.2 Preparation of Fe NPs

In this study, Fe nanoparticle modification was carried out in two ways: 1) pre-agglomeration modification, i.e., adding stabilizers before or during the growth of nanoparticles; and 2) post-agglomeration modification, where stabilizers are applied to the formed Fe NP aggregates. Commercial ZVI NPs (M-Fe) were purchased from Nanostructured & Amorphous Materials, Inc., and used as the formed Fe NPs in post-agglomeration modification process. The purchased ZVI NPs were also used as representative unmodified bare Fe NPs.

Two kinds of stabilizers were used for post-agglomeration modification including CMC and potassium oleate (PO). Stock solutions of each stabilizer at various concentrations were prepared to prepare modified Fe NPs in post-agglomeration method. 0.04 g of M-Fe were, then, added to 10 mL of PO stock solutions for PO modified Fe NPs via post-agglomeration modification (PoOl-Fe) and to 40 mL of CMC stock solutions for CMC modified Fe NPs via post-agglomeration modification (PoCMC-Fe) in 24 mL vials, and mixed by an end-over-end rotator at 45 rpm following ultrasonic irradiation using an ultrasonic water bath for 30 min.

CMC modified Fe NPs via pre-agglomeration modification (CMC-Fe) were prepared according to the methods described in He and Zhao (2007). In brief, the preparation was carried out in a 250 mL flask attached to a vacuum line. 0.5% (w/w) CMC solution was prepared in DW and purged with N_2 gas for 20 min. Ten mL of 0.18 M ferrous sulfate stock solution was added and mixed into 90 mL of CMC solution for 30 min to enable the formation of Fe-CMC complexes during N_2 purging. CMC-Fe were then formed by reducing Fe^{2+} ions using ten mL of a borohydride solution at a BH_4^-/Fe^{2+} molar ratio of 2.0. The reactor was operated under anoxic conditions through continuous vacuuming until gas evolution ceased. The resultant Fe concentration used in this study was 1 g/L.

Oleic acid (fatty acid) coated Fe NPs (OFe) were synthesized according to one of the thermal decomposition method for synthesis of OFe described in Kim et al. (2007). The synthesis was carried out under an argon atmosphere using standard Schlenk line techniques. 2 mM of ferrous stearate was added to 10 g of oleic acid in three necks round bottom flask. The mixture was degassed at 105 ℃ for 1 hour under continuous vacuuming. The solution was then heated to 380 ℃ at the rate of 5 ℃/min with vigorous magnetic stirring. The color of the mixture gradually changes to dark-black, which indicates the formation of Fe NPs. The temperature of the mixture was maintained at 380 ℃ for one h. The end product is a black gelatinous Fe NPs containing slurry. After cooling the slurry to room temperature, the slurry was stored without any purification in an N_2 filled glove box for further process. A small amount of the slurry was collected and added to a mixture of acetone and a small fraction of n-hexane and ethanol. The solution was then centrifuged to precipitate the Fe NPs. This washing process was repeated several times, and the separated particles were used for TEM and XRD analysis. To adding a second fatty acid layer onto hydrophobic OFe for the formation of the fatty acid double layer mimic lipid bilayer membrane and the colloidal stability in the aqueous phase, PO stock solution (100 g/L) was used. 9.78 g of oleic acid was added to 50 mL DDW filled 100 mL volumetric flask and magnetically stirred for preparing the PO stock solution, and 50 mL of 0.7 N KOH was added to the flask slowly during vigorous stirring. After six h stirring, clear PO solution, indicating complete dissociation of oleic acid into PO, was prepared. Mechanical (with magnetic stirring) mixing was, then, applied to coat additional fatty acid layer onto the surface of OFe using the hydrophobic-hydrophobic reaction between the hydrocarbon chains on OFe and in PO solution. Eight mL of OFe slurry was added to 100 mL of PO solutions with various concentrations and vigorously stirred with magnetic spin bar for 24 h. The dispersed nanoparticles in the mixture were centrifuged at 40,000 rpm for 15 min, and the supernatant with excess unreacted oleic

acid and PO was decanted before filled with DDW or PO solutions of 16 mM or 0.32 mM. The concentrated and washed dispersions (oleic acid and potassium oleate double layer coated Fe NPs, PO-OFe) were stored in an N_2 filled glove box until used for further experiments.

3.2.3 Physical characterization

The particle size of Fe NPs was measured through transmission electron microscope (TEM) analyses. TEM micrographs of Fe NPs were obtained using an FEI Titan 80-300 TEM. Samples for TEM analysis were prepared by dispersing Fe NPs in water or hexane, dropping the suspensions onto a carbon TEM support grid and allowing solvent volatilization for over two h. Mineral compositions of Fe NPs were estimated by X-ray diffraction analysis (XRD, Dmax2500, Rigaku) with a Cu X-ray source at 40 kV and 200 mA. Continuous scans from 10 to 80° 2θ were conducted at a scan rate of 1° 2θ/min. The stabilizer mass of coated particles was quantified by thermogravimetric analysis (TGA) under an N_2 atmosphere from room temperature up to 800 ℃ with a heating rate of 10 ℃/min (SDT Q600, TA Instruments).

3.2.4 Iron content

Total Fe was determined by dissolving the aliquot of sample (0.1 mL, dispersed in aqueous media) in 0.5 mL of 6 N HCl (1:5 v/v ratio) for two h and diluted to 10 mL with DW. UV spectrometer was used to calculate Fe concentration in the solution according to ASTM method (ASTM, 2000).

3.3 Results and discussion

3.3.1 Strategy for development of fatty acid double layer coated Fe NPs

The main reason why the lipid bilayer can permeate only hydrophobic materials through the membrane and preventing ion and ionic materials from permeating is that the hydrophobic carbon chain is gathered in the central part of the membrane and the local polarity is close to zero (Xiang et al., 1998). It is a condition similar to the difficulty of water penetrating the oil layer. Through the solubility-diffusion mechanism, ions can pass through the lipid bilayer, but the rate is prolonged. Most of the ions penetrate through some hydrophilic spaces in the middle of the lipid bilayer where no carbon chain structure exists (i.e., hydrophilic pore in lipid bilayer) or pass through proteins as carriers (Nagle et al., 2008; Tepper and Voth, 2006). Therefore, fatty acid should be densely bonded to the surface of Fe NPs and build the area where the polarity is close to zero inside the stabilizer layer to form a stabilizer layer onto the surface of Fe NPs having a selective permeability like lipid bilayer that blocks hydrophilic substances and penetrates only hydrophobic substances using fatty acid layer.

The critical point of this chapter is to find the answer to the question of how oleic acid can be densely bonded to the surface of Fe NPs and an additional layer of metal oleate combined to form a fatty acid double layer. The pre- and post-agglomeration modification were applied to prepare oleic acid bonded Fe NPs. The difference in surface density of oleic acid bonded to the surface of Fe NPs was evaluated by the weight of oleic acid bonded per unit weight of Fe NPs. Moreover, commercially available Fe NPs (M-Fe) were used as a representative of bare unmodified Fe NPs and raw materials for

post-agglomeration modification. CMC was chosen as a representative modification reagent based on its various application cases in the environmental engineering field.

3.3.2 Synthesis of oleic acid-coated Fe NPs (OFe) via thermal decomposition and formation of fatty acid double layer onto Fe NPs

The traditional synthesis approach to Fe NPs has relied on the aqueous precipitation or hydrolysis of ferrous and/or ferric salt(s) (Huber, 2005). This approach is based on the aqueous medium. Therefore, it may be challenging to apply hydrophobic oleic acid as the stabilizer of pre-agglomerate modification to this approach. Another popular synthesis method of Fe NPs is a thermal decomposition method. In a typical laboratory synthesis using thermal decomposition method, iron precursor (mostly hydrophobic iron complex precursor) is mixed with a stabilizer and boiled in a high boiling point solvent under reflux conditions. The most notable examples of this type of synthesis are refluxing iron acetylacetonate, oleic acid, oleylamine and 1,2-hexadecanediol in diphenyl ether (Sun et al., 2004), heating iron acetate in oleic acid and trioctylamine (Yu et al., 2004), and refluxing iron oleate or stearate mixed with oleic acid and 1-octadecene (Kim et al., 2007; Park et al., 2004).

Unlike typical aqueous precipitation by which polydispersed Fe NPs are synthesized (Yu et al., 2004), thermal decomposition method can synthesize monodisperse Fe NPs with uniform particle size and can change its size in a wide range (Bronstein et al., 2007). The flexibility in the synthesis method is attributed to the stabilizer added during the synthesis process, which can efficiently prevent the particle aggregation during the nucleation and growth of Fe NPs. Oleic acid is widely used as a stabilizer in thermal decomposition synthesis methods for synthesis of Fe NPs, and oleic acid bonded stable Fe NPs can be obtained by thermal decomposition method (Ullrich et al., 2014; Zhang

et al., 2006). In this study, to synthesize 'fatty acid double layer' on the surface of Fe NPs, firstly, oleic acid-coated Fe NPs were synthesized via thermal decomposition method and, then, dispersed in aqueous phase using the formation of an additional dispersible layer with metal oleate (sodium or potassium oleate). Metal oleate possesses the same hydrocarbon chain structure as oleic acid, thereby, allowing for a hydrophobic-hydrophobic interaction between attached oleic acid and oleate molecules (Fig. 3.2, 3.3). The carboxylate group of PO in the outer layer is hydrophilic so that it can transfer OFe to stable in the aqueous phase (Fig. 3.3).

In general, the phase transfer process requires washing or purification steps. This process removes excess ligand and solvent that remain unreacted during the synthesis of Fe NPs. It is because excess unreacted remained materials can interfere with the reaction of the synthesized Fe NPs to the transferring reagent in the process. However, during this process, as-synthesized Fe NPs can react with oxygen and water in the atmosphere. Therefore, in this study, washing and purification processes were excluded to simplify the process of producing Fe NPs and protect the particles. After the particle synthesis, black colored viscous OFe slurry was directly injected into glass bottle filled with PO solution of various concentrations and stirred for one day, and water dispersed OFe can be recovered.

The amount of recovered iron increased with the increase of the concentration of PO solution (Fig. 3.4). At a concentration of PO solution above 50 g/L, the recovery of iron was kept constant, and the amount of recovered iron decreased sharply as the concentration of PO solution decreased below 25 g/L. Especially at the concentration of 5 g/L or less, aggregated Fe NPs can be confirmed by visual observation, which can be due to the excess oleic acid. The amount of iron that can theoretically be recovered in the recovering method prescribed in this study is about 0.07 g. More than 80% of iron could be recovered at PO solution concentrations of 50 g/L or more. This results

indicated that using a high concentration of the transferring agent, Fe NPs synthesized based on organic matters including thermal decomposition can be recovered simplifying the washing process.

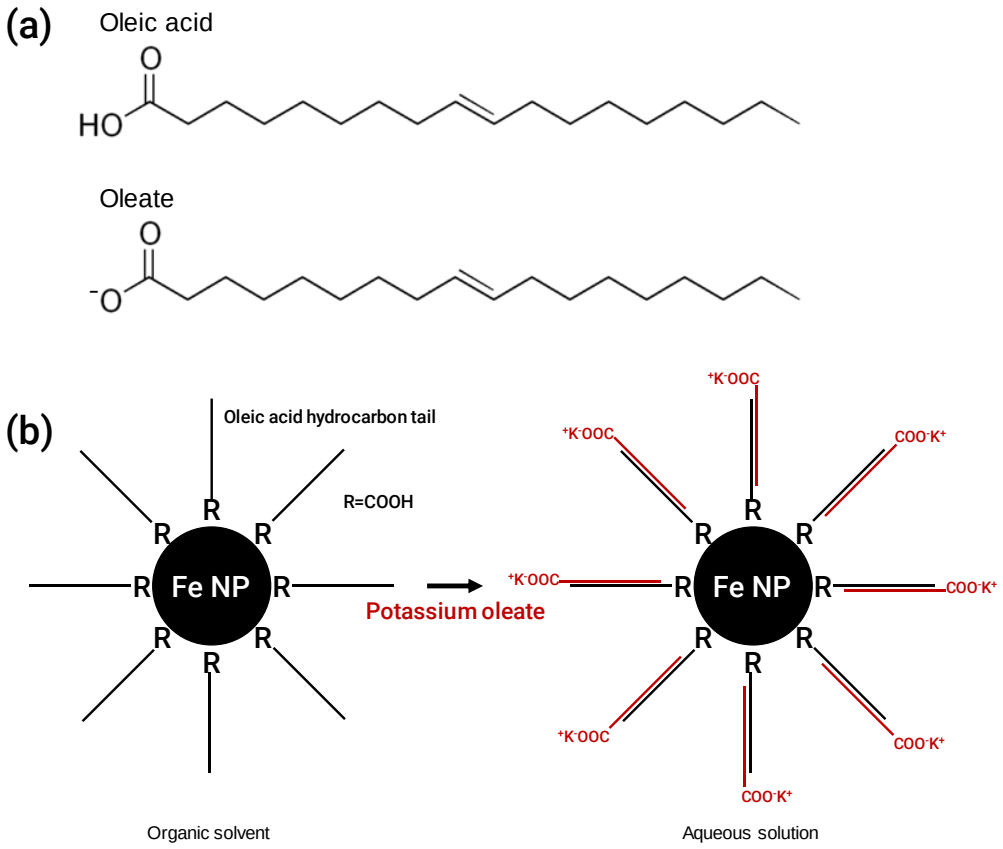

Figure 3.3 Schematic diagram of (a) structures of oleic acid and oleate, and (b) phase transferring of oleic acid coated Fe NPs to water dispersed fatty acid double layer coated Fe NPs with potassium oleate

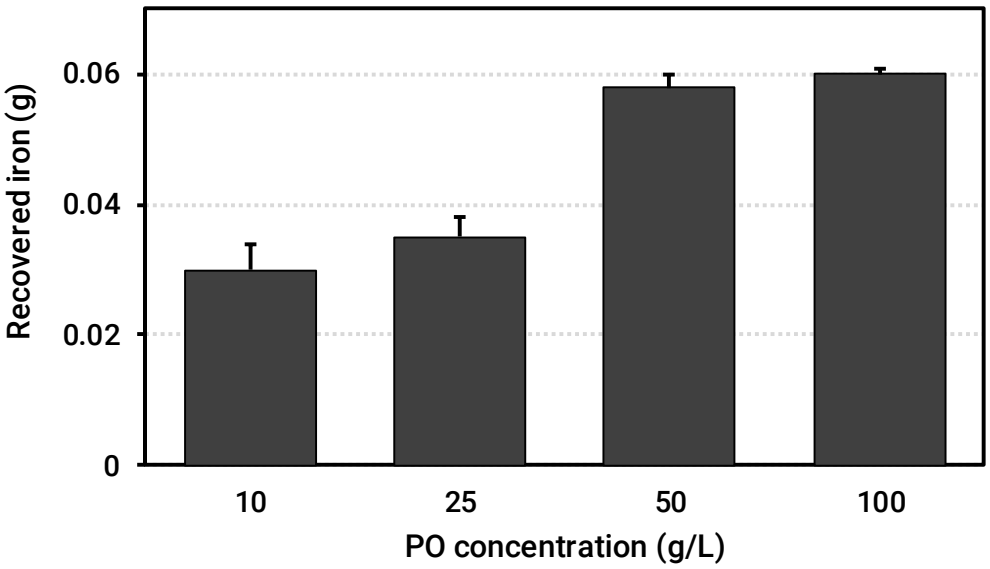

Figure 3.4 Effect of PO concentration on the amount of recovered iron in phase transferring process. In the process, 8 mL of OFe slurry containing 0.07 g iron or so was added to 100 mL of PO solution. Error bar means standard deviation of triplicate experiments

Recovered Fe NPs were no longer dispersed in water in the case when particles were precipitated by centrifugation and washed with DDW. Moreover, the iron particles that lose their water dispersibility can be readily re-dispersed when an organic solvent was added. These surface characteristics of the Fe NPs related to the dispersivity can be seen as a result of the relatively weak bonding between the oleic acid hydrocarbon chains coated on the surface of Fe NPs and the PO tails. Therefore, to maintain the aqueous dispersibility of the recovered Fe NPs, the concentration of PO solution had to be maintained at a specific concentration or more. Wang et al. (2013) revealed the relation between initial (added) surfactant (e.g. sodium oleate) concentration and Fe NPs stability in aqueous solution, and introduced that the best possible dispersion was obtained when the surfactant concentration in solution at equilibrium with the adsorbed surfactant should be close or slightly above its critical micelle concentration (MC). Washed Fe NPs in this study could be re-dispersible in aqueous solution when the concentration of background PO solution was above 0.32 mM. Considering the MC of PO, 0.8 mM (Molchanov et al., 2005), the concentration of background PO solution was prepared in two different concentrations, 0.32 mM (minimum concentration, LPO-OFe) and 16 mM (high concentration, HPO-OFe). In this study, all experiments proceeded with PO-OFe in 16 mM PO solution unless otherwise mentioned.

3.3.3 Nanoparticle characterization

Figure 3.5 shows the TEM images of Fe NPs used in this study (M-Fe, CMC-Fe, OFe, PO-OFe). TEM analysis for the post-agglomeration modified Fe NPs (PoOl-Fe, PoCMC-Fe) was excluded based on the assumption that coated stabilizer by post-agglomeration modification method should not affect the morphology of the particle. The M-Fe were spherical with chain network structure as shown in Fig. 3.5, consistent with those in other research works (Nurmi et al., 2005; Sun et al., 2006). The aggregation of ZVI NPs (in this study, M-Fe) in aqueous solution is also a typical behavior. CMC-Fe in the TEM image appeared as discrete particles, which can be attributed to the stabilizer added into Fe NPs synthesis process. Oleic acid coated Fe NPs (OFe) and stabilized OFe in PO solution (PO-OFe) were highly uniform in size and monodispersed in organic and PO solution, respectively due to the capping by oleic acid (Fig. 3.5), which is consistent with previous works (Kim et al., 2007; Park et al., 2004).

The mean size of the nanoparticles was estimated based on measuring 100 particles on TEM images for each sample except for M-Fe of which mean size is 25 nm given from the manufacturer. CMC-Fe had a mean size of 5.13 nm (standard deviation = 2.82 nm). Using a similar synthesis method, Raychoudhury et al. (2010) and He et al. (2007) reported that CMC-Fe with an average diameter of 5.7 ± 0.9 nm and 4.3 ± 1.8 nm, respectively. It was expected that CMC-Fe could have higher reactivity than that of M-Fe due to the larger surface area which is attributed to the smaller particle size of it. The reactivity of Fe NPs was discussed in the following chapter 5. There was little change in the mean size of OFe and PO-OFe. The mean size of OFe is 22.4 nm (standard deviation = 1.1 nm), which is also consistent with previous work (the nanoparticles synthesized by Kim et al. (2007) had the mean size of 23 nm).

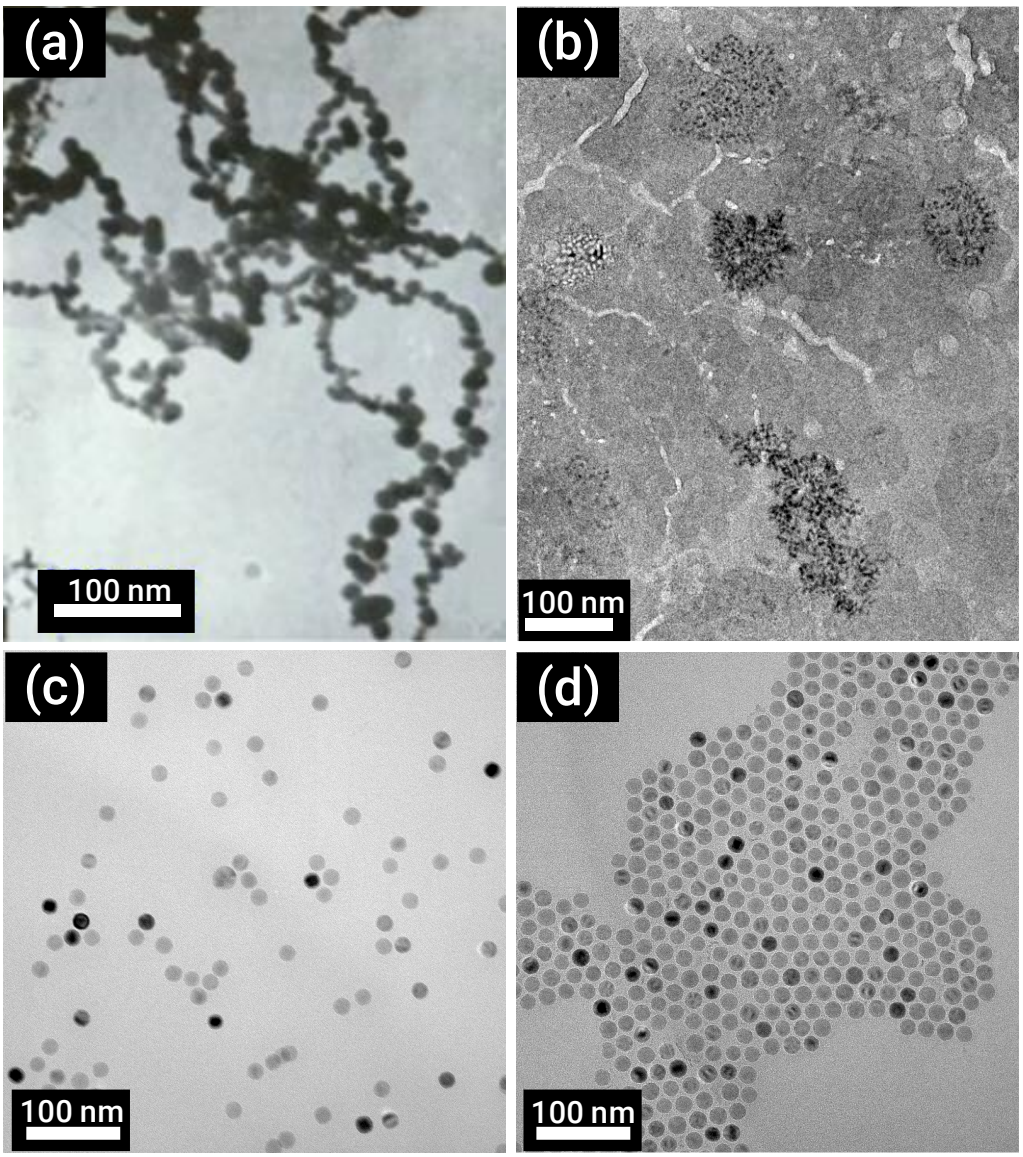

Figure 3.5 TEM image of Fe NPs (a)* commercial ZVI NPs (M-Fe), (b) CMC modified Fe NPs before particle agglomeration (CMC-Fe), (c) oleic acid coated Fe NPs via thermal decomposition method (OFe), and (d) Fatty acid double layer coated Fe NPs (PO-OFe)
* obtained from the manufacturer

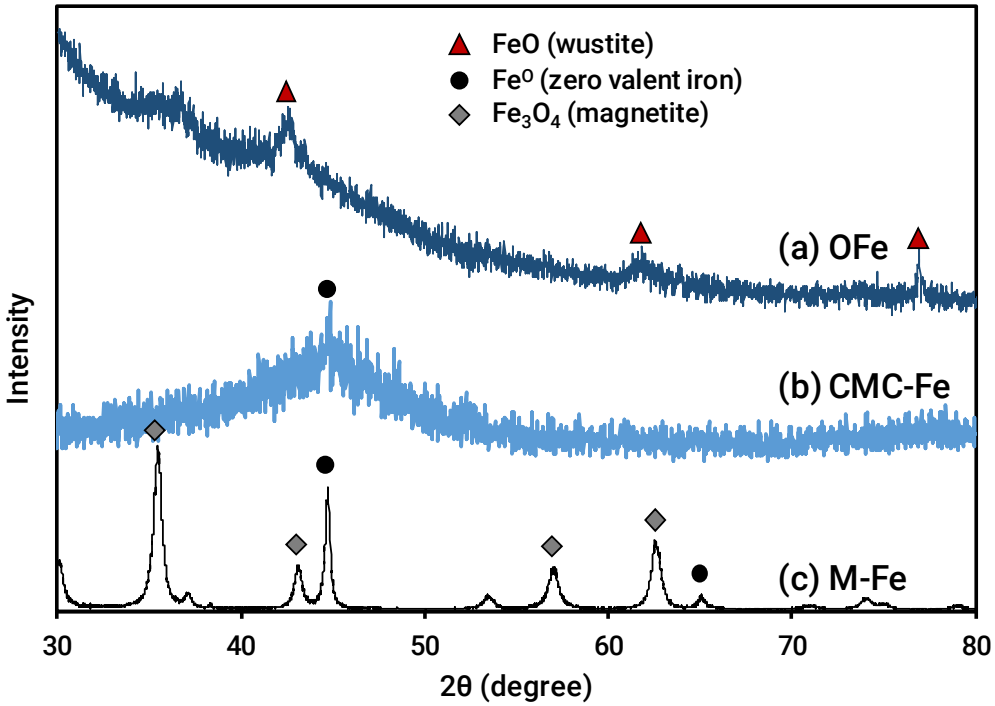

Figure 3.6 X-ray diffraction pattern of (a) OFe, (b) CMC-Fe, and (C) M-Fe

XRD patterns in Fig. 3.6 revealed FeO (wustite) structure of OFe. The synthesis method for OFe in this study followed the method from Kim et al. (2007) by which highly crystalline α-Fe (zero valent) can be synthesized and magnetite. FeO is generally formed in the condition of an insufficient amount of oxygen in magnetite synthesis and can be decomposed into α-Fe and magnetite (Redl et al., 2004). The formation of FeO may be due to the different synthesis conditions that difficult to control including the purity of compounds and gas used and applied vacuum pressure with those of Kim et al. (2007). In contrast, the TEM image of M-Fe and CMC-Fe confirmed the presence of ZVI in both samples. Magnetite was also confirmed in M-Fe, which is a common oxide mineral frequently found at the surface of ZVI.

3.3.4 Stabilizer mass coated onto Fe NPs surface

An essential goal of this chapter is to develop Fe NPs with a sufficient amount of oleic acid combined with an oleate capable of stabilizing it in aqueous solution. For this purpose, oleic acid-coated Fe NPs was synthesized by thermal decomposition method (OFe), and PO was used to disperse the particles in aqueous solution. Commercial Fe NPs (M-Fe) were purchased as a control, and stabilizer coated M-Fe by CMC (PoCMC-Fe) and PO (PoOl-Fe) were also prepared. Moreover, CMC-Fe synthesized via the pre-agglomeration modification method in which borohydride reduction of iron is carried out after the complexation reaction between CMC molecules and iron ions were prepared to compare the difference of the amount of the stabilizer coated onto the surface of Fe NPs by post- and pre-agglomeration modification. TGA analysis quantitatively determined the amount of stabilizer bonded to the surface of the Fe NPs.

The mass loss in TGA graph (Fig. 3.7) related to the mass of bonded stabilizer. The initial mass loss is due to the evaporation of physically adsorbed water or degradation of surface hydroxyl groups (Araújo-Neto et al., 2014). Subsequent mass loss corresponds to the decomposition of the stabilizer (Zhang et al., 2006). The mass ratios of the stabilizers to the Fe NPs evaluated from TGA were 0.15% of M-Fe, 4.63% of PoCMC-Fe, 5.09% of PoOl-Fe, 37.65% of CMC, and 52.07% of PO-OFe.

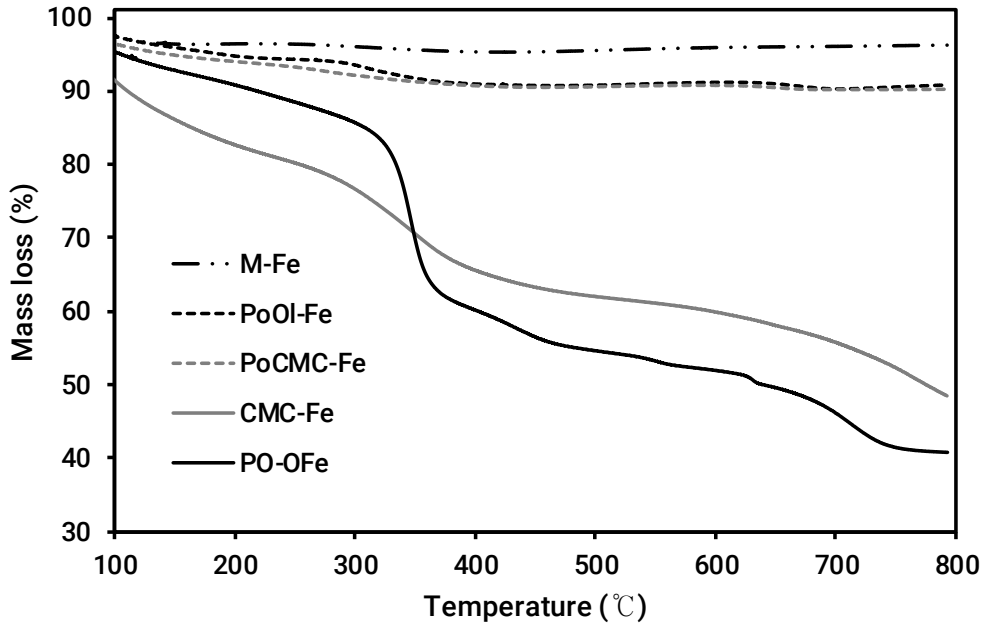

Figure 3.7 TGA curves of commercial unmodified Fe NP and modified Fe NPs

There was a significant difference in the amount of bonded stabilizer for each modification method. The amount of stabilizer coated on the Fe NPs prepared by the pre-agglomerated modification method was more than seven times larger than that of prepared by the post-agglomerated method. In the case of Fe NPs coated with CMC (PoCMC-Fe and CMC-Fe), it can be seen that the difference in the amount of bonded stabilizer is caused by the difference in particle size. The amount of the stabilizer of CMC-Fe was more than 1.5 times greater than that of PoCMC-Fe prepared by the post-agglomerated modification method, even though the difference in the specific surface area was considered. On the other hand, it is hard to confirm that the amount of bonded stabilizer is attributed to the difference in specific surface area between PO-OFe and PoOl-Fe because of the similar particle size. It can be seen that the difference of the

amount of bonded stabilizer was attributed to the difference of modification method. In the post-agglomerated modification method, there should be a portion of the surface that cannot react with the stabilizer due to the presence of Fe aggregates. Although it is possible to break up the aggregates and lead the entire surface of the particle to participate in a bonding reaction with the stabilizer, the ultrasound irradiation method introduced in this study cannot be considered to break the aggregates completely. In the pre-agglomerated modification method, the entire surface of the particles can participate in bonding with the stabilizer because the aggregation is prevented at the growing stage where the nanoparticles are formed and become larger.

TGA provided additional qualitative evidence of fatty acid double layer coating on the PO-OFe and PoOl-Fe. The curves show a mass loss in a two-step process, from 300 to 400 ℃ and from 600 to 750 ℃. The mass loss in the low-temperature region can be attributed to the decomposition of outer part of the fatty acid double layer, while the loss in the high-temperature region results from physically adsorbed oleate molecules (Roth et al., 2016). These results support the formation of a fatty acid double layer onto the Fe NPs in aqueous solution and agree with other works (Roth et al., 2016; Yang et al., 2010).

3.4 Conclusions

The fatty acid double layer coated Fe NPs (PO-OFe) was able to be synthesized by the following fatty acid coating; dispersing oleic acid-coated Fe NPs (OFe) into potassium oleate solution after synthesis of OFe using thermal decomposition method. When oleic acid is bonded to the surface of the metal particles, the surface of the metal particles becomes hydrophobic and, thus cannot be dispersed in water. Hydrophobic OFe could be recovered in aqueous solution using potassium oleate solution in this study, which can be considered as evidence that a bilayer was formed onto the particle surface. The TGA results also showed that a bilayer was formed on the iron surface. The amount of coated stabilizer of Fe NPs synthesized by thermal decomposition method was larger than that of other iron synthesis methods. Since the water dispersibility and mobility in porous media of the nanoparticles are greatly influenced by the surface characteristics of the particles, it can be expected that the Fe NPs coated with a remarkable amount of fatty acid as the double-layered structure will have prominent characteristics compared with the Fe NPs prepared by other synthetic methods.

Chapter 4. Transport of fatty acid double layer coated iron-based nanoparticles in porous media

4.1 Introduction

The objective of this chapter is to evaluate the mobility of newly developed modified Fe NPs (PO-OFe) in Chapter 3. The most important result in this chapter is the results of column experiments in that Fe NPs were injected into a sand filled column to obtain a breakthrough curve. The breakthrough curve derived from the column experiment can be used to quantitatively evaluate the mobility of Fe NPs using the filtration theory. Factors that are deeply related to the mobility of nanoparticles are particle size and surface potential (i.e., zeta potential). These two factors have been used as a significant factor in identifying the mechanism to improve the mobility of Fe NPs as a factor that determines inter-particle stability and particle-collector response. For comparative analysis, bare unmodified Fe NPs and Fe NPs coated with CMC, which is the most commonly used stabilizer in laboratory and field scale studies, were also tested for mobility evaluation.

4.2 Materials and methods

4.2.1 Chemicals

The following chemicals from Sigma-Aldrich (St. louis) were used as received: ferrous sulfate heptahydrate (ACS reagent), sodium borohydride (98%), sodium carboxymethyl cellulose (CMC, average molecular weight = 90k), potassium oleate (technical grade, 87%), oleic acid (technical grade), potassium chloride (ACS reagent), acetone (HPLC grade), ethanol (ACS reagent), n-hexane (GC grade), hydrochloric acid (ACS reagent). Toluene (GC grade, JT baker), potassium hydroxide (extra pure, 85%, Daejung), ferrous stearate (9% Fe, Strem) were also used as received. Deionized water produced from Milli-Q (Millipore) was used as standard aqueous matrix.

4.2.2 Fe NPs synthesis and characterization

The main content of this chapter is to evaluate the mobility of fatty acid double layer coated Fe NPs (PO-OFe) in the subsurface. To evaluate the mobility of PO-OFe, Commercial ZVI NPs (M-Fe), potassium oleate modified Fe NPs via post-agglomeration modification (PoOl-Fe), carboxymethyl cellulose (CMC) modified Fe NPs via post-agglomeration modification (PoCMC-Fe), and CMC modified Fe NPs via pre-agglomeration modification (CMC-Fe) were prepared and used as a control group. The detailed synthesis procedure of above Fe NPs was described in Chapter 3.2.

4.2.3 Porous media

Jumunjin silica sand (Yesung Inc.), with a median diameter, d_{50}, of 440 μm, was used as a model porous media. The sand grains were 30% by weight in size range of 250 ~ 420 μm, 70% in size range of 420 ~ 595 μm. Prior to use, the sand was acid washed with concentrated hydrochloric acid to remove the background iron oxide, rinsed with water and dried in an oven overnight at 550 °C to remove background organic matter.

4.2.4 Sedimentation tests

Colloidal stability of Fe NPs (M-Fe, CMC-Fe, PoCMC-Fe, PoOl-Fe, OFe, PO-OFe) in aqueous media or hexane were assessed by visual observation and monitoring the optical absorbance at 508 nm as a function of time for the concentration of 0.1 g-Fe/L by UV-vis spectrophotometry (Scinco, Korea) in duplicate. All prepared Fe NPs dispersions were stored in glass vials and routinely monitored for 6 h.

4.2.5 Column experiments

Glass columns with 12 cm in length and 1.17 cm (for average and fast pore water velocity) and 2.5 cm (for slow pore water velocity) in diameter were packed with sand and gently vibrated at several stages to ensure uniform packing. The sand packed column was first saturated with CO_2 then flushed with DW for more than 5 pore volumes (PVs) to remove air bubbles. A sheet of ASTM mesh No. 100 (the size of sieve hole is 150 μm) were placed at both ends of the column to prevent sand loss. The column was set up vertically and sealed with screw caps at both ends. Tracer KCl was injected from the bottom of the column until the effluent concentration is equal to the influent. The effluent chloride was collected at a selected time interval with a fraction collector, and the

concentration was analyzed. Then, the influent was switched to the de-aired, de-ionized water (DDW) for 5 PVs to elute the tracer thoroughly.

The column feeding solutions containing CMC-Fe and PO-OFe were pumped upwards through the column at several velocities (0.04 cm/min, 0.2. cm/min, 1.4 cm/min). CMC-Fe and PO-OFe suspensions were diluted to 0.5 g/L using DDW for the column experiments. Additional column experiment was performed with PO-OFe at the concentration of 1 g/L at 0.2 cm/min to evaluate the effect of nanoparticle concentration on column transport. The suspension was vigorously mixed with magnetic stirring during the suspension injection to prevent particle sedimentation. The nanoparticle breakthrough curves were obtained by measuring the concentration of total iron in the effluent at a selected time interval. The transport of unmodified Fe NPs (M-Fe) was also conducted as a control test. Main parameters of the column experiments are summarized in Table 4.1.

Table 4.1 Experimental conditions and parameters for column experiments

Column inner diameter (cm)	1.75, 2.5
Column length (cm)	12
Iron concentration of suspension feed (g/L)	0.5
Pore water velocity (cm/min)	0.04, 0.2, 1.4
Porosity	0.4
Median diameter of the sand particles (um)	440

4.2.6 Analytical methods

Chloride was analyzed by ion chromatography (IC) (ICS-1000, Dionex Co., Sunnyvale, CA) equipped with IonPac® AS23 column for anion analysis.

Total Fe was determined by dissolving the aliquot of sample (0.1 mL, dispersed in aqueous media) in 0.5 mL of 6 N HCl (1:5 v/v ratio) for 2 h and diluted to 10 mL with DW. UV spectrometer was used to calculate Fe concentration in the solution according to ASTM method (ASTM, 2000).

The particle size of Fe NPs was measured through transmission electron microscope (TEM) analyses. Detailed procedure was described in Chapter 3.2. DLS tests were also performed with a Zetasizer Nano NS (Malvern Instruments) to obtain a hydrodynamic diameter of the sample. Stock solutions of 1 g/L Fe NPs (for M-Fe, PoCMC-Fe, PoOl-Fe, and CMC-Fe) were diluted to 0.1 g/L with DW except for OFe, the hydrophobic sample. For the DLS measurement of OFe, toluene was used as a dispersant. About 0.1 mL of non-washed OFe slurry was diluted to 10 mL of toluene. Zeta potential was also measured in the DLS measurements. In this study, all data on particle size and zeta potentials are given as mean ± standard deviation of at least triplicate samples.

4.3 Results and discussion

In Chapter 3, the fatty acid double layer using oleic acid and PO was formed on the surface of Fe NPs by simulating the structure of the lipid bilayer membrane. Compared with other prepared Fe NPs by different manufacturing methods (PoOl-Fe, PoCMC-Fe, CMC-Fe), the amount of coated stabilizer onto the surface was the highest when synthesized by thermal decomposition method and confirmed by TGA analysis. In this chapter, the mobility of PO-OFe in subsurface was evaluated by the analysis of particle size, zeta potential, colloidal stability, and 1-D column transport experiment. As in Chapter 2, the mobility was compared with those of stabilized Fe NPs prepared by other methods including M-Fe and CMC-Fe.

4.3.1 Nanoparticle characterization

The particle size of the Fe NPs used in this study was measured with TEM images in Chapter 3. Although TEM images provide direct visualization of the size, shape, and morphology of nanoparticles, it is difficult to distinguish the nanoparticles from the coated stabilizer in the resultant image, and it is difficult to judge the dispersion and coagulation state of the nanoparticles because the analysis proceeds in a dried condition. On the other hand, the DLS analysis can measure the size of suspended particles in the original solution, and it is possible to analyze the hydrodynamic diameter which reflects the particle and the stabilizer together in the measurement of size so that it can be more relevant to the transport of the nanoparticles. In this study, a hydrodynamic diameter from DLS measurements was used in the subsequent model calculation.

Table 4.2 Characteristics of different types of Fe NPs used in this study

Fe NPs	Particle size (nm) (Mean ± SD)		Zeta potential (mV) (Mean ± SD)		
	by TEM	by DLS	Value	pH	Background solution
M-Fe	25	N.A.*	-38.2 ± 1.3	7	DW
PoCMC-Fe	-	1035.0 ± 5.5	-79.7 ± 2.1	7	1/10 dilution of Fe stock solution
PoOl-Fe	-	965.1 ± 12.1	-72.8 ± 2.5	7	
CMC-Fe	5.1 ± 2.8	250.1 ± 5.4	-57.4 ± 1.0	8	
PO-OFe	22.4 ± 1.1	204.1 ± 2.9	-91.2 ± 1.8	6	0.032 mM PO
		89.4 ± 9.6	-115.2 ± 5.1	8	1.6 mM PO

Table 4.2 shows the size of Fe NPs with different methods. Although M-Fe suspension was soaked in an ultrasound bath for ultrasonic irradiation to break down the aggregates, the rapid settlement was occurred even in a short measuring time for DLS analysis apparently because of the particles' aggregation. It is natural that insufficient colloidal stability and mobility of the sediments, M-Fe, is expected. The aggregation of M-Fe can be also confirmed in the TEM image, and these results show one of the reasons why the modification of Fe NPs is necessary. Due to the added stabilizers, both of PoOl-Fe and PoCMC-Fe showed a smaller hydrodynamic diameter than that of M-Fe. However, in general, above the size of 1 μm, particles begin to sediment out of suspension (Hotze et al., 2010). Therefore, Fe NPs prepared by the post-agglomerated modification based on M-Fe are also unlikely to be stable in aqueous solution.

The Fe NPs prepared by the pre-agglomerated modification methods had a relatively small hydrodynamic diameter. The reason for this is that the stabilizer prevents the aggregation of the particles during the formation of the ripen iron particles. This stabilizing mechanism is also consistent with the fact that a more massive amount of stabilizer is combined with the Fe NPs prepared by the pre-agglomeration modification methods.

Significant differences were noted between the particle size by TEM and DLS (hydrodynamic diameter) in Fe NPs prepared by the pre-agglomerated modification methods. The mean particle sizes of CMC-Fe were 5.1 (by TEM) and 250.1 (by DLS). Even considering the increased diameter due to the attached stabilizer, the diameter difference between the two value is not fully explained. It may be attributed to the bridging of polymer coated nanoparticles by the free polyelectrolytes in solution (Chen et al., 2007; Syrbe et al., 1998). According to Chen et al. (2007) and Syrbe et al. (1998), polyelectrolytes such as CMC attached to the surface of nanoparticles can make inter-polymer bridging between the particle surfaces and result in enhanced aggregation of nanoparticles. It is presumed that several CMC-Fe are connected each other by surface attached CMC or free CMC in the solution like Fig. 4.1(b) and it is consistent with the stabilizing concepts of researchers on polyacrylic acid stabilized ZVI NPs (Lin et al., 2010; Schrick et al., 2004).

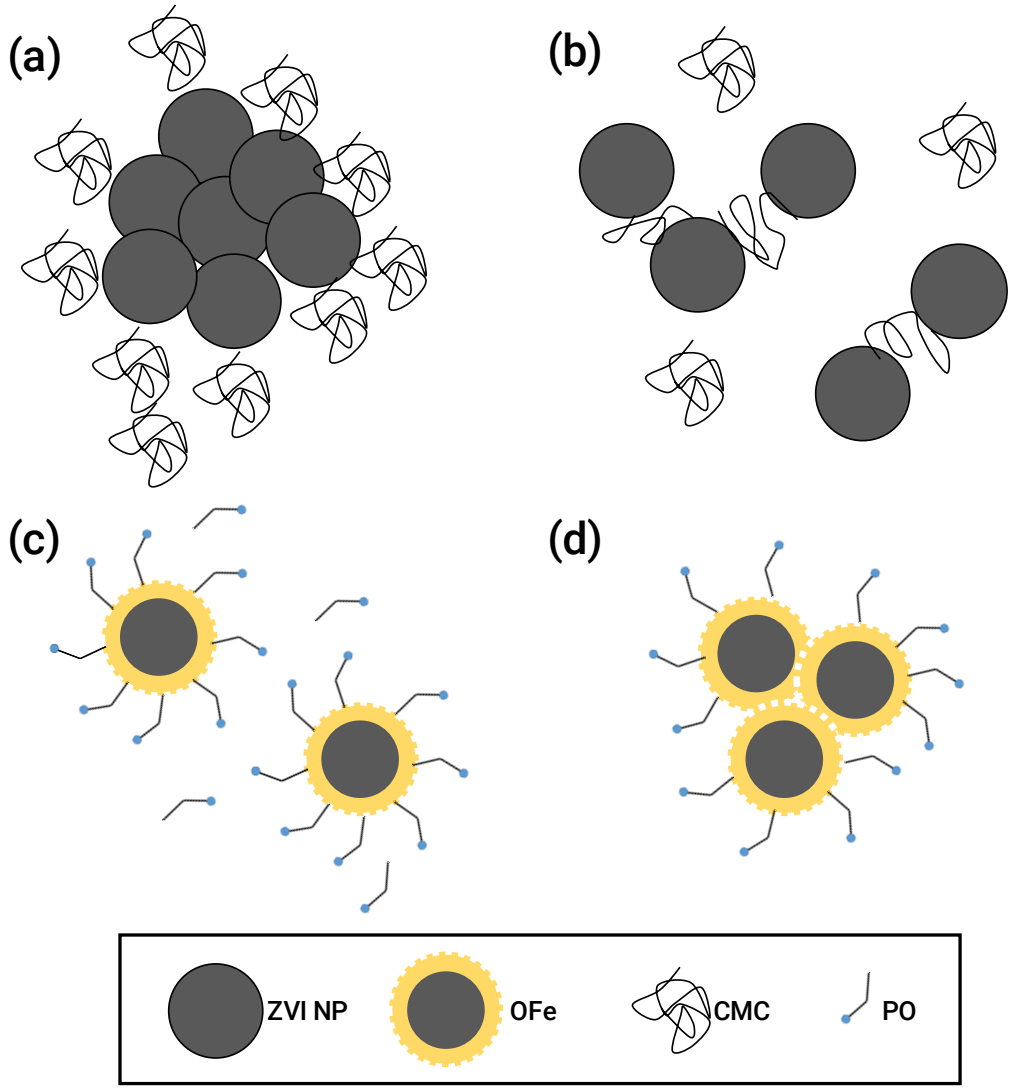

Figure 4.1 Schematic of stabilizing mechanisms of (a) PoCMC-Fe*, (b) CMC-Fe, (c) PO-OFe in high concentration of PO (e.g. 16 mM), and (d) PO-OFe in low concentration of PO (e.g. 0.32 mM)

* A stabilizer cannot coat the surface of nanoparticle fully enough to be stable in aqueous solution when aggregates are already formed

In the case of PO-OFe, it can be expected that several nanoparticles in PO-OFe suspension are clustered similar to the case of CMC-Fe. However, the mechanism of clustering should be different from that of CMC-Fe because of the inherent structural difference between coating methods, the single layer of polyelectrolyte and the double layer of fatty acid. Xu et al. (2005) reported that when oleate ions were adsorbed on the nanoparticle surface, nonpolar chains extending towards aqueous media render the nanoparticle surface strongly hydrophobic whereby oleate coated particles (single layer) may unite with each other by hydrophobic-hydrophobic interaction. However, with the increased concentration of oleate ion in the solution, oleate tail attached onto the particle surface and oleate molecules in the solution as free phase may cause a double layer by which oleate bilayer coated nanoparticles can remain stable in aqueous solution. Yu et al. (2010) observed the aggregation of paramagnetic nanoparticles stabilized with oleic acid bilayer by injecting in sedimentary rocks and explained the mechanism of the aggregation that high shear stress resulted from interaction with rock surface breaks the weak bond between first and second oleic acid layer, so that oleic acid monolayer coated nanoparticles become aggregate in aqueous media due to its hydrophobic surface.

With the stabilizing concept from above literature, the difference in the hydrodynamic diameter due to the difference in PO concentration can be explained. In a relatively high PO concentration (e.g., 16 mM), almost every nanoparticle can form an oleic acid-PO double layer along with smaller hydrodynamic diameter (Fig. 4.1(c)). On the other hand, clusters of several hydrophobic OFe would be formed first and then fatty acid double layer coated OFe cluster will be formed that also can be stable in aqueous solution where the concentration of PO is relatively low (e.g., 0.32 mM) (Fig. 4.1(d)).

Measurements of particle zeta potential indicated that all types of Fe NPs were negatively charged as shown in Table 4.2. Notably, two types of PO-OFe had a high magnitude of negative surface charge. This result should originate from the adsorption

an anionic oleate on OFe (oleic acid coated Fe NPs) surface. In an alkaline environment, metal oleate such as potassium oleate is dissociated, so, the higher the pH of the solution, the higher the amount of dissociated metal oleate. Liposome, aspherical vesicle formed by phospholipids bilayer, also had a lower negative surface charge than -100 mV in alkaline condition (Yandrapati, 2012). It can be confirmed that a higher magnitude of negative surface charge is attributed to the presence of fatty acid double layer. Similar to hydrodynamic diameter, the results indicated that zeta potential of PO-OFe could be changed depending on the background solution. Bare ZVI NPs would be expected to have a lower magnitude of surface charge, zeta potential for bare ZVI NPs has been reported to be -31.7 mV (Kocur et al., 2014). CMC coated Fe NPs synthesized using a similar method have been reported to have a zeta potential of -55.8 mV (He et al., 2009), consistent with the values of zeta potential in this study.

4.3.2 Colloidal stability of modified Fe NPs

Sedimentation tests were performed with different types of Fe NPs to compare the colloidal stability. The absorbance at 508 nm in suspension of M-Fe in a measurement vial was reduced rapidly by almost 90% of the initial absorbance only in 2 h under quiescent conditions as expected (Fig. 4.2). Much of this change in absorbance is attributable to the rapid settling of M-Fe (Raychoudhury et al., 2010). In comparison, for the Fe NPs prepared by the post-agglomerated modification methods, PoOl-Fe, PoCMC-Fe, about 70% and 50% of the initial absorbance was reduced in 2 h. However, over 80% of the initial absorbance was reduced over 6 h in both case and the clear supernatant was observed due to the sedimentation of the nanoparticles in the vials even though the addition of stabilizer was effective to reduce the particle size (hydrodynamic diameter) and zeta potential by which obtaining colloidal stability of the particle was more favorable.

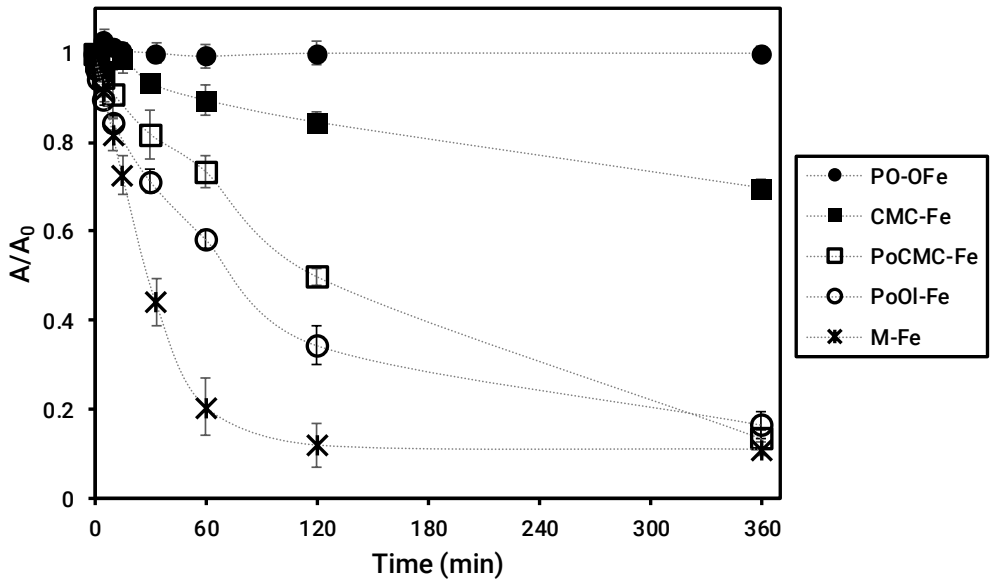

Figure 4.2 Changes in relative absorbance over time in sedimentation tests with different Fe NPs at a suspension concentration of 0.2 g/L

In vials containing a suspension of CMC-Fe, the absorbance was reduced by 30% or so of the initial absorbance in 3h. However, the absorbance remained for 24 h. Only a few large particles seemed to sediment in the vial under quiescent conditions. The hydrodynamic diameter of remaining suspended particle at 24 h after synthesis was maintained within around 10% change from the original particle diameter. He et al. (2009) also observed the change in particle size of CMC modified ZVI NPs synthesized by a similar method with used in this study as increasing time and reported that the particle size unchanged for 6 days. The particle size and zeta potential of CMC-Fe stored in a glove box after 24 h from the synthesis were unchanged. PO-OFe (in this experiment, the background PO solution was 1.6 mM, 1/10 dilution of 16 mM PO solution) showed

the most excellent aqueous stability among the Fe NPs in this study. The suspension of PO-OFe was well dispersed and remained as a homogeneous dark gray-colored solution for 6 h (for over 7 days, the absorbance remained at almost 95% of the initial absorbance). This data demonstrates that fatty acid double layer as a stabilizing agent kept the particles suspended and superior mobility of PO-OFe in 1-D column experiment was also expected.

4.3.3 Transport of modified Fe NPs in 1-D sand packed column

Based on the results of the colloidal stability of Fe NPs, in this study, CMC-Fe and two types of PO-OFe (stabilized in high concentration of PO solution, e.g., 16 mM, and low concentration of PO solution, e.g., 0.32 mM) suspensions were used for the transport experiments in 1-D sand packed columns as representatives of modified Fe NPs, and M-Fe as an unmodified Fe NPs was also used to compare the mobility. Column transport experiment with M-Fe with 0.5 g/L iron concentration at a pore water velocity of 1.4 cm/min (fastest pore water velocity used in this study) resulted in negligible transport of M-Fe with less than 0.05 mg/L iron concentration in the effluent. Photographs of the collected eluents after the injection of M-Fe and PO-OFe are presented for comparison (Fig. 4.3). No visible black iron can be seen in the effluent within the entire range of the column experiment in the case of M-Fe, while the black color from Fe NPs through the column was apparently visible in the collected effluents with gradually increasing concentration during the period of 3 pore volumes (PV) injection. Most of M-Fe deposited at the bottom section of the column as shown in a small picture inserted in Fig. 4.3.

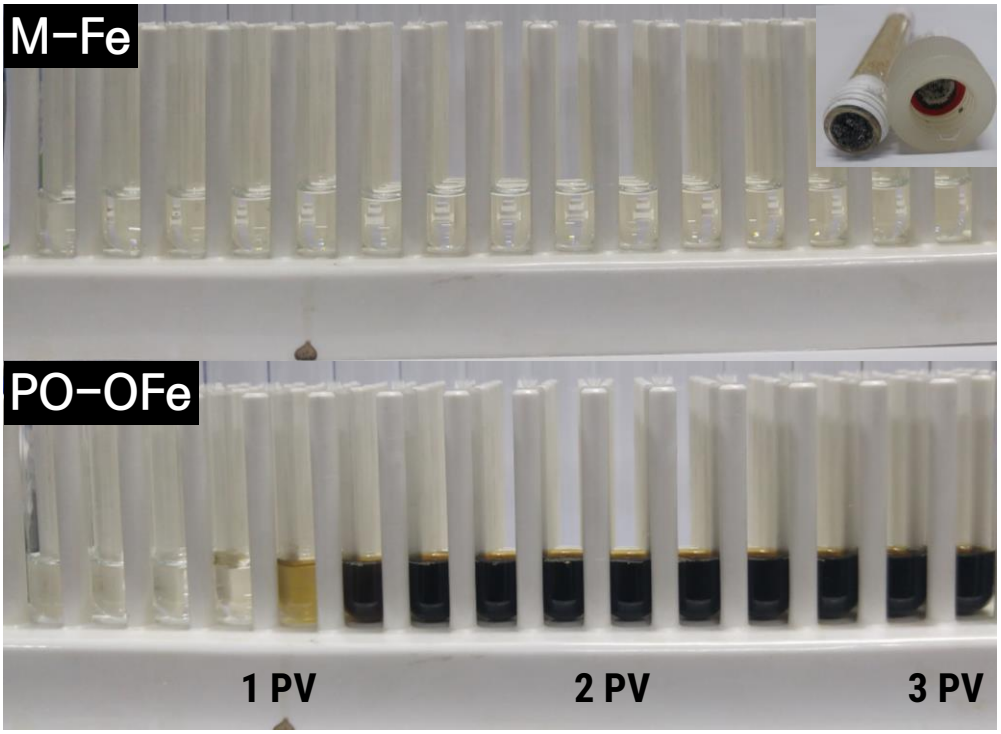

Figure 4.3 Photograph of the collection of the effluent containing M-Fe and PO-OFe (PV means pore volume). An inserted picture shows the bottom part of the column used after the injection of M-Fe during 3 PV, confirming the deposition of M-Fe during the column experiment

Fig. 4.4 shows the breakthrough curves of column experiments for CMC-Fe and two types of PO-OFe with different pore water velocities which are known as a parameter mainly affecting the mobility of Fe NPs in porous media. The pore water velocity range (0.04-1.4 cm/min) was chosen to simulate typical groundwater flow and possible injection velocity. In all cases, the iron concentration of effluent rapidly reached a plateau at around 2 PVs with different values according to the Fe NPs injected and the pore water velocity, suggesting that the transport of CMC-Fe and PO-OFe in porous media follows the model of the classical filtration theory (Tufenkji and Elimelech, 2004). With the adaption of the filtration theory, one can evaluate the mobility of nanoparticles quantitatively. In the model, deposition of colloidal particles is typically described by three mechanisms: Brownian diffusion, interception, and gravitational sedimentation. Tufenkji and Elimelech (2004) developed a correlation equation for calculating individual contributions from each transport mechanism using dimensionless parameters; η_D, η_I, η_G. Particle deposition rate (in particle attachment favorable conditions), then, is calculated by summing these dimensionless parameters as shown in Eq. (2.11).

Following the method of Tufenkji and Elimelech (2004), values of various parameters were obtained for the tests and summarized in Table 4.3. The attachment efficiency α, representing a fraction of collisions between particles and surface of collectors that result in particle deposition, is then calculated via Eq. (2.15).

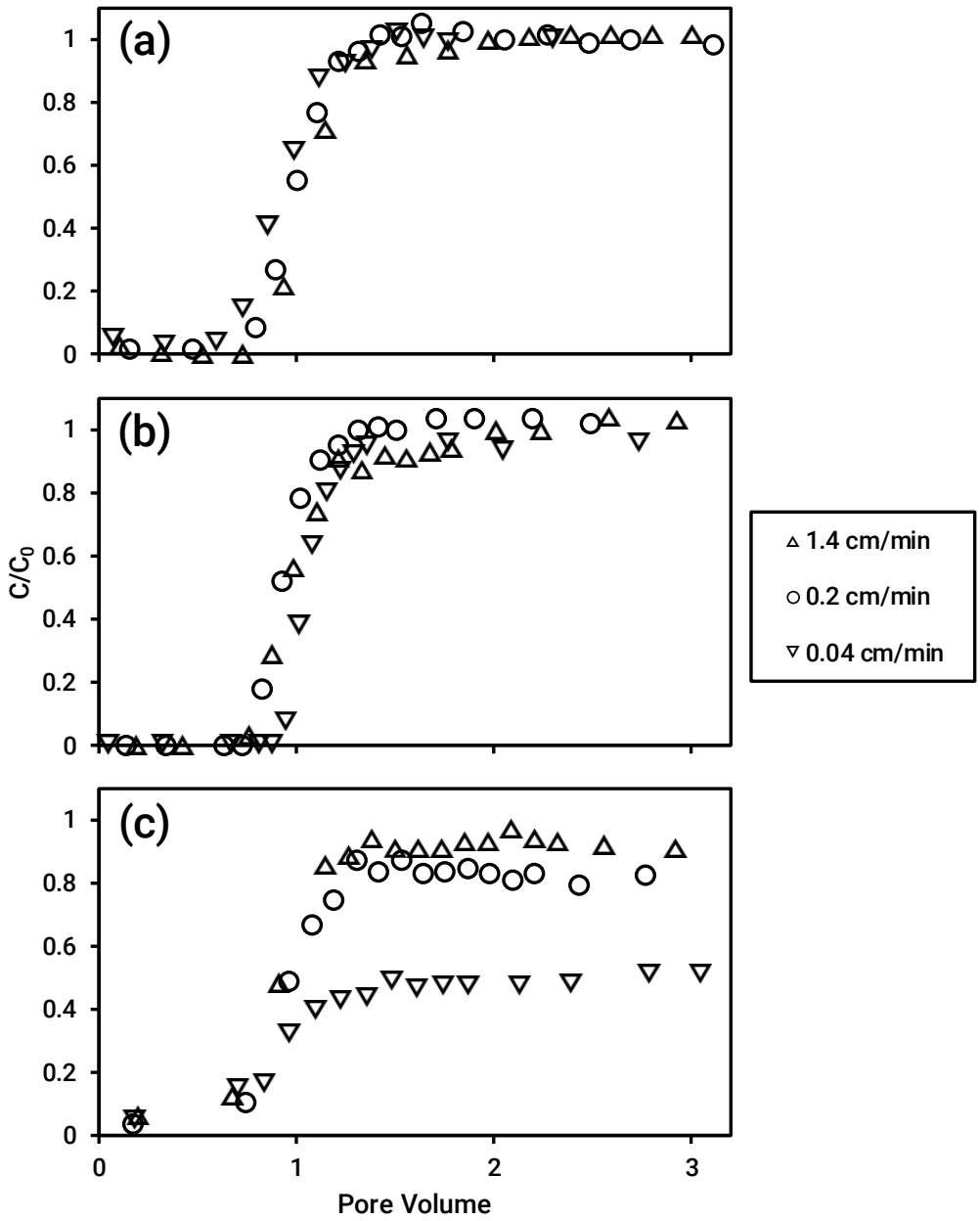

Figure 4.4 Breakthrough curves of column experiments for two types of PO-OFe; (a) HPO-OFe, (b) LPO-OFe, and (c) CMC-Fe with different pore water velocities (0.04 – 1.4 cm/min)

Table 4.3 Parameters for Fe NPs breakthrough experiments and results of filtration model fitting

Fe NPs	Deposition rate	Maximum distance	Attachment efficiency	Single collector contact efficiency	Transport by diffusion	Transport by interception	Transport due to gravity	Pore water velocity	Particle diameter
	C_e/C_0	$L_{0.1}$ (m)	α	η_0	η_D	$\eta_I \times 10^{-4}$	η_G	U (cm/min)	d_p (μm)
PO-OFe (16 mM)	1	-	-	0.1783	0.1738	0.1986	0.0045	0.04	0.089
	1	-	-	0.0558	0.0550	0.1624	0.0008	0.2	0.089
	1	-	-	0.0138	0.0137	0.1274	0.0001	1.4	0.089
PO-OFe (0.32 mM)	0.96	6.63	0.0015	0.1132	0.0901	0.6435	0.0230	0.04	0.204
	1	-	-	0.0324	0.0285	0.5263	0.0038	0.2	0.204
	1	-	-	0.0076	0.0071	0.4126	0.0004	1.4	0.204
CMC-Fe	0.47	0.37	0.0277	0.1111	0.0764	0.8647	0.0346	0.04	0.251
	0.83	1.48	0.0253	0.0300	0.0242	0.7072	0.0058	0.2	0.251
	0.93	3.81	0.0439	0.0067	0.0060	0.5545	0.0007	1.4	0.251

From the slowest velocity of 0.04 cm/min to the fastest velocity of 1.4 cm/min, the iron concentration of PO-OFe stabilized in 16 mM PO solution reached a maximum relative concentration of 1, the same level of KCl tracer (Fig. 4.4 and Table 4.3), suggesting completely breakthrough without particle deposition. However, the full breakthrough (C_e/C_0) level of CMC-Fe decreased with decreasing the pore water velocity. The maximum C_e/C_0 of CMC-Fe was 0.93 at the pore water velocity of 1.4 cm/min, i.e. only 7% of the nanoparticles deposited on the sand grain packed in the column. Decreasing the velocity to 0.2 cm/min decreased the value of C_e/C_0 from 0.93 to 0.83 (10.8%). At the slowest pore water velocity of 0.04 cm/min, especially, the C_e/C_0 value reached only 0.47, more than a half of iron particles in CMC-Fe were deposited during transport through the sand packed column.

The difference in particle size is one of the reasons inducing the difference in deposition rate. According to the Derjaguin-Landau-Verwey-Overbeek (DLVO) theory, the van der Waals force, which is one of the prime attraction forces between particles and particles or between particles and collectors, is proportional to the particle size (Hotze et al., 2010). As the particle size of CMC-Fe is about 2.8 times larger than that of PO-OFe stabilized 16 mM PO (HPO-OFe) (Table 4.3), CMC-Fe should have a larger attraction with the sand particles compared with HPO-OFe. Raychoudhury et al. (2010) calculated extended-DLVO (XDLVO) energies between the PAA coated ZVI NPs and the surface of the sand particles, and reported that the larger the size of ZVI NP, the larger the negative secondary minima, which contributes to the higher van der Waals force. In other words, the larger the particle size, the more likely it is that the particle is difficult to be detached when it collides with the sand surface and is liable to deposit on the sand surface, leading to an increase in the α value. In this study, α value of CMC-Fe was 0.03 and α value of HPO-OFe could not be quantified in the column test conditions performed in this study (i.e., extremely low).

Table 4.4 Contribution (%) of each transport mechanism to η_0

Fe NPs	Pore water velocity (cm/min)	Brownian diffusion (%)	Interception (%)	Gravitational sedimentation (%)
PO-OFe (16 mM)	0.04	95.49	0.02	4.49
	0.2	97.52	0.05	2.43
	1.4	98.71	0.15	1.14
PO-OFe (0.32 mM)	0.04	79.64	0.06	20.30
	0.2	87.96	0.16	11.87
	1.4	93.60	0.54	5.86
CMC-Fe	0.04	68.76	0.08	31.17
	0.2	80.45	0.24	19.31
	1.4	89.24	0.82	9.93

The difference in particle size also brought about differences in colloidal transport mechanisms related to particle deposition. Brownian diffusion was the primary mechanism in all experiments performed in this study (Table 4.4). In the case of HPO-OFe, more than 95% of the particle transport leading to the collision (quantitatively expressed as η_0) was caused by Brownian diffusion. On the other hand, the contribution of gravitational sedimentation to η_0 was 31% at the lowest flow rate (0.04 cm/min) in the case of CMC-Fe. Gravitational sedimentation is a factor influenced greatly by the size and density of particle (Phenrat et al., 2007). Considering the comparatively high density of iron (7.87 g/cm^3), it can be seen that the change of particle size dramatically affects the contribution of gravitational sedimentation. This contribution is consistent with the experimental results of HPO-OFe with less than 5% contribution of gravitational sedimentation.

At the lowest flow rate of 0.04 cm/min, C_e/C_0 value of CMC-Fe rapidly decreased to 0.47, that can be related to the sedimentation test result. CMC-Fe showed about 30% decrease in absorbance over 6 hours in the experiment (Fig. 4.2). This result can be induced by the sedimentation of some large particles in CMC-Fe suspension. After the experiment, some settled Fe NPs on the bottom of the measurement cell were also observed. The retention times of Fe NPs injected at each flow rate are 11 min, 1 h, and 5 h, respectively, in the column experiments conducted in this study. In the case of the experiment at the slowest flow rate, low C_e/C_0 value can be attributed to the sedimentation of some particles due to long residence time. On the other hand, no evidence of precipitation was found in the sedimentation experiment of PO-OFe. Superior colloidal stability of PO-OFe should be a factor contributing to the high mobility of it.

The particle size of PO-OFe stabilized by a low concentration of PO, 0.32 mM (LPO-OFe), is 200 nm or so and is similar to that of CMC-Fe. However, it showed higher mobility in all cases. This higher mobility can be interpreted regarding the solution and surface chemistry. Electrical repulsion and steric repulsion are the key mechanisms for stabilizing surface coated Fe NPs to prevent aggregation and reduce deposition on the surface of soil particles. The electrical repulsive force is determined by the electrical properties of the stabilizer bond to the particle surface (Sen and Khilar, 2006). The higher the negative charge, the stronger the repulsive force between the particles or between the particle and the soil particle surface, and the higher the mobility of the particles. The zeta potential of CMC-Fe was -30 mV, which is larger than the zeta potential of the unmodified Fe-NPs, M-Fe, but lower than the zeta potential of PO-OFe. The zeta potential of PO-OFe was -90 mV, which is lower than that of stabilized Fe NPs reported in several documents (-31.6 to -55.8 mV from Saleh et al. (2008), He et al. (2009), Kocur et al. (2014), and Raychoudhury et al. (2010)). Due to the high magnitude of negative

zeta potential, PO-OFe has high colloidal stability and a low α value. In particular, the zeta potential of HPO-OFe was -115 mV, by which HPO-OFe showed higher mobility than LPO-OFe and CMC-Fe as well as no deposition even at the lowest pore water velocity. Although it was not quantitatively evaluated in this study, PO-OFe may have greater steric repulsion than CMC-Fe. Steric repulsion is proportional to the mass of the surface bonded stabilizer (Phenrat et al., 2008). The TGA results in Chapter 3 showed that PO-OFe is associated with about 1.4 times larger amount of stabilizer per unit weight of iron than CMC-Fe. However, since the steric repulsive force is affected not only by the mass of the combined stabilizer but also by the thickness (Phenrat et al., 2008), the additional examination is required to verify the difference in the steric repulsion between the two stabilization methods.

CMC-Fe had the α of about 0.027 in the groundwater relevant pore water velocity range (from 0.04 to 0.2 cm/min), and LPO-OFe had the α of about 0.002 at the lowest pore water velocity (HPO-OFe had less α value but could not be measured in this study). It is lower than the typical value of colloid in nature (α = 0.05) (Jiemvarangkul et al., 2011). In other words, it can be interpreted that the modified Fe NPs have the mobility comparable to naturally occurring colloidal particles. Schrick et al. (2004) reported an α value of 0.36 for PAA coated ZVI NPs and 0.07 for hydrophilic carbon supported ZVI NPs. Kanel et al. (2007) reported α values of 0.21 for surfactant coated ZVI NPs. He et al. (2009) reported α value of 0.002 for CMC coated ZVI NPs and Phenrat et al. (2009a) reported α values in the range of 0.0.005-0.01 for PSS modified Fe NPs. These reported α values indicated that the α value of PO-OFe might match the low-end value of stabilized Fe NPs, indicating considerable mobility in porous media.

Another means of expressing mobility can be obtained by rearranging Eq. (2.15) to express maximum distance (L). The distance was calculated as a function of the pore water velocity with the selected α values and arbitrary selected C_e/C_0 value. In this study, a level of $C_e/C_0 = 0.1$ has adopted to calculate the distance $L_{0.1}$ over which 90% removal of the nanoparticles occurs. For the α values of 0.0015 (for LPO-OFe), 0.0147, and 0.0277 (for CMC-Fe), the relationship between the maximum distance and the pore water velocity is plotted in Fig. 4.5 and shown in Table 4.3. At a pore water velocity of 0.04 cm/min and using α value of 0.0277 (the same value with CMC-Fe), $L_{0.1}$ is only about 40 cm. Only when the pore water velocity was artificially controlled, the maximum distance was more than 6 m (at 1.41 cm/min). Therefore, this result suggests that CMC-Fe is somewhat confined under the natural groundwater flow condition and controlling the pore water velocity should be needed for CMC-Fe to be mobile in porous media of which physical conditions is like that used in the column tests. On the other hand, when the α value of 0.0015, it showed a maximum distance of more than 6 m even under typical pore water velocity, showing that PO-OFe can be injected into the ground and transported without further adjustment of the hydrodynamic gradient.

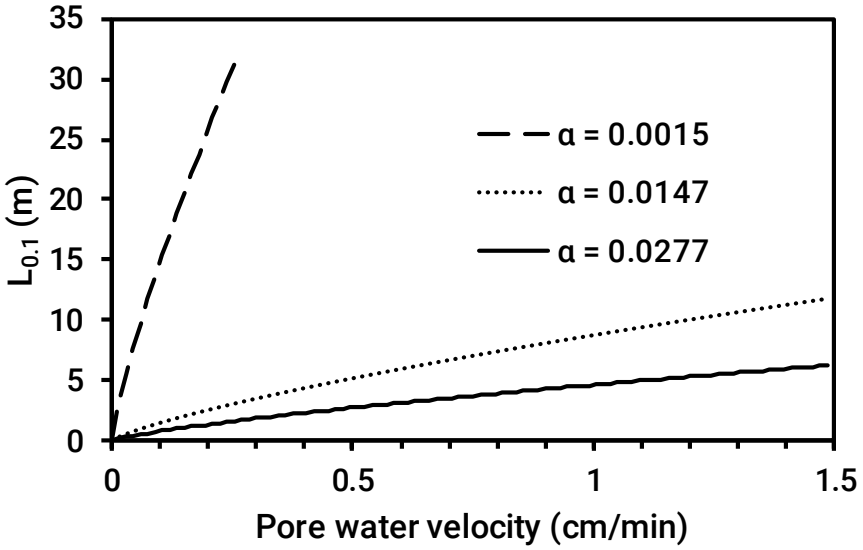

Figure 4.5 Calculated maximum distance over which 90% of Fe NPs are removed in the sand packed column as a function of pore water velocity

The experimental results so far show that PO-OFe, especially HPO-OFe, have the higher mobility than or the equivalent mobility to those of the existing modified Fe NPs, considering zeta potential, sediment test results, and the results from the lab. scale 1-D column experiments such as the maximum C_e/C_0 level and α values. However, the high mobility of PO-OFe can appear under limited conditions. The stabilizing layer of PO-OFe developed in this study consists of sequential bonded layers of oleic acid and PO on the iron surface. The primary layer, oleic acid, is firmly bound to the iron surface, but the bond between PO and OA layer is strongly influenced by the solution conditions because it is based on a weak hydrophobic-hydrophobic interaction. Other studies on the formation of bilayers onto the surface of Fe NPs with sodium oleate (SO), a kind of metal oleate such as PO, have shown that the formation and structure of the bilayer formed (Shen et al., 1999) is dependent on the oleate concentration and pH of the background solution (Roth et al., 2016; Wang et al., 2013; Yang et al., 2010). The size and structure of PO-OFe developed in this study were also changed by the concentration of PO solution added during the manufacturing process, and the mobility was also changed. As mentioned above, there has been reported a case where the oleate bilayer structure coating the nanoparticles was deformed by the high shear stress occurred during the flow through a dense porous medium in sedimentary rock and deposition of nanoparticles stabilized by the oleate bilayer was observed (Yu et al., 2010).

When a suspension containing nanoparticles is injected into a saturated porous medium, a concentration gradient occurs around the boundary between the suspension and the porous medium saturated solution, so that the suspension concentration is diluted, followed by the change in solution chemistry conditions such as pH and ionic strength. To investigate the effect of reduction of background PO concentration originated form dilution on the PO-OFe formation, the changes of particle size, zeta potential, and pH in suspension according to the dilution ratio of PO-OFe suspension were investigated.

The molar ratio of FeO (wustite, the core of PO-OFe) to PO in the LPO-OFe suspension was 43.5 and 0.9 in the case of HPO-OFe. The particle size did not change even as the dilution ratio increased and the background concentration decreased in the case of LPO-OFe (Fig. 4.6). This change in the particle size is because the reduction of the background concentration reduces the number of iron particles in solution and thus the surface area required to bond with the oleate molecule to be dispersed in an aqueous solution is also reduced. Interestingly, for PO-OFe stabilized at a molar ratio of 0.9 (HPO-OFe), the particle size increased as PO concentration in the background solution decreased accompanied by dilution. Unlike the synthesis case of LPO-OFe where a particle cluster of 200 nm or more is formed due to a relatively low PO concentration, it seems that a specific concentration of PO should be maintained in the background solution to disperse the particle cluster within the size range of 100 nm or less. Also, Po-OFe stabilized at 0.9 molar ratio is presumed to secure the amount of PO required for stabilization by decreasing the surface area exposed to the aqueous solution by gradually increasing the particle cluster size when the PO concentration of the background solution is decreased. Therefore, it is expected that the PO-OFe, especially the one stabilized with a high PO concentration solution enough to maintain the cluster size less than 100 nm, injected into the groundwater will change their form from the type described in Fig. 4.1(c) to (d) as the dilution progresses, which is expected to lead to an increase in α value and a decrease in mobility. Zeta potential and pH of the suspension were independent to the mole ratio and related only to the PO concentration in the solution.

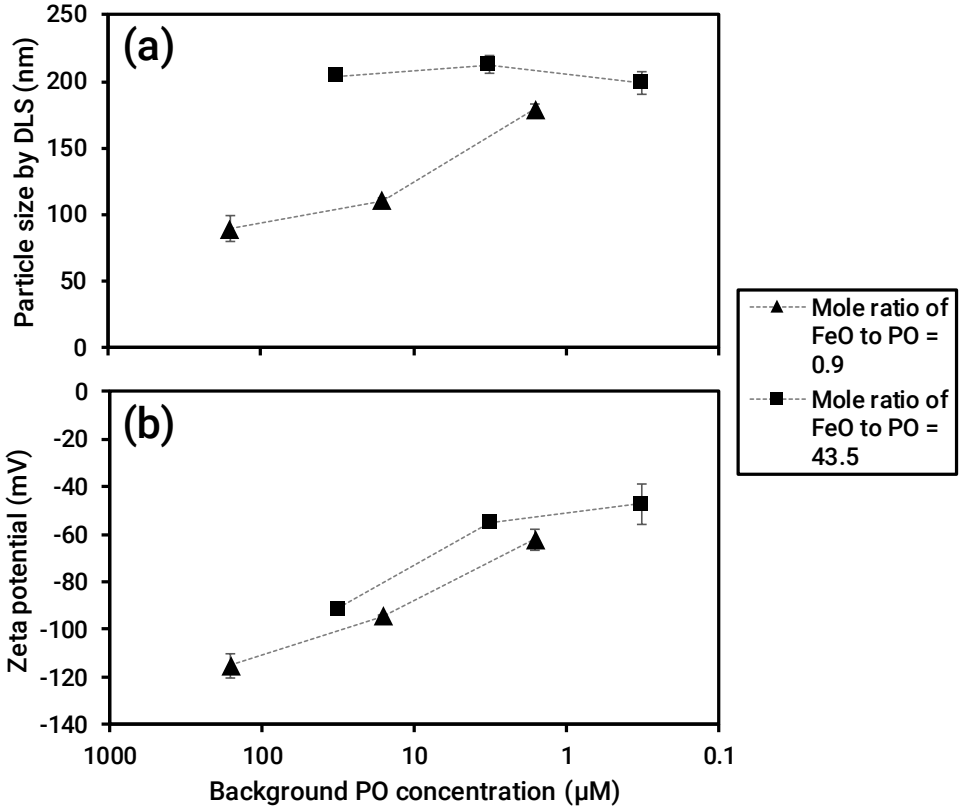

Figure 4.6 Changes in zeta potential and particle size of HPO-OFe (FeO/PO = 0.9) and LPO-OFe (FeO/PO = 43.5) as a function of background PO concentration adjusted by dilution

The results above suggest the possibility of preparing stabilized nanoparticles with adjustable mobility in porous media. The transport and fate in groundwater and toxicity to the environment of engineered nanoparticles have not yet been fully understood (Aiken et al., 2011; Maurer-Jones et al., 2013). Therefore, nanoparticles engineered for superior mobility with the α value is close to 0, thus the particle deposition rate is negligible, can be regarded as another harmful substance from an ecosystem perspective. In the case of PO-OFe developed in this study, it was possible to control the cluster size and α value of the PO-OFe cluster only by adjusting the mole ratio of the stabilizer (PO) and the core (FeO). Also, changes in ionic strength and pH may result in different mobility from the results reported in this study. Moreover, thermal decomposition method used for the synthesis of Fe NPs coated with oleic acid in this study can manipulate the size and distribution of the particles by nano-meter range according to the synthesis conditions and change the mineral phase of the core (Bronstein et al., 2007; Park et al., 2004; Yu et al., 2004). Therefore, the combination of thermal decomposition method for the synthesis of the core and fatty acid double layer stabilization method for the surface modification applicable in an aqueous phase can be an alternative to the existing methods of preparing engineered nanoparticles that minimize the environmental impact, thus are suitable to be applied for remediation of underground environment.

4.4 Conclusions

Fatty acid double layer coated Fe NPs (PO-OFe) showed the best dispersibility in aqueous phase and mobility among the samples used in this study because of the hydrodynamic diameter and high negative zeta potential. CMC modified Fe NPs (CMC-Fe) showed the greater mobility in the column tests compared with unmodified Fe NPs, presenting low attachment efficiency that can be in the mid-range of reported efficiencies in the literature. PO-OFe showed even better mobility than CMC-Fe that can be attributable to the formation of a fatty acid double layer onto the surface of PO-OFe. Of particular interest is that the particle size (hydrodynamic diameter) and surface charge of the PO-OFe changes with the conditions of the background PO solution. The molar ratio of Fe to PO and the free phase PO concentration of the background solution affect the size and surface potential of PO-OFe and, of course, the mobility. These results suggests the possibility of preparing PO-OFe with adjustable mobility.

Chapter 5. Selective removal of carbon tetrachloride using fatty acid double layer coated iron-based nanoparticles in modeled groundwater containing dissolved solutes

5.1 Introduction

In Chapter 3 and 4, the formation of the fatty acid double layer on PO-OFe surface was confirmed. However, it is not yet clear how the selective permeability of the lipid bilayer can be exerted in the fatty acid double layer, given that is a common phospholipid, and the bilayer produced in this study consists of oleic acid. The primary factors to be verified in this chapter are as follows: 1) Reactivity of FeO (core mineral of PO-OFe) to hydrophobic contaminants, 2) effect of the fatty acid double layer on the reaction rate, 3) reactivity of PO-OFe to ionic pollutants, 4) change in reactivity of PO-OFe to hydrophobic pollutants in the presence of dissolved groundwater solutes.

In this study, carbon tetrachloride (k_{ow} = 2.83) as a hydrophobic contaminant and nitrate as an ionic contaminant were selected because both model contaminants in this study are well known as easily reducible contaminants by Fe NPs and of which reductive degradation mechanisms and pathways are relatively simple. For comparative analysis, bare unmodified Fe NPs and CMC coated Fe NPs were also tested for reactivity evaluation.

5.2 Materials and methods

5.2.1 Chemicals

Ferrous sulfate heptahydrate (ACS reagent), sodium borohydride (98%), sodium carboxymethyl cellulose (CMC, average molecular weight = 90k), odium salts of bicarbonate (ACS reagent), sulfate (ACS reagent), phosphate (ACS reagent) and humic acid (technical grade), potassium oleate (technical grade, 87%), oleic acid (technical grade, 90%), acetone (HPLC grade), ethanol (ACS reagent), methanol (ACS reagent), n-hexane (GC grade), carbon tetrachloride (HPLC grade), and chloroform (HPLC grade) were acquired from Sigma-Aldrich (St. Louis). Others were methylene chloride (HPLC grade, JT Baker), potassium hydroxide (extra pure, 85%, Daejung), ferrous stearate (9% Fe, Strem), potassium nitrate (99.0 %, Showa chemical Co.). Deionized water produced from Milli-Q (Millipore) was used as standard aqueous matrix, and N_2 purged deionized water (DDW) was also used to minimize surface passivation of Fe NPs by the aqueous matrix.

5.2.2 Fe NPs preparation

Fatty acid double layer coated Fe NPs (PO-OFe) were prepared as described in Chapter 3. For the comparison, carboxymethyl cellulose coated Fe NPs (CMC-Fe) as a representative of polyelectrolytes modified Fe NPs were synthesized by the method described in Chapter 3, and commercial Fe NPs from Nanostructured & Amorphous Materials, Inc. (M-Fe) were purchased and used as a representative of unmodified bare Fe NPs.

5.2.3 Fe NPs reactivity tests in batch type experiments

Batch type carbon tetrachloride (CT) reductive removal experiments were conducted in transparent borosilicate glass vials (25 mL) capped by Teflon Mininert valves (24 mm, VICI) for minimizing the intrusion of oxygen and volatilization losses of CT and daughter products (e.g., chloroform and methylene chloride) form the reaction. For all experiments, the batch reactors were prepared in an anaerobic glovebox (N_2), and DDW was used as a standard aqueous matrix. All batch reactors for CT reductive removal experiments contained 24 mL of the Fe NPs suspensions (PO-OFe stabilized 16 mM PO solution, CMC-Fe, and M-Fe suspension) at the concentration of 0.5 g-Fe/L with a small headspace less than 1 mL.

CT stock solutions were made with a dilution of CT in methanol, and then 20 μL of the stock solution was spiked into the reactors to yield initial CT concentration of 100 μM. Each reactor was then rotated on an end-over-end rotator at 45 rpm at 25 ± 3 ℃. At each sampling event, 20 μL of the aqueous samples including Fe NPs were withdrawn and transferred to 2 mL GC sample vials that were filled with 1 mL of hexane for solvent extraction to analyze CT, chloroform (CF), and methylene chloride (DCM) concentrations. To analyze the concentration of chloride via reductive removal of CT in the batch reactor vials, a vial was extracted and sacrificed at predetermined time intervals. The extracted sample for chloride analysis was, then, centrifuged at 40k rpm for 15 min to precipitate the Fe NPs in the sample followed by analysis of chloride in the aliquot using ion chromatography.

Batch experiments for nitrate reduction using Fe NPs were also conducted in 45 mL glass vials. 35 mL of Fe NPs suspensions containing 0.6 g/L Fe were placed in the vials. Then, the vials were injected with 5 mL of nitrate concentrate (180 mg-NO_3^-/L) to achieve an initial concentration of 30 mg-NO_3^-/L and 0.5 g-Fe/L, sealed with PTFE-lined septa and aluminum caps, and stirred on an end-over-end rotator at 45 rpm under room

temperature. At predetermined time intervals, a vial was extracted for 1 mL sample including suspended Fe NPs using a plastic syringe (1 mL) with a 23-gauge needle for analyzing residual concentrations of nitrate, nitrite, and ammonium in the sample after filtering through a 3 kDa MWCO Amicon-0.5 centrifugal filter unit (Millipore).

The effect of dissolved groundwater solutes on the reactivity of Fe NPs was evaluated by as similar batch type experiments as for CT reductive removal experiments with slight modifications. 20 mL of the Fe NPs suspensions at the concentration of 0.6 g-Fe/L was placed in 25 mL vials. Then the vials were injected with 4 mL of stock solutions containing model groundwater solutes (nitrate, bicarbonate, sulfate, phosphate, humic acid (HA) as a representative of dissolved organic matter) at the fixed concentrations, thus the concentration of Fe in the reactors was 0.5 g/L. A vial contained only one kind of solutes in the batch experiments. After 5 min of the injection, 20 μL of CT stock solution was also spiked into the reactors to yield initial CT concentration of 100 μM. The concentrations of model dissolved groundwater solutes were selected based on the field concentration data from various literature (Choi et al., 2014; Kim et al., 2014; Liu et al., 2007; Phenrat et al., 2015) and summarized in Table 5.1.

All samples were prepared in duplicates or triplicates, and control tests were conducted using a vial without Fe NPs.

Table 5.1 Concentration of model dissolved groundwater solutes and Fe to solutes ratios in batch experiments

Model dissolved groundwater solutes	Concentration		Fe/solutes[1)] (mole/mole or g/g)
	mg/L	mM	
NO_3^-	30	0.48	17.9
HCO_3^-	100	1.64	5.5
SO_4^{2-}	50	0.31	28.9
HPO_4^{2-}	50	0.52	17.2
DOC[2)] (by HA)	15	-	33.3

[1)] Calculated based on the iron loading (0.5 g-Fe/L) and the solution volume (24 mL) in a reactor vial
[2)] Dissolved organic carbon measured by TOC

5.2.4 Analytical methods

The concentration of CT, CF, and DCM was analyzed by GC/ECD (GC-2010, Shimadzu) equipped with a 30 m length DB-5 capillary column (J & W Scientific). The temperature of the injector port and the detector were set at 250 and 300 ℃, respectively. The oven temperature program was as follows: 50 ℃ for 5 min, 50-150 ℃ at 10 ℃/min, 150 ℃ for 5 min. Nitrogen was used as both carrier gas (3 mL/min) and as makeup gas (40 mL/min). Split ratio was 10:1. External calibration standards prepared in hexane were used to quantification.

Nitrogen species (nitrate, nitrite, and ammonium) and chloride were analyzed using ion chromatography (ICS-1000, Dionex, Sunnyvale, CA, USA) equipped with IonPac AS23 column for anions (nitrate, nitrite, and chloride) and IonPac CS12A column for cation (ammonium).

Dissolved organic carbon (DOC) in HA was determined using a TOC analyzer (TOC-L CPH, Shimadzu).

The reactivity of Fe NPs of interest in this study was evaluated by comparing pseudo-first order rate constants, k_{obs}, obtained by fitting the concentration vs. time data to the kinetic model:

$$\frac{dC}{dt} = -k_{obs}C \tag{5.1}$$

where C is the concentration of Fe reducible target contaminant in the aqueous phase (mg/L); k_{obs} is the observed pseudo-first order rate constant (h^{-1}); and t is time (h). To better compare the reaction rates observed with different Fe loading and particle size, it is useful to normalize the reactivity per unit Fe NP surface area. The surface area normalized rate constants, k_{SA}, can be obtained using:

$$k_{obs} = k_{SA}a_s\rho_m \tag{5.2}$$

where k_{sa} is the surface area normalized rate constant ($L/h/m^2$); a_s is the specific surface area of Fe (m^2/g); ρ_m is the mass concentration of Fe (g/L). The value of ρ_m is 0.5 in all batch experiments conducted in this chapter, and the specific surface area was calculated using the particle diameter with the assumption that all Fe NP are spherical following the equation below:

$$SA = \frac{6}{\rho D} \tag{5.3}$$

where SA is the specific surface area (m^2/g); ρ is the particle density (kg/m^3); D is the particle diameter (m). The values of the specific surface area were 149 m^2/g (from the diameter of 5.1 nm), 46.99 m2/g (from the diameter of 22.4 nm), and 40 m^2/g (from the manufacturer) for CMC-Fe, PO-OFe, and M-Fe respectively.

To obtain the k_{obs} value, the experimental results only up to 6 hours after the start of the reaction were used with the exceptions for the cases showing less than 50% removal for 6 hours. As dealt with in results and discussion section, the experimental results for CT removal, using M-Fe and CMC-Fe without the dissolved solutes, were well-fitted with the pseudo-first order kinetic model where the values of coefficient of determination, r^2, were more than 0.99. However, it was found that the k_{obs} decreases as the reaction progresses under some experimental conditions. The coefficient of determination dropped to a minimum of 0.53, and the relationship between the log-concentration value and time was likely shown to be represented by two straight lines rather than a single straight line, indicating that the reactivity of the sample decreased as the reaction progresses.

To quantify the rate limiting effect, in addition to k_{obs} and k_{SA}, two different reactive constants were adopted in this study. For obtaining the additional constants, the fitting interval for the analysis was divided into two phases (initial phase and second phase), and the rate constants were obtained from each phase. The distinction between the initial phase and the second phase is based on the time by that the sum of the decision coefficients derived from each interval is closest to 2 (maximum value). The rate constant from the initial phase was defined as k_I and from the second phase was defined as k_s. Four rate constants (k_{obs}, k_{SA}, k_I, and k_S) were obtained from all experiments dealing CT and used to evaluate the reactivity of Fe NPs as well as the change in the reactivity as the reaction progress.

5.3 Results and discussion

5.3.1 Reductive removal of carbon tetrachloride and nitrate

CT reductive removal and byproducts formation were illustrated in Fig. 5.1 and 5.2., and calculated reaction rate constants from the results were summarized in Table 5.2. Both M- and CMC-Fe showed high reactivity to reduce 95% of CT within 6 hours. The k_{obs} value of CMC-Fe is 0.944, which is about 20% larger than that of M-Fe. However, the k_{sa} value of M-Fe, which is the specific surface area normalized k_{obs}, was larger by 3 times than that of CMC-Fe, indicated that the high reactivity of CMC-Fe is based on the relatively large specific surface area, and the 'intrinsic' reactivity of the M-Fe is more than three times greater than that of CMC-Fe. M-Fe have been used for the reactivity test more than one month after the purchasing. Therefore, the XRD results (Chapter 3) of M-Fe showed that some the particles are oxidized and magnetite, one of the Fe oxides, is formed on the surface. The iron oxide layer formed on the surface of iron particles can be attributed to lower the reactivity of the particles. Also, the TEM (Chapter 3) and sediment experiments (Chapter 4) showed that M-Fe got clustered into micro-sized aggregates, and even if ultrasonic irradiation was applied into the suspension of M-Fe to detach them physically, the particles were likely to agglomerate within a short time and precipitate easily under quotient conditions. Therefore, it would be reasonable to infer that the 'effective reaction surface area' of M-Fe to react with CT is less than the value form the manufacturer, 40 m^2/g.

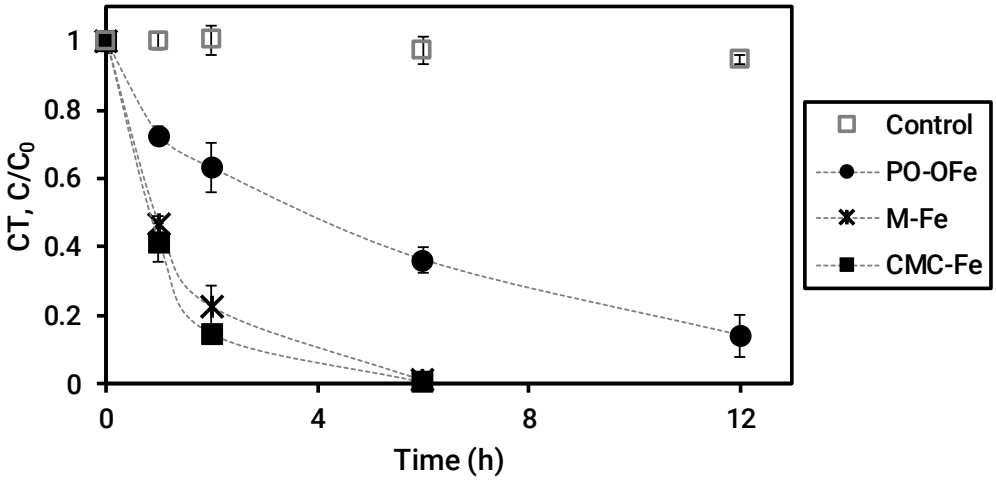

Figure 5.1 CT reductive removal using M-Fe, CMC-Fe, and PO-OFe. $[CT]_0$ = 100 μM, [Fe] = 0.5 g/L. Dotted lines are used only to guide the eye

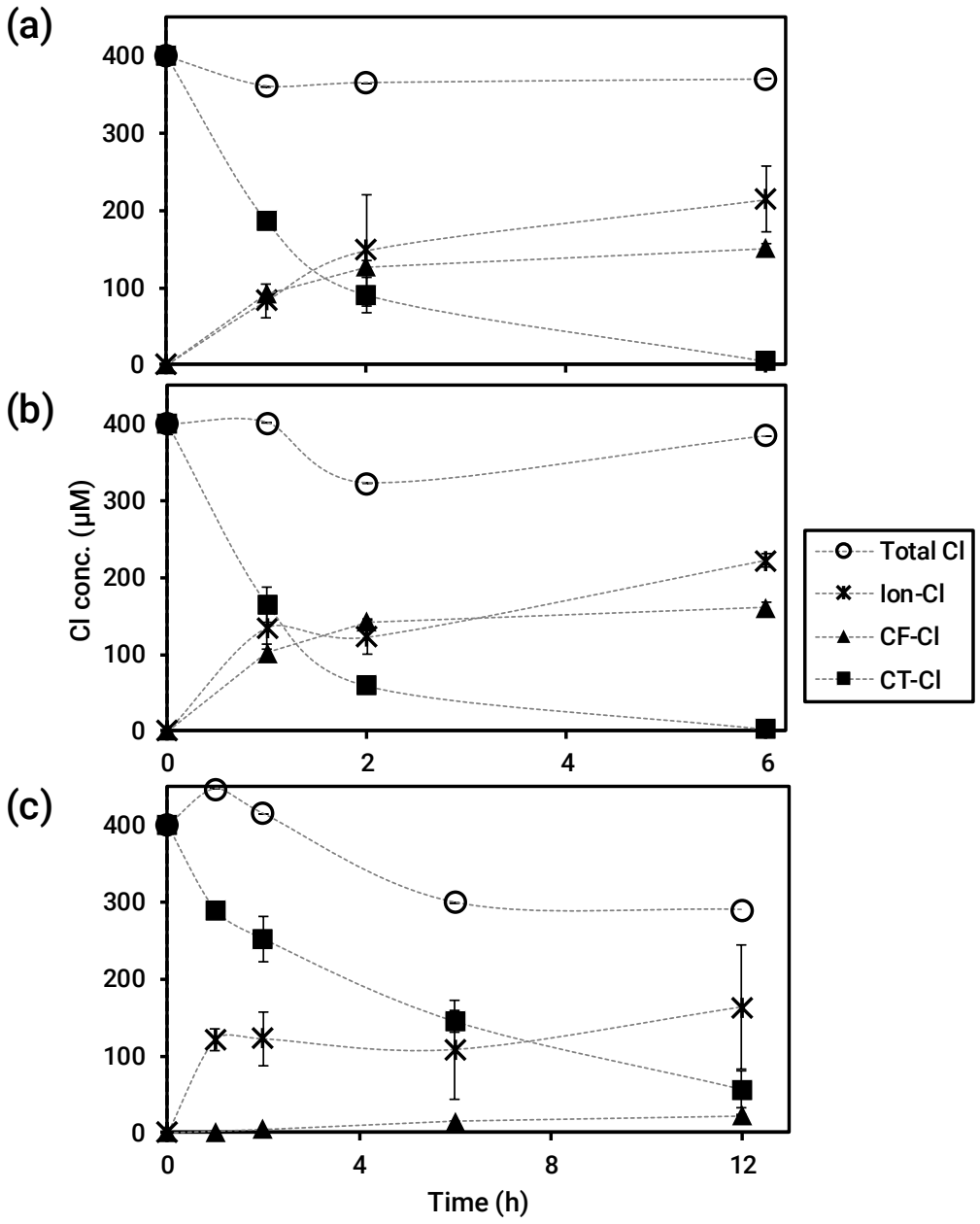

Figure 5.2 By-products formation from the CT removal experiment using (a) M-Fe, (b) CMC-Fe, and (c) PO-OFe. $[CT]_0$ = 100 μM, [Fe] = 0.5 g/L. Dotted lines are used only to guide the eye

Table 5.2 CT reductive removal rate constants of Fe NPs with different groundwater solutes condition

Fe NPs	Condition	k_{obs} value	r^2	k_I	k_S	k_s/k_I	k_{SA} ($\times 10^{-2}$)
M-Fe	CT only	0.775	1.00	0.797	0.737	0.92	3.875
	w/ HCO_3^-	0.378	0.94	0.539	0.270	0.50	1.890
	w/ SO_4^{2-}	0.356	0.93	0.517	0.251	0.49	1.780
	w/ HA	0.163	0.85	0.122	0.110	0.90	0.815
	w/ NO_3^-	0.050	0.53	0.181	0.024	0.13	0.250
	w/ HPO_4^{2-}	0.038	0.84	0.096	0.026	0.27	0.190
CMC-Fe	CT only	0.944	1.00	0.886	1.030	1.16	1.263
	w/ HCO_3^-	0.575	0.97	0.764	0.435	0.57	0.769
	w/ SO_4^{2-}	0.133	1.00	0.141	0.134	0.95	0.178
	w/ HA	0.403	0.97	0.521	0.318	0.61	0.539
	w/ NO_3^-	0.526	0.98	0.668	0.425	0.64	0.704
	w/ HPO_4^{2-}	0.104	0.99	0.076	0.113	1.49	0.139
PO-OFe	CT only	0.167	0.98	0.322	0.139	0.43	0.711
	w/ HCO_3^-	0.171	0.98	0.322	0.145	0.45	0.728
	w/ SO_4^{2-}	0.161	0.97	0.314	0.147	0.47	0.685
	w/ HA	0.177	0.98	0.317	0.149	0.47	0.753
	w/ NO_3^-	0.165	0.98	0.356	0.141	0.40	0.702
	w/ HPO_4^{2-}	0.155	0.95	0.307	0.156	0.51	0.660

CMC-Fe was used for the reactivity test experiments within 2 hours after synthesis in the laboratory. The XRD test results also showed broad peaks indicating the presence of amorphous iron and the peaks related with iron oxides such as magnetite was not detected. When M- and CMC-Fe dispersed in an aqueous solution in a laboratory were left in aerobic condition, the color of the solution containing the particles was gradually changed to red only in the solution with CMC-Fe be, but unchanged in M-Fe solution. M-Fe were not vulnerable to corrosion induced by the exposure to oxygen, perhaps due to the presence of the passivated iron oxide layer on the surface of the particles. On the other hand, CMC-Fe which had been protected from contact with oxygen since its synthesis did not have a protective layer of iron oxide on the surface, meaning that it is susceptible to be oxidized by the exposure to oxygen.

In addition to the presence or absence of a surface oxide layer, the improvement in dispersibility due to CMC coating and the prevention of agglomeration and precipitation of particles are also factors that lead to increasing the reactivity. The reason why the k_{SA} of CMC-Fe is 3 times smaller than the value of M-Fe is that the reactivity of Fe NPs can be lowered by coated polyelectrolyte molecules. Phenrat et al. (2009b) reported that the polyelectrolyte coated on the iron surface could occupy the effective reaction sites of the iron surface and, thus reduce the reactivity of the iron to target contaminants. Moreover, it was also suggested that hydrophobic contaminants could be partitioned into the polymer layer, resulting in a decrease in local contaminant concentrations around the iron surface, causing the decrease in the reactivity. Tratnyek et al. (2011) also proposed that stabilizers may compete for the reaction sites with target contaminants, thereby inhibiting reactions between Fe NPs and the contaminants. In Chapter 4, although CMC-Fe synthesized in this laboratory was revealed to have a small particle size of around 5 nm by TEM analysis, it was expected that small sized CMC-Fe clusters of around 250 nm would be formed in the aqueous phase by the bridging effect of CMC-Fe. It can be

concluded that the bonding among iron particles by the bridging of CMC molecules reduces the effective specific surface area involved in the actual reaction so that the reactivity per unit area of CMC-Fe could be inhibited as compared with M-Fe. Although it is difficult to quantify the magnitude, the effect of reaction inhibiting due to contaminants partitioning can be higher than that reported in the existing literature as the hydrophobicity of CT higher than that of TCE (partition coefficient of CT and TCE is 2.83 and 2.61). All of the studies presented above used TCE as the target contaminant.

PO-OFe showed relatively low reactivity compared to M- and CMC-Fe, and had nearly 5 times lower k_{obs} and k_{sa} than those of M-Fe (Fig. 5.1, 5.2, and Table 5.2). It may be contributable to the difference in the core of Fe NPs. The core of PO-OFe consists of FeO, otherwise ZVI as in the case of M- and CMC-Fe. Until now, the reductive dechlorination of CT using FeO NPs has not been reported, and any further experiments to identify the exact removal mechanism have not been tried in this study. It is presumed that the CT reduction will be caused by the reduction potential generated when the metastable FeO changes into magnetite (Rakshit et al., 2005; Redl et al., 2004). In this case, the reduction potential induced by the oxidation of FeO NPs should be expected to be smaller than the reduction potential of ZVI NPs.

Another cause is inhibition of the reactivity by the surface coating stabilizer as in the case of CMC. The coating layer of PO-OFe is a newly developed fatty acid double layer simulating a lipid bilayer using oleic acid and oleate. If the coating layer of PO-OFe is prepared as expected, it will have a selective permeability as the lipid bilayer. Only neutral small or hydrophobic molecules can permeate across lipid bilayer by passive diffusion (Mulder, 2012). The mass transport rate through the lipid bilayer membrane is determined by the following equation (Tepper and Voth, 2006):

$$\frac{dn}{dt} = A\frac{KD}{x}\left(C_1^{aq} - C_2^{aq}\right) \quad (5.4)$$

where A is the membrane surface area; K is the partition coefficient; D is the diffusion coefficient of the substance within the membrane; x is the membrane thickness, C_1^{aq}-C_2^{aq} is the concentration gradient between the areas divided with the lipid bilayer.

For CT molecules to reach the FeO surface of PO-OFe and be reductively degraded, it has to pass through the fatty acid double layer surrounding FeO, which can be controlled by the diffusion mechanism, that may act as a rate-limiting step for the reaction.

The reaction rate, expressed as pseudo-first order rate constants, of PO-OFe decreased slightly as the reaction progresses and can be estimated from the divided reaction time into two phases as shown in Fig. 5.3. In this experimental condition, reductive removal of CT by PO-OFe can be divided into two phases based on 1 h reaction time, and the reaction rate of the second phase decreases to less than half of that of the initial phase. On the other hand, M- and CMC-Fe showed a high coefficient of determination (almost 1) and the reaction rate was also 0.92 and 1.16, respectively. The decrease in the reaction rate of PO-OFe seems to be due to the characteristic of the fatty acid double layer. The diffusion rate is proportional to the partition coefficient of the material passing through the bilayer as well as the concentration gradient inside and outside the bilayer. Therefore, at the initial stage of the reaction, the concentration gradient of the inner and outer parts of the bilayer is maximum, and thus the diffusion rate is also maximized. However, the concentration gradient is decreased due to the accumulation of CT inside the bilayer. The permeated CT also spreads from the inside of the bilayer to parallel to the iron surface, resulting in further decrease in the concentration gradient between inside and outside the bilayer (Lodish et al., 2000). Also,

since the diffusion rate is proportional to the partition coefficient of the material, it is speculated that the fatty acid double layer can prevent penetration of dissolved ionic groundwater solutes and pass only hydrophobic contaminants such as CT through the layer (Fig. 5.4).

In reductive degradation of CT using M- and CMC-Fe, the major by-products of the reaction were CF (Fig. 5.2). DCM was not detected in this study. The concentration of chloride ion (Cl^-) in the solution was measured and the total chlorine mass balance (($[CT]_t \times 4 + [CF]t \times 3 + [Cl^-]_t$)/($[CT]_0 \times 4$)) was calculated. As a result, more than 81% chlorine was confirmed in the remaining aliquot by CT, CF, and Cl^- analysis, suggesting no by-products containing chlorine other than CT are formed in the batch system. This result can be commonly found in the CT dechlorination experiments using ZVI (Lien and Zhang, 1999; Song and Carraway, 2006). CT degradation using M- and CMC-Fe is considered to be proceeded by sequential dechlorination as explained in the literature (Feng et al., 2008; Lien and Zhang, 1999; Matheson and Tratnyek, 1994), and the kinetics of by-product formation from these Fe NPs (M- and CMC-Fe) was not different from each other mainly because their core NPs were as same as ZVI.

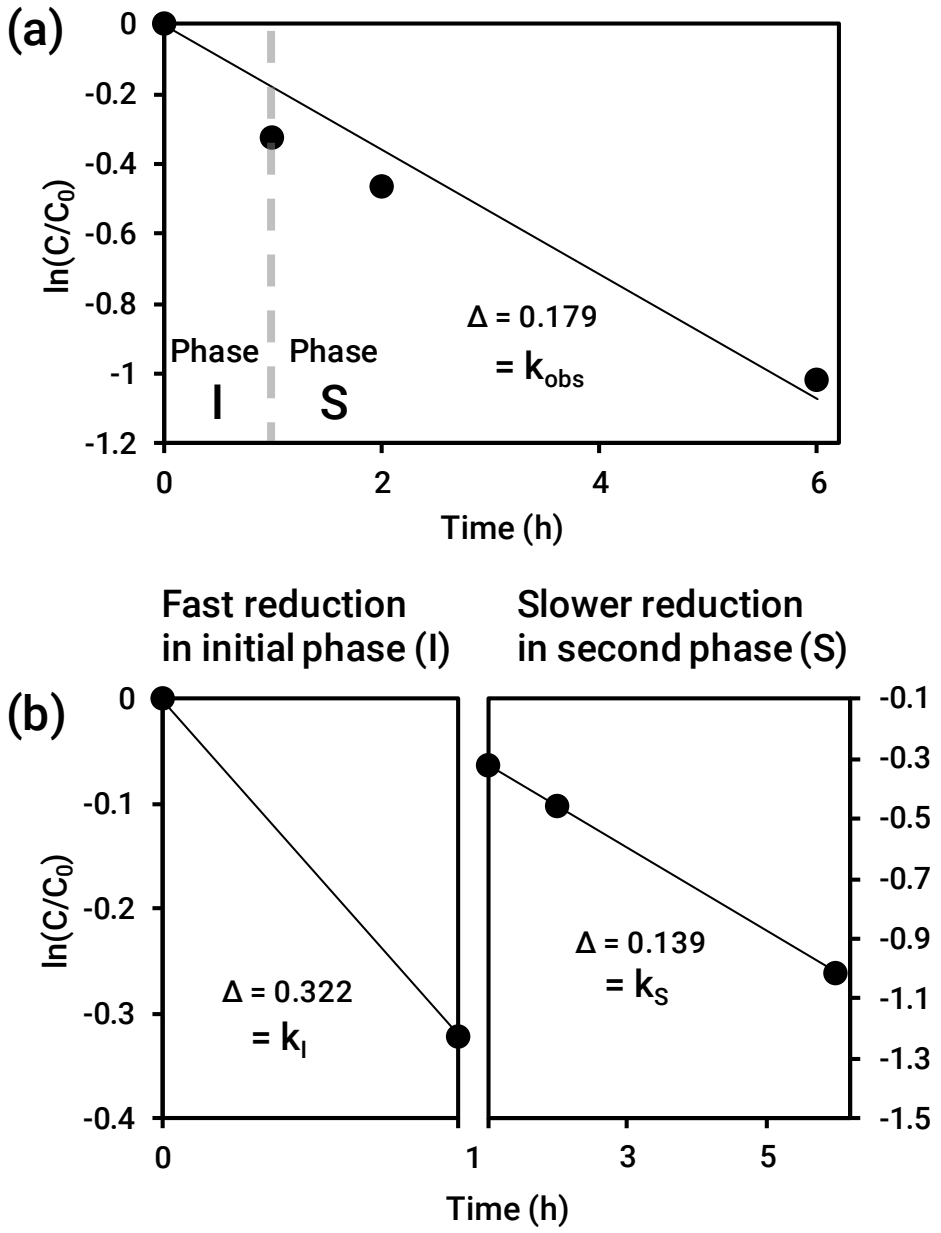

Figure 5.3 CT reductive removal and pseudo-first order fitted line using PO-OFe with lognormal y axis to obtain (a) k_{obs} over 6 h, (b) k_I and k_S

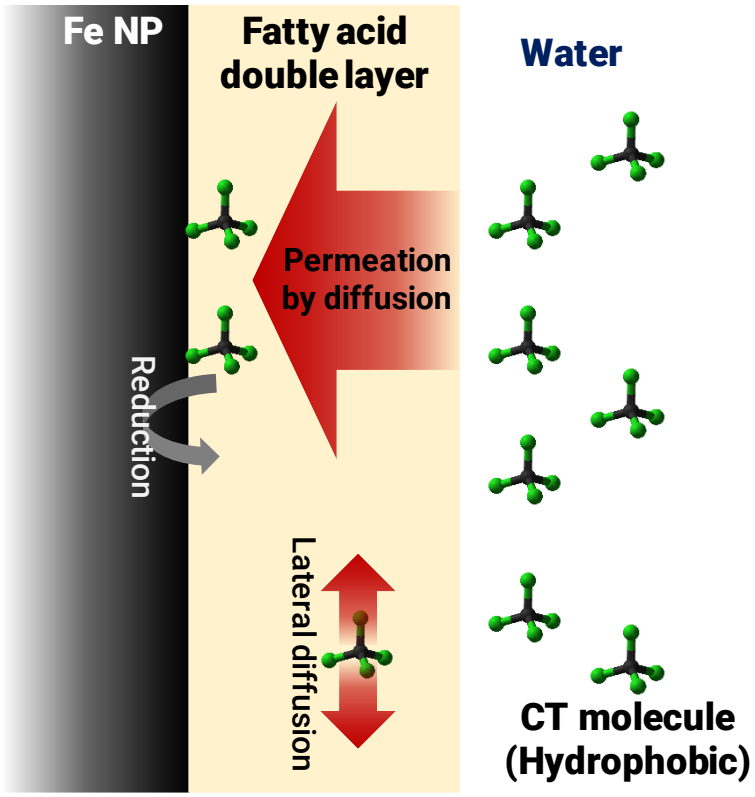

Figure 5.4 Schematic diagram illustrating permeation characteristics of the fatty acid double layer

On the other hand, in the case of the decomposition experiments of CT using PO-OFe, only up to 7.5% CF compared to the initial concentration of CT occurred as a by-product. DCM was not detected as in the case of M- and CMC-Fe. Nevertheless, more than 73% of chlorine could be measured in CT, CF, and Cl^- concentration in the remaining aliquot. It can be seen that the CT reductive removal mechanism by FeO coated with a fatty acid double layer (PO-OFe) is different from the mechanism using zero valence iron. In the researchers using green rust (O'Loughlin et al., 2003) and magnetite (McCormick and Adriaens, 2004), one of the iron oxides, to degrade CT, it has been reported that CT is not reduced to CF but to CH_4 directly via the formation of carbine species. PO-OFe, developed in this study, may also be regarded as having a different reaction pathway with limited CF formation. Accurate degradation mechanism identification through qualitative and quantitative analysis of the by-products will be performed later.

Nitrate is a typical ionic contaminant found in groundwater and can be reduced by zero valence iron (Hwang et al., 2011). Figures 5.5 and 5.6 show the results of nitrate reduction using M-Fe, CMC-Fe, and PO-OFe. At the iron concentration of 0.5 g/L, M- and CMC-Fe reduced 66 and 45% nitrate, respectively, and nitrite was not detected for 6 h. The sum of the nitrogen in remained nitrate and the ammonium ion maintained at least 55% of the total nitrogen. The same tendency was found in the literature (Xiong et al., 2009) in which nitrate was removed from the ZVI NPs coated with CMC.

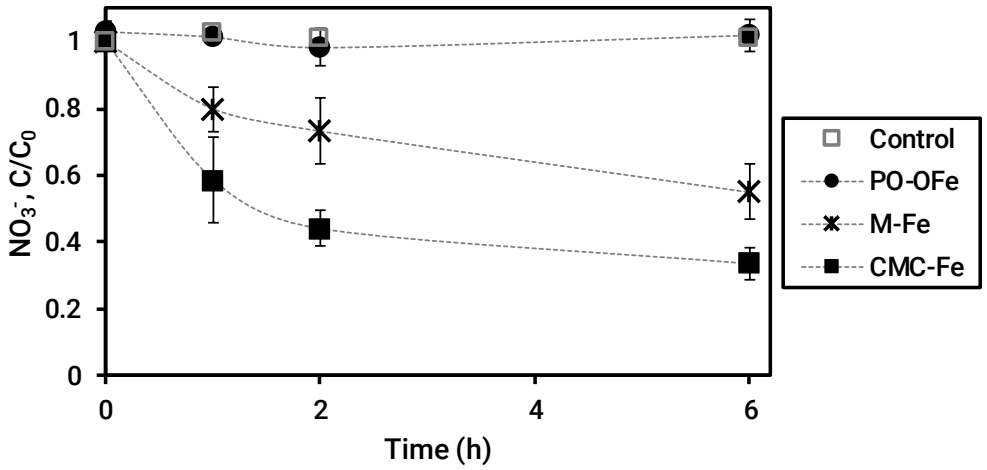

Figure 5.5 NO_3^- reductive removal using PO-OFe, M-Fe, and CMC-Fe. $[NO_3^-]_0$ = 0.48 mM, [Fe] = 0.5 g/L. Dotted lines are used only to guide the eye

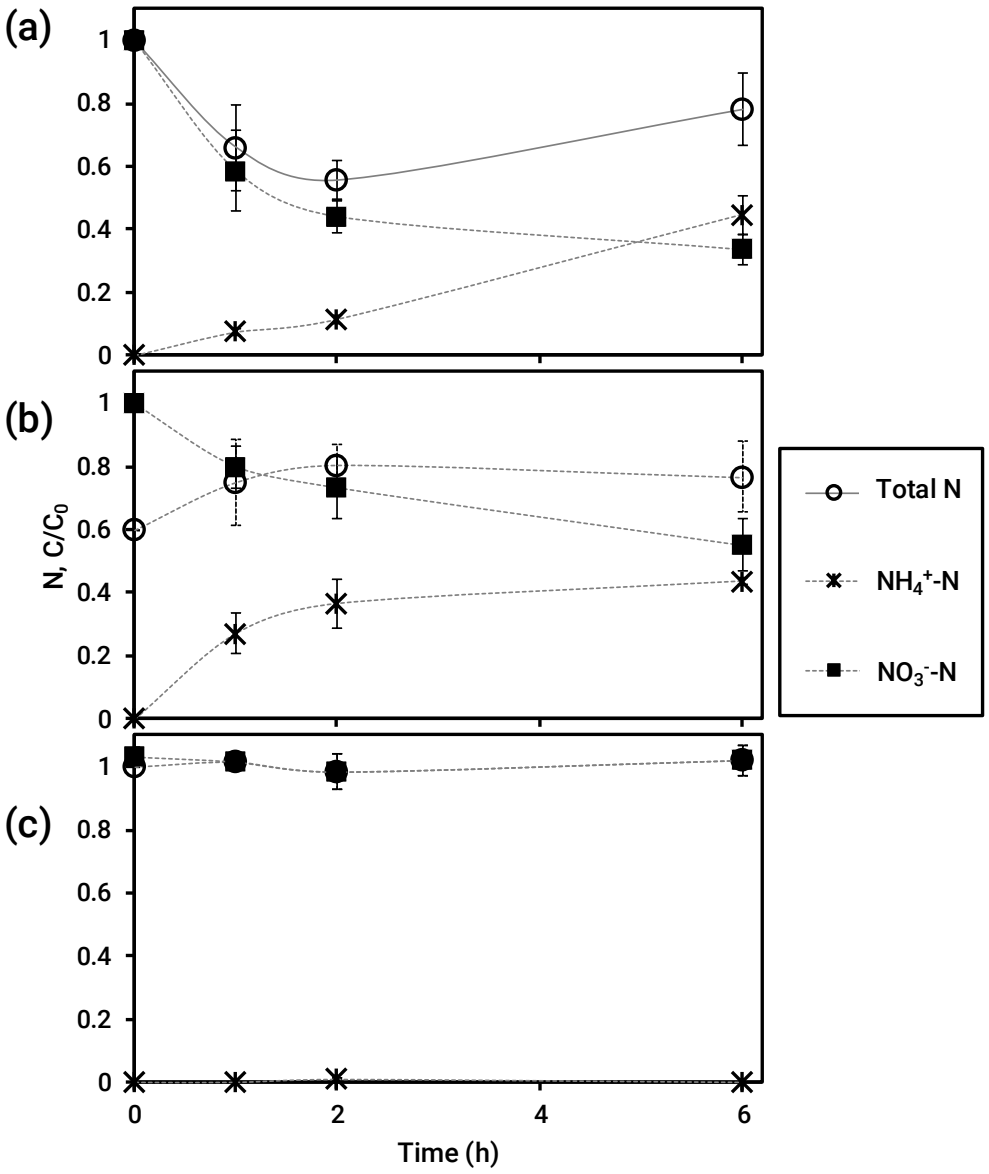

Figure 5.6 By-products formation from the NO_3^- removal experiment using (a) M-Fe, (b) CMC-Fe, and (c) PO-OFe. $[NO_3^-]_0$ = 0.48 mM, [Fe] = 0.5 g/L. Dotted lines are used only to guide the eye

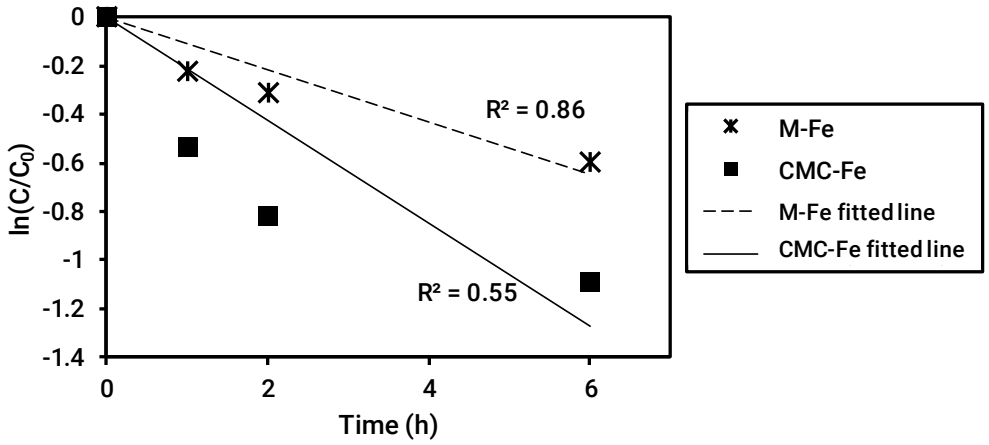

Figure 5.7 Pseudo-first order fitting results of NO_3^- reductive removal using M-Fe and CMC-Fe showing incompatibility of applying first order due to decrease in the reaction rate over time

As can be seen in the Fig. 5.7. the reaction rate of both Fe NPs obviously deceased with reaction time increase in nitrate removal reaction using M- and CMC-Fe. The reaction rate of M- and CMC-Fe in the second phase decreased to 33% and 17% of the initial phase, respectively. Reinsch et al. (2010) reported that ZVI is oxidized by dissolved anions, which are commonly found in groundwater containing nitrates. According to the results, nitrate mostly tends to passivate the surface of iron particle among nitrate, carbonate, phosphate, and sulfate. Once the passivating layer is formed on the surface of iron particle, ZVI was found in the core even after 6 months. In the experiments conducted in this study, it can be considered that the protective/passive layer was formed on the surface of M- and CMC-Fe due to reaction with nitrate, and thus the reaction rate became considerably slower compared to the reaction rate at the initial phase.

Meanwhile, FeO was also reported to reduce nitrate by corresponding oxidation of FeO to magnetite. However, FeO nanoparticles protected by the fatty acid double layer (PO-OFe) did not react with nitrate. No reaction by-products occurred at all during the reaction. According to the selective permeation principle of the lipid bilayer described above, ionic substances such as nitrate are extremely difficult to pass through the lipid bilayer because they cannot be partitioned in the hydrophobic region. It can be concluded that PO-OFe having the fatty acid double layer also prevented nitrate from penetrating into the surface of FeO based on the same principle as applied in the lipid bilayer.

5.3.2 Effect of dissolved groundwater solutes

To investigate the effect of dissolved groundwater solutes on the reactivity of Fe NPs, the selected solutes shown in Table 5.1 were added to a batch vial containing CT and Fe NPs. CT reductive removal by M-Fe, CMC-Fe, and PO-OFe in the presence of dissolved groundwater solutes typically found in groundwater are shown in Figure 5.8. The reaction rate constants were also calculated using the experimental results and shown in Table 5.2. The effect of dissolved groundwater solutes on the value of k_{obs} is shown in Fig. 5.9.

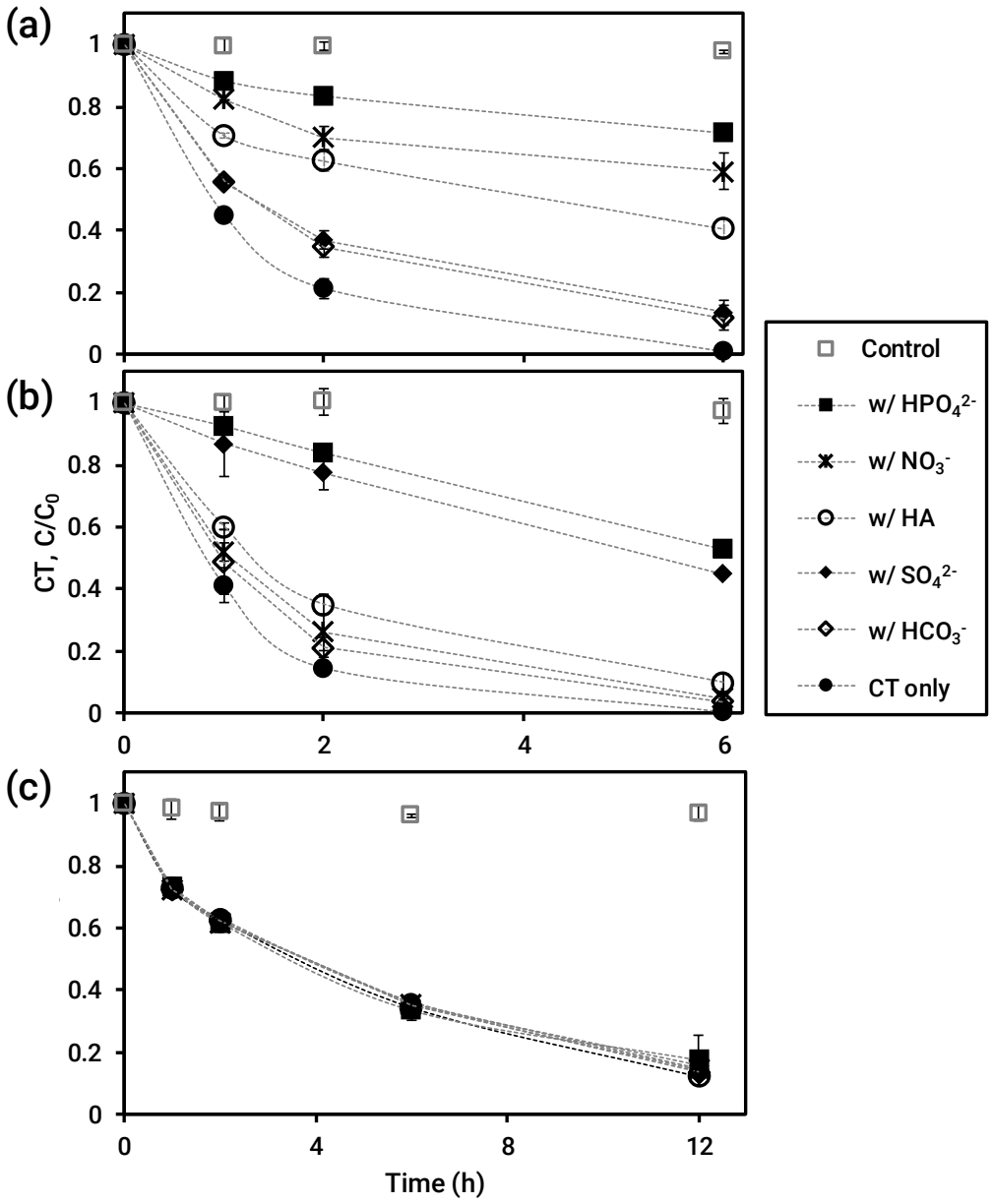

Figure 5.8 CT reductive removal in the presence of dissolved groundwater solutes using (a) M-Fe, (b) CMC-Fe, and (C) PO-OFe. Dotted lines are used only to guide the eye

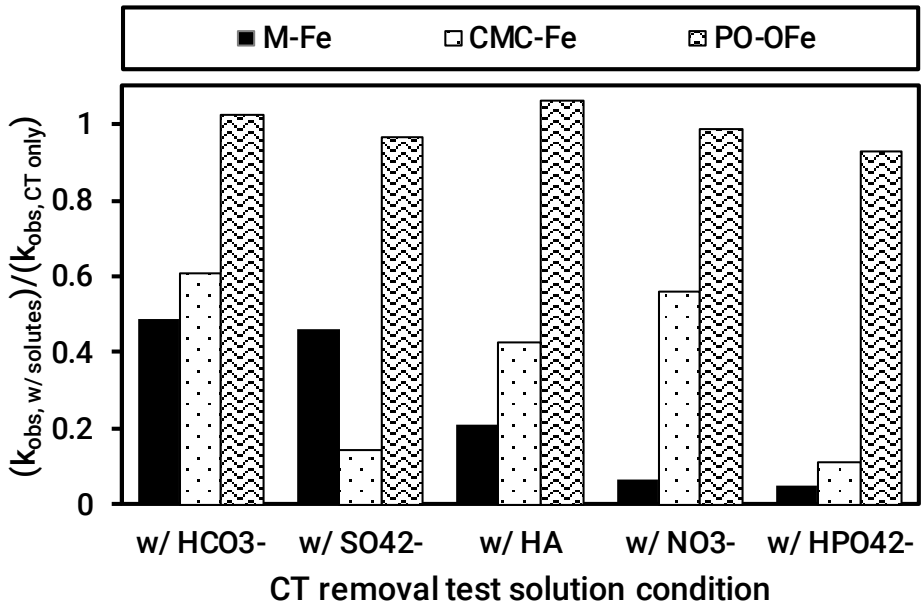

Figure 5.9 Ratio of k_{obs} for the experiments w/o dissolved groundwater solutes to k_{obs} with the solutes

All of the dissolved groundwater solutes selected in this study decreased the reactivity of M-Fe with CT in increasing order HCO_3^- < SO_4^{2-} < HA < NO_3^- < HPO_4^{2-}. This tendency is consistent with the results from Liu et al. (2007) in which the effect of dissolved groundwater solutes on the reactivity of uncoated bare ZVI NPs with TCE was evaluated. Liu et al. (2007) reported that the sequence of the decrease in reactivity was consistent with the complexation affinity with iron, suggesting that iron and anion were combined and passivated the iron surface. The reactivity inhibition by passivation of the reactive sites can be considered as the main reason for the reactivity decrease of M-Fe with dissolved groundwater solutes in this study.

The presence of nitrate also decreased the reactivity of TCE in Liu et al. (2007), but the reactivity decreased only if the nitrate concentration was > 3 mN. The magnitude of reactivity decrease was insignificant at a nitrate concentration lower than 3 mN. The molar ratio of iron to nitrate was 11.9 when 3 mN nitrate was present under the experimental conditions in Liu et al. (2007), which is 30% lower than the ratio used in this study, 17.9. When the molar ratio of iron to nitrate of 17.9, equivalent to 2 mN nitrate, the reactivity slightly increased in the research of Liu et al. (2007). It is considered that the difference in sensitivity to nitrate concerning the reactivity is caused by the different characteristic of contaminants. In Liu et al. (2007)'s study, TCE was the target contaminant, on the other hand, CT was used as the target contaminant. CT is more sensitive to the reduction reaction induced by iron than TCE, and the reaction rate of CT is generally 10 times greater than that of TCE using ZVI (Lien and Zhang, 1999; Lien and Zhang, 2001; Matheson and Tratnyek, 1994; Wang and Zhang, 1997). Therefore, it can be concluded that the reducing sensitive contaminants such as CT are more likely affected by changes in solution chemistry, resulting in a significant decrease in the reaction rate.

The presence of dissolved groundwater solutes has also brought the effect of changing in the reaction rate over time. Except for the presence of HA in the reaction solution, the reaction rate in the second phase was reduced by more than 50% in the presence of dissolved groundwater solutes, compared to the reaction rate in the initial phase. Especially in the presence of nitrate, the reaction rate was reduced by 87%, corresponding to the results of the nitrate reduction experiments using M-Fe. In this study, when both CT and nitrate were present as reducible contaminants with M-Fe, both contaminants reduced simultaneously by M-Fe. Therefore, it can be interpreted that the reaction rate of the second phase decreased significantly due to the passive layer formed by the reaction associated with the reduction of nitrate. In the presence of nitrate, CT and

nitrate may compete with each other in the effective reaction site on the surface of iron particle. Therefore, in the presence of nitrate, the reaction rate of CT removal by M-Fe can be seen to be significantly reduced as compared with the conditions in the presence of carbonate and sulfate.

In the presence of HA, the reaction rate change with time was almost negligible as compared to the change in the reaction rate by the other solutes. This rate change can be seen as a result of the difference in the mechanism by which the dissolved anions and HA reduce the reactivity of M-Fe. Dissolved anions have been reported to passivate the reactive sites of iron by complexing with iron surfaces (Liu and Lowry, 2006; Liu et al., 2007; Su and Puls, 2004). On the other hand, the reaction between the dissolved organic matters such as HA and the iron surface is explained by the adsorption (Tratnyek et al., 2011; Tratnyek et al., 2001) and can be regarded as an instantaneous reaction rather than the complexation reaction induced by anions (Phenrat et al., 2015; Vindedahl et al., 2016). In the presence of HA, it can be seen that binding of HA to the iron surface take place rapid enough to affect the reactivity even in the initial phase, reducing the reactive site for CT.

Unlike M-Fe, which had a 94% decrease in the reaction rate in the presence of nitrate, the reaction rate of CMC-Fe maintained 56% of the reaction rate when CT alone was present in the reaction solution. Even in the presence of HA, the degree of decrease in the reactivity was smaller than that of M-Fe. As described in Section 5.3.1, the polyelectrolyte molecules coated on the iron surface can reduce the reactivity of iron particle to the contaminants because they can occupy the reactive site of iron particle and block the approach of the contaminants to the reactive site, and cause the contaminants to partition into the polyelectrolytes layer, by which the local concentration of the contaminants right around the surface of iron particle can decrease. These effects seem to have helped to reduce the reactivity inhibition effect of dissolved groundwater solutes.

According to Phenrat et al. (2015), for ZVI NPs coated with PAP polyelectrolyte, the coated polymer reduces the anion concentration right around iron surface and increases the concentration of cation compared with for bare unmodified ZVI NPs due to the negative charge of PAP. CMC molecules of CMC-Fe also seems to reduce the anion concentration around the iron surface like PAP. Therefore, it can be inferred that the reaction rate of CMC-Fe to nitrate decreased and the passivation effect by the presence of nitrate decreased concurrently. In the case of HA, it seems that the amount of HA adsorption to the surface of iron particle decreased because the adsorption site is occupied by the polyelectrolytes, resulting in a relieved decrease in the reaction rate of CMC-Fe. Partitioning of HA into the CMC layer or binding to CMC may also be a cause of the relieved decrease in the reaction rate.

In the presence of sulfate and phosphate, the reactivity of CMC-Fe to CT reduced remarkably by more than 86%. In particular, in the presence of sulfate, the extent of decrease in the reactivity was higher than that of M-Fe. Also, for CMC-Fe, the value of k_s/k_I is close to 1, which means that the reactivity reduction by both dissolved substances is instantaneously occurred. In the presence of divalent anions in the CMC-Fe solution, the coated CMC layer may be compressed, resulting in more reactive sites being blocked by the CMC than in the presence of monovalent anions, thereby significantly reducing the reactivity of the CMC-Fe. However, further study should be needed to find out the mechanisms related to the reactivity decrease of CMC-Fe in the presence of sulfate and phosphate.

In the case of the experiments using PO-OFe, all the effects associated with reactivity decrease mentioned above did not appear. The effect of reducing the k_{obs} by passivation of the iron surface or adsorption to the site by dissolved anions and organic substances could not be found, and the additional decrease related to the reactivity of Fe NPs induced by the reaction among contaminant, stabilizer, and dissolved groundwater

solute were not observed also. These results should be originated from the fatty acid double layer formed on the surface of iron particle and it can be regarded as a proof of success to coat the surface of Fe NPs with fatty acid double layer imitating lipid bilayer membrane that has selective permeability by which ions are blocked to pass through the layer, and only hydrophobic materials can pass across the layer, producing selective reactivity to the Fe NPs.

5.4 Conclusions

As expected in the hypothesis that fatty acid double layer onto the surface of Fe NPs can have a selective permeability like as the lipid bilayer of cell, dissolved groundwater solutes that commonly encountered in field groundwater such as bicarbonate, sulfate, nitrate, phosphate, and humic acids at the concentration relevant to field groundwater concentrations (except phosphate) have not affected the reactivity of PO-OFe. Nitrate is one of the reducible contaminants by Fe NPs, however, it was not able to be reduced by the contact of PO-OFe. M- and CMC-Fe have been passivated in the solution with the presence of model groundwater solutes regarding the reactivity to CT as reported in literature. Especially in the presence of phosphate, CT reduction rate of M- and CMC-Fe, estimated by k_{obs}, decreased by almost 95 and 89%, respectively. These results suggested that the injecting PO-OFe may be more efficient in the application that needs longer transport distance or residence time in the subsurface due to the reactivity protection by the fatty acid double layer preventing reactivity loss from the groundwater solutes.

Chapter 6. Conclusions and recommendation

6.1 Summary

This dissertation presents a newly developed Fe-based nanoscale groundwater remediation reagent overcoming the two significant drawbacks for ZVI NPs within the consideration of subsurface remediation apply. Three main contents including 'introducing the synthesis and preparation procedure', 'mobility in 1-D column', and 'reactivity evaluation' were prepared for this dissertation exploring essential aspects of ZVI NP application.

Pre-agglomeration modification seems to have potential to add the larger amount of stabilizer onto the surface of Fe NPs. Less than only 5% mass of Fe NPs was accounted for the mass of stabilizer in case of post-agglomeration modification, which results in agglomeration and sedimentation of the particles. Thermal decomposition of iron stearate with oleic acid formed FeO nanoparticles coated with oleic acid. The fatty acid double layer was successfully formed onto the surface of FeO nanoparticles by adding the PO solution at various concentrations into OFe slurry followed by vigorous mixing. Experimental results such as TGA and performance test results (mobility and reactivity tests) have confirmed the formation of the fatty acid double layer. Hydrodynamic diameter and zeta-potential of the fatty acid double layer coated Fe NPs developed in this study were variable with the solution condition such as the concentration of PO solution in the suspension and the molar ratio of Fe to PO. The Fe to PO molar ratio of less than 43.5 is necessary to prepare stable OA coated Fe NPs in PO solution.

Two kinds of Fe NPs modified with post-agglomeration methods, CMC-Fe and PO-OFe, only showed stability in the aqueous phase. Sedimentation of PO-OFe was not observed, and only 40% of absorbance decreased in 24 h in case of CMC-Fe indicated the partial sedimentation, although post-agglomeration modified Fe NPs and unmodified Fe-NPs, PoOl-Fe, PoCMC-Fe, and M-Fe, rapidly agglomerated and sediment within 6 h, consistent with the results of particle size measurement and TGA.

As reported earlier in previous literature, unmodified ZVI NPs, M-Fe, showed insufficient mobility in a 1-D sandy packed column transport experiment, stuck in the initial influent pregnant of the column. With various pore water velocities from 0.04 to 1.4 cm/min (representative of typical groundwater velocity and artificially increased velocity, respectively), the normalized Fe concentrations of CMC-Fe at a steady plateau increased dramatically from 0.47 to 0.93 in the column experiments condition conducted in this study. However, the normalized Fe concentrations in case of HPO-OFe reached unity in all transport experiments in this study suggesting great mobility in subsurface transport. Attachment efficiencies (α) of 0.0015, the extent of which is in the range of low-end value among reported values, and 0 were calculated for PO-OFe in the column experiments. Low α can be attributed to the high magnitude of zeta potential (-115.2 and -91.2), and the steric force originated from the fatty acid double layer. A variable form of the fatty acid double layer coated Fe NPs may be used as a reaction agent with controlled mobility in the subsurface.

Distinct reactivity characteristics for PO-OFe were confirmed in this study. Comparing with the case of M-Fe and CMC-Fe, lower CT reductive dechlorination rate constant (estimated using pseudo-first-order kinetic model) of PO-OFe was observed. Moreover, a model hydrophilic contaminant, nitrate, was not reduced at all by PO-OFe. Although observed ration rates, k_{obs}, of M-Fe and CMC-Fe decreased by 89% and 95% at maximum respectively, only 7% reduction in k_{obs} was observed in case of PO-OFe.

These reaction experiments result can be explained by the surface protection of the fatty acid double layer formed onto the surface of Fe NPs. As expected in the hypothesis that fatty acid double layer onto the surface of Fe NPs can have a selective permeability like as the lipid bilayer of cell, it seems that hydrophilic contaminant and dissolved groundwater solutes that commonly encountered in field groundwater such as bicarbonate, sulfate, nitrate, phosphate, and humic acids at the concentration relevant with field groundwater concentrations (except phosphate) cannot permeate the fatty acid double layer and have not affect the reactivity of PO-OFe.

6.2 Conclusions and implications

The major conclusions and implications that were drawn from these studies are as follows:

Experimental results in this study suggested that fatty acid double layer coating can have the same role as lipid bilayer protecting the cell regarding selective permeability. Nitrate, hydrophilic contaminant, cannot be reduced by the fatty acid double layer coated Fe NPs. The reactivity of the coated Fe NPs to CT remained even in the presence of dissolved groundwater solutes including anions and natural organic matter. The selective reactivity is attributable to permeability characteristic of the fatty acid double layer protecting Fe NPs. Well organized structure of fatty acid double layer may be attributable to the high magnitude of zeta potential of PO-OFe, results in very low attachment efficiency and better mobility of PO-OFe than those of CMC-Fe. Sufficient steric repulsion may work in interactions of Fe NPs to each other or soil grains primary due to the mass of fatty acid coated onto the surface of Fe NPs, which aid to make Fe NPs stable in the aqueous phase.

A reactive particle for in-situ groundwater remediation have selective reactivity can be considered as having longer remaining reactivity, that is longevity, to target contaminants. Remedial action using the reactants have the longevity, and high mobility can offer the chance to clean-up the site where as-used technologies cannot be economically applied. Fatty acid double layer coated Fe NPs may be a suitable remediation alternative for these sites (Fig. 6.1). For example, 1) existing infrastructure on the contaminated subsurface to be remediated, causing too expensive costs to dismantle the infrastructure before remediation; 2) deep depth contamination that inapplicable by other remediation methods; 3) contamination in fractured bedrock.

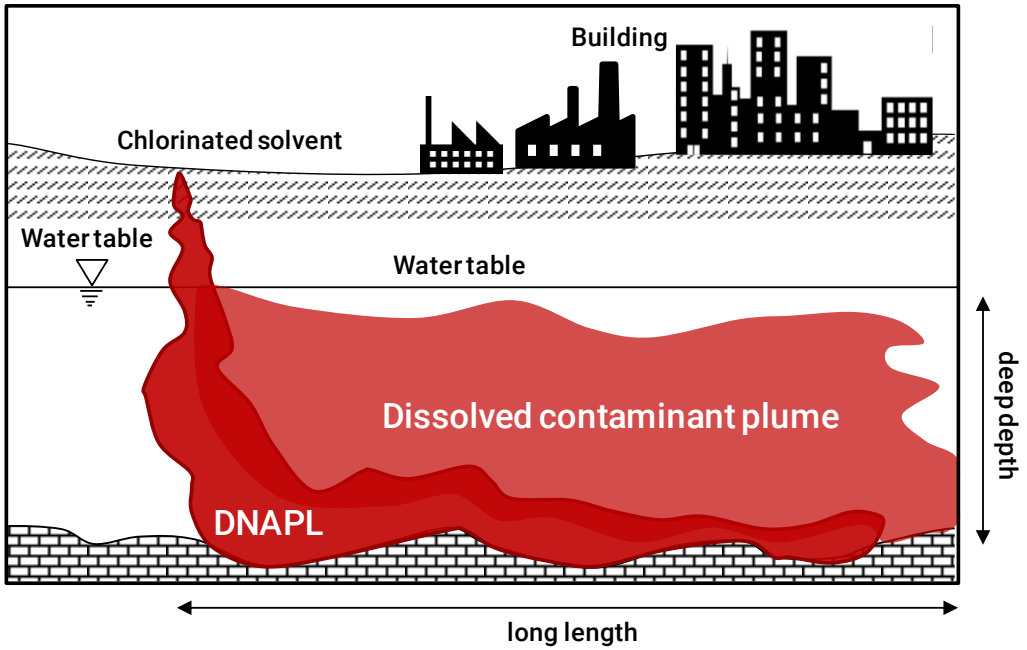

Figure 6.1 Schematic diagram illustrating the cases where PO-OFe may be a suitable remediation alternative

Forming a fatty acid double layer onto Fe NPs should not be necessary to follow the synthesis and preparation method used in this study. Other methods can be adapted to give a protective layer onto the surface of Fe NPs. Moreover, the core is also changeable accompanied by the use of other synthesis and preparation methods. Reactivity and mobility may be improved or controlled with the combination of the core and fatty acid double layer characteristics with proper development methods.

6.3 Research needs

It is the first try to use a fatty acid double layer to stabilize Fe NPs in the aqueous phase as well as protect surface reactivity of Fe NPs from dissolved groundwater solutes. In this study, the contents are focused on the ideas to secure the mobility and selective reactivity of Fe NPs and develop the synthesis and preparation methods for fatty acid double layer coating. Therefore, optimization of the nanoparticle formation and detailed investigation of the effect originated from the fatty acid double layer have not been sufficiently explored. For example, the relation of fatty acid mass bonded to the particles' surface to the performances (i.e., mobility and reactivity) should be revealed. Developing the methods to control the thickness of the fatty acid double layer and unveiling the role of the thickness are also meaningful. Minimal tests to confirm the possibility of the advantages by the surface coating concerning mobility and reactivity were conducted in this study. After the optimization with the aid of supplement experiments, pilot or filed scale remediation trials should be followed to confirm the applicability of this developed technology.

Bibliography

Agrawal, A., Ferguson, W.J., Gardner, B.O., Christ, J.A., Bandstra, J.Z., Tratnyek, P.G. (2002) Effects of carbonate species on the kinetics of dechlorination of 1,1,1-trichloroethane by zero-valent iron. Environmental science & technology 36, 4326-4333.

Aiken, G.R., Hsu-Kim, H., Ryan, J.N., (2011) Influence of dissolved organic matter on the environmental fate of metals, nanoparticles, and colloids. ACS Publications.

Araújo-Neto, R., Silva-Freitas, E., Carvalho, J., Pontes, T., Silva, K., Damasceno, I., Egito, E., Dantas, A.L., Morales, M.A., Carriço, A.S. (2014) Monodisperse sodium oleate coated magnetite high susceptibility nanoparticles for hyperthermia applications. Journal of magnetism and magnetic materials 364, 72-79.

Arnold, W.A., Roberts, A.L. (2000) Pathways and kinetics of chlorinated ethylene and chlorinated acetylene reaction with Fe (0) particles. Environmental science & technology 34, 1794-1805.

ASTM, (2000) E394-00: Standard test method for iron in trace quantities using the 1,10-phenanthroline method, Annual book of ASTM standards, pp. 1-4.

Bardos, P., Bone, B., Daly, P., Elliott, D., Jones, S., Lowry, G., Merly, C., (2015) A risk/benefit appraisal for the application of nano-scale zero valent iron (nZVI) for the remediation of contaminated sites, WP9 NanoRem.

Bennett, P., He, F., Zhao, D., Aiken, B., Feldman, L. (2010) In situ testing of metallic iron nanoparticle mobility and reactivity in a shallow granular aquifer. Journal of contaminant hydrology 116, 35-46.

Bronstein, L.M., Huang, X., Retrum, J., Schmucker, A., Pink, M., Stein, B.D., Dragnea, B. (2007) Influence of iron oleate complex structure on iron oxide nanoparticle formation. Chemistry of materials 19, 3624-3632.

Carpenter, E., Calvin, S., Stroud, R., Harris, V. (2003) Passivated iron as core−shell nanoparticles. Chemistry of materials 15, 3245-3246.

Chen, J., Xiu, Z., Lowry, G.V., Alvarez, P.J. (2011) Effect of natural organic matter on toxicity and reactivity of nano-scale zero-valent iron. Water research 45, 1995-2001.

Chen, K.L., Mylon, S.E., Elimelech, M. (2007) Enhanced aggregation of alginate-coated iron oxide (hematite) nanoparticles in the presence of calcium, strontium, and barium cations. Langmuir 23, 5920-5928.

Choi, B.-Y., Yun, S.-T., Kim, K.-H., Kim, J.-W., Kim, H.M., Koh, Y.-K. (2014) Hydrogeochemical interpretation of South Korean groundwater monitoring data using self-organizing maps. Journal of geochemical exploration 137, 73-84.

Comba, S., Dalmazzo, D., Santagata, E., Sethi, R. (2011) Rheological characterization of xanthan suspensions of nanoscale iron for injection in porous media. Journal of hazardous materials 185, 598-605.

Comba, S., Sethi, R. (2009) Stabilization of highly concentrated suspensions of iron nanoparticles using shear-thinning gels of xanthan gum. Water research 43, 3717-3726.

Cook, S.M., (2009) Assessing the use and application of zero-valent iron nanoparticle technology for remediation at contaminated sites. Jackson State University.

Council, N.R. (1994) Alternatives for ground water cleanup. National Academies Press.

Crane, R.A., Scott, T.B. (2012) Nanoscale zero-valent iron: Future prospects for an emerging water treatment technology. Journal of hazardous materials 211-212, 112-125.

Cundy, A.B., Hopkinson, L., Whitby, R.L.D. (2008) Use of iron-based technologies in contaminated land and groundwater remediation: A review. Science of the total environment 400, 42-51.

Danielsen, K.M., Hayes, K.F. (2004) pH dependence of carbon tetrachloride reductive dechlorination by magnetite. Environmental science & technology 38, 4745-4752.

Elliott, D.W., Zhang, W.-X. (2001) Field assessment of nanoscale bimetallic particles for groundwater treatment. Environmental science & technology 35, 4922-4926.

Erbs, M., Bruun Hansen, H.C., Olsen, C.E. (1999) Reductive dechlorination of carbon tetrachloride using iron (II) iron (III) hydroxide sulfate (green rust). Environmental science & technology 33, 307-311.

Faraji, M., Yamini, Y., Rezaee, M. (2010) Magnetic nanoparticles: synthesis, stabilization, functionalization, characterization, and applications. Journal of the Iranian chemical society 7, 1-37.

Feng, J., Zhu, B.-w., Lim, T.-T. (2008) Reduction of chlorinated methanes with nano-scale Fe particles: Effects of amphiphiles on the dechlorination reaction and two-parameter regression for kinetic prediction. Chemosphere 73, 1817-1823.

Frascari, D., Zanaroli, G., Danko, A.S. (2015) In situ aerobic cometabolism of chlorinated solvents: A review. Journal of hazardous materials 283, 382-399.

Gavaskar, A.R., Gupta, N., Sass, B., Janosy, R., OSullivan, D. (1998) Permeable barriers for groundwater remediation.

Gschwend, P.M. (2016) Environmental organic chemistry. John Wiley & Sons.

He, F., Zhang, M., Qian, T., Zhao, D. (2009) Transport of carboxymethyl cellulose stabilized iron nanoparticles in porous media: Column experiments and modeling. Journal of colloid and interface science 334, 96-102.

He, F., Zhao, D. (2005) Preparation and characterization of a new class of starch-stabilized bimetallic nanoparticles for degradation of chlorinated hydrocarbons in water. Environmental science & technology 39, 3314-3320.

He, F., Zhao, D. (2007) Manipulating the size and dispersibility of zerovalent iron nanoparticles by use of carboxymethyl cellulose stabilizers. Environmental science & technology 41, 6216-6221.

He, F., Zhao, D., Liu, J., Roberts, C.B. (2007) Stabilization of Fe-Pd nanoparticles with sodium carboxymethyl cellulose for enhanced transport and dechlorination of trichloroethylene in soil and groundwater. Industrial & engineering chemistry research 46, 29-34.

He, F., Zhao, D., Paul, C. (2010) Field assessment of carboxymethyl cellulose stabilized iron nanoparticles for in situ destruction of chlorinated solvents in source zones. Water research 44, 2360-2370.

Henn, K.W., Waddill, D.W. (2006) Utilization of nanoscale zero-valent iron for source remediation—A case study. Remediation journal 16, 57-77.

Hotze, E.M., Phenrat, T., Lowry, G.V. (2010) Nanoparticle aggregation: Challenges to understanding transport and reactivity in the environment. Journal of environmental quality 39, 1909-1924.

Hou, Y., Xu, Z., Sun, S. (2007) Controlled synthesis and chemical conversions of FeO nanoparticles. Angewandte chemie international edition 46, 6329-6332.

Huber, D.L. (2005) Synthesis, properties, and applications of iron nanoparticles. Small 1, 482-501.

Hwang, Y.H., Kim, D.G., Shin, H.S. (2011) Mechanism study of nitrate reduction by nano zero valent iron. Journal of hazardous materials 185, 1513-1521.

Jiemvarangkul, P., Zhang, W.-x., Lien, H.-L. (2011) Enhanced transport of polyelectrolyte stabilized nanoscale zero-valent iron (nZVI) in porous media. Chemical engineering journal 170, 482-491.

Johnson, R.L., Johnson, G.O.B., Nurmi, J.T., Tratnyek, P.G. (2009) Natural organic matter enhanced mobility of nano zerovalent iron. Environmental science & technology 43, 5455-5460.

Johnson, T.L., Fish, W., Gorby, Y.A., Tratnyek, P.G. (1998) Degradation of carbon tetrachloride by iron metal: Complexation effects on the oxide surface. Journal of contaminant hydrology 29, 379-398.

Kanel, S.R., Nepal, D., Manning, B., Choi, H. (2007) Transport of surface-modified iron nanoparticle in porous media and application to arsenic (III) remediation. Journal of nanoparticle research 9, 725-735.

Karn, B., Kuiken, T., Otto, M. (2009) Nanotechnology and in situ remediation: a review of the benefits and potential risks. Environmental health perspectives 117, 1813.

Keely, J.F., Boulding, J. (1989) Performance evaluations of pump-and-treat remediations. EPA Environmental Engineering Sourcebook.

Kim, D., Park, J., An, K., Yang, N.-K., Park, J.-G., Hyeon, T. (2007) Synthesis of hollow iron nanoframes. Journal of the American chemical society 129, 5812-5813.

Kim, D.K., Mikhaylova, M., Zhang, Y., Muhammed, M. (2003) Protective coating of superparamagnetic iron oxide nanoparticles. Chemistry of materials 15, 1617-1627.

Kim, K.-H., Yun, S.-T., Park, S.-S., Joo, Y., Kim, T.-S. (2014) Model-based clustering of hydrochemical data to demarcate natural versus human impacts on bedrock groundwater quality in rural areas, South Korea. Journal of hydrology 519, 626-636.

Klausen, J., Ranke, J., Schwarzenbach, R.P. (2001) Influence of solution composition and column aging on the reduction of nitroaromatic compounds by zero-valent iron. Chemosphere 44, 511-517.

Kocur, C.M., Chowdhury, A.I., Sakulchaicharoen, N., Boparai, H.K., Weber, K.P., Sharma, P., Krol, M.M., Austrins, L., Peace, C., Sleep, B.E., O'Carroll, D.M. (2014) Characterization of nZVI mobility in a field scale test. Environmental science & technology 48, 2862-2869.

Korolev, V., Ramazanova, A., Blinov, A. (2002) Adsorption of surfactants on superfine magnetite. Russian chemical bulletin 51, 2044-2049.

Lecoanet, H.F., Bottero, J.-Y., Wiesner, M.R. (2004) Laboratory assessment of the mobility of nanomaterials in porous media. Environmental science & technology 38, 5164-5169.

Lee, W., Batchelor, B. (2002) Abiotic reductive dechlorination of chlorinated ethylenes by iron-bearing soil minerals. 1. Pyrite and magnetite. Environmental science & technology 36, 5147-5154.

Li, L., Fan, M., Brown, R.C., Leeuwen, J.V., Wang, J., Wang, W., Song, Y., Zhang, P. (2006a) Synthesis, properties, and environmental applications of nanoscale iron-based materials: A review. Critical reviews in environmental science & Technology 36, 405-431.

Li, S., Yan, W., Zhang, W.-x. (2009) Solvent-free production of nanoscale zero-valent iron (nZVI) with precision milling. Green chemistry 11, 1618-1626.

Li, X.-q., Elliott, D.W., Zhang, W.-x. (2006b) Zero-valent iron nanoparticles for abatement of environmental pollutants: Materials and engineering aspects. Critical reviews in solid state and materials sciences 31, 111-122.

Lien, H.L., Elliott, D.W., Sun, Y.P., Zhang, W.X. (2006) Recent progress in zero-valent iron nanoparticles for groundwater remediation. Journal of environmental engineering and management 16, 371.

Lien, H.L., Zhang, W. (1999) Transformation of chlorinated methanes by nanoscale iron particles. Journal of environmental engineering 125, 1042-1047.

Lien, H.L., Zhang, W.X. (2001) Nanoscale iron particles for complete reduction of chlorinated ethenes. Colloids and Surfaces A: Physicochemical and engineering aspects 191, 97-105.

Lim, T.-T., Zhu, B.-W. (2008) Effects of anions on the kinetics and reactivity of nanoscale Pd/Fe in trichlorobenzene dechlorination. Chemosphere 73, 1471-1477.

Lin, Y.H., Tseng, H.H., Wey, M.Y., Lin, M.D. (2009) Characteristics, morphology, and stabilization mechanism of PAA250K-stabilized bimetal nanoparticles. Colloids and surfaces A: Physicochemical and engineering aspects 349, 137-144.

Lin, Y.H., Tseng, H.H., Wey, M.Y., Lin, M.D. (2010) Characteristics of two types of stabilized nano zero-valent iron and transport in porous media. Science of the total environment 408, 2260-2267.

Liu, Y., Lowry, G.V. (2006) Effect of particle age (Fe0 content) and solution pH on NZVI reactivity: H2 evolution and TCE dechlorination. Environmental science & technology 40, 6085-6090.

Liu, Y., Majetich, S.A., Tilton, R.D., Sholl, D.S., Lowry, G.V. (2005) TCE dechlorination rates, pathways, and efficiency of nanoscale iron particles with different properties. Environmental science & technology 39, 1338-1345.

Liu, Y., Phenrat, T., Lowry, G.V. (2007) Effect of TCE concentration and dissolved groundwater solutes on NZVI-promoted TCE dechlorination and H_2 evolution. Environmental science & technology 41, 7881-7887.

Lodish, H., Berk, A., Zipursky, S.L., Matsudaira, P., Baltimore, D., Darnell, J. (2000) Molecular cell biology 4th edition.

Matheson, L.J., Tratnyek, P.G. (1994) Reductive dehalogenation of chlorinated methanes by iron metal. Environmental science & technology 28, 2045-2053.

Maurer-Jones, M.A., Gunsolus, I.L., Murphy, C.J., Haynes, C.L. (2013) Toxicity of engineered nanoparticles in the environment. Analytical chemistry 85, 3036-3049.

McCormick, M.L., Adriaens, P. (2004) Carbon tetrachloride transformation on the surface of nanoscale biogenic magnetite particles. Environmental science & technology 38, 1045-1053.

McDowall, L., (2005) Degradation of toxic chemicals by zero-valent metal nanoparticles-A literature review. DTIC Document.

McKinney, D.C., Lin, M.-D. (1996) Pump-and-treat ground-water remediation system optimization. Journal of water resources planning and management 122, 128-136.

Molchanov, V., Shashkina, Y.A., Philippova, O., Khokhlov, A. (2005) Viscoelastic properties of aqueous anionic surfactant (potassium oleate) solutions. Colloid journal 67, 606-609.

Müller, N.C., Nowack, B. (2010) Nano zero valent iron–The solution for water and soil remediation? Report of the ObservatoryNANO.

Mulder, J. (2012) Basic principles of membrane technology. Springer science & business media.

Nagle, J.F., Mathai, J.C., Zeidel, M.L., Tristram-Nagle, S. (2008) Theory of passive permeability through lipid bilayers. The Journal of general physiology 131, 77-85.

Nurmi, J.T., Tratnyek, P.G., Sarathy, V., Baer, D.R., Amonette, J.E., Pecher, K., Wang, C., Linehan, J.C., Matson, D.W., Penn, R.L. (2005) Characterization and properties of metallic iron nanoparticles: spectroscopy, electrochemistry, and kinetics. Environmental science & technology 39, 1221-1230.

O'Loughlin, E.J., Kemner, K.M., Burris, D.R. (2003) Effects of Ag(I), Au(III), and Cu(II) on the reductive dechlorination of carbon tetrachloride by green rust. Environmental science & technology 37, 2905-2912.

Park, J., An, K., Hwang, Y., Park, J.-G., Noh, H.-J., Kim, J.-Y., Park, J.-H., Hwang, N.-M., Hyeon, T. (2004) Ultra-large-scale syntheses of monodisperse nanocrystals. Nature materials 3, 891-895.

Phenrat, T., Kim, H.-J., Fagerlund, F., Illangasekare, T., Tilton, R.D., Lowry, G.V. (2009a) Particle size distribution, concentration, and magnetic attraction affect transport of polymer-modified Fe^0 nanoparticles in sand columns. Environmental science & technology 43, 5079-5085.

Phenrat, T., Liu, Y., Tilton, R.D., Lowry, G.V. (2009b) Adsorbed polyelectrolyte coatings decrease Fe^0 nanoparticle reactivity with TCE in water: Conceptual model and mechanisms. Environmental science & technology 43, 1507-1514.

Phenrat, T., Saleh, N., Sirk, K., Kim, H.J., Tilton, R.D., Lowry, G.V. (2008) Stabilization of aqueous nanoscale zerovalent iron dispersions by anionic polyelectrolytes: adsorbed anionic polyelectrolyte layer properties and their effect on aggregation and sedimentation. Journal of nanoparticle research 10, 795-814.

Phenrat, T., Saleh, N., Sirk, K., Tilton, R.D., Lowry, G.V. (2007) Aggregation and sedimentation of aqueous nanoscale zerovalent iron dispersions. Environmental science & technology 41, 284-290.

Phenrat, T., Schoenfelder, D., Kirschling, T.L., Tilton, R.D., Lowry, G.V. (2015) Adsorbed poly (aspartate) coating limits the adverse effects of dissolved groundwater solutes on Fe^0 nanoparticle reactivity with trichloroethylene. Environmental science and pollution research, 1-13.

Ponder, S.M., Darab, J.G., Mallouk, T.E. (2000) Remediation of Cr (VI) and Pb (II) aqueous solutions using supported, nanoscale zero-valent iron. Environmental science & technology 34, 2564-2569.

Rakshit, S., Matocha, C.J., Haszler, G.R. (2005) Nitrate reduction in the presence of wüstite. Journal of environmental quality 34, 1286-1292.

Ramos-Tejada, M., Ontiveros, A., Viota, J., Durán, J. (2003) Interfacial and rheological properties of humic acid/hematite suspensions. Journal of colloid and interface science 268, 85-95.

Raychoudhury, T., Naja, G., Ghoshal, S. (2010) Assessment of transport of two polyelectrolyte-stabilized zero-valent iron nanoparticles in porous media. Journal of contaminant hydrology 118, 143-151.

Redl, F.X., Black, C.T., Papaefthymiou, G.C., Sandstrom, R.L., Yin, M., Zeng, H., Murray, C.B., O'Brien, S.P. (2004) Magnetic, electronic, and structural characterization of nonstoichiometric iron oxides at the nanoscale. Journal of the American chemical society 126, 14583-14599.

Reinsch, B.C., Forsberg, B., Penn, R.L., Kim, C.S., Lowry, G.V. (2010) Chemical transformations during aging of zerovalent iron nanoparticles in the presence of common groundwater dissolved constituents. Environmental science & technology 44, 3455-3461.

Rockenberger, J., Scher, E.C., Alivisatos, A.P. (1999) A new nonhydrolytic single-precursor approach to surfactant-capped nanocrystals of transition metal oxides. Journal of the American chemical society 121, 11595-11596.

Roth, H.-C., Schwaminger, S., Fraga García, P., Ritscher, J., Berensmeier, S. (2016) Oleate coating of iron oxide nanoparticles in aqueous systems: the role of temperature and surfactant concentration. Journal of nanoparticle research 18, 99.

Saleh, N., Kim, H.J., Phenrat, T., Matyjaszewski, K., Tilton, R.D., Lowry, G.V. (2008) Ionic strength and composition affect the mobility of surface-modified Fe^0 nanoparticles in water-saturated sand columns. Environmental science & technology 42, 3349-3355.

Sarathy, V., Tratnyek, P.G., Nurmi, J.T., Baer, D.R., Amonette, J.E., Chun, C.L., Penn, R.L., Reardon, E.J. (2008) Aging of iron nanoparticles in aqueous solution: effects on structure and reactivity. The journal of physical chemistry C 112, 2286-2293.

Schlicker, O., Ebert, M., Fruth, M., Weidner, M., Wüst, W., Dahmke, A. (2000) Degradation of TCE with iron: the role of competing chromate and nitrate reduction. Groundwater 38, 403-409.

Schrick, B., Hydutsky, B.W., Blough, J.L., Mallouk, T.E. (2004) Delivery vehicles for zerovalent metal nanoparticles in soil and groundwater. Chemistry of materials 16, 2187-2193.

Sen, T.K., Khilar, K.C. (2006) Review on subsurface colloids and colloid-associated contaminant transport in saturated porous media. Advances in colloid and interface science 119, 71-96.

SERDP, ESTCP, (2004) Annual report: DNAPS source zone initiative, pp. 1-18.
Shen, L., Laibinis, P.E., Hatton, T.A. (1999) Bilayer surfactant stabilized magnetic fluids: synthesis and interactions at interfaces. Langmuir 15, 447-453.

Smith, J.A., Burns, S.E. (2002) Physicochemical groundwater remediation. Springer.

Song, H., Carraway, E.R. (2006) Reduction of chlorinated methanes by nano-sized zero-valent iron. Kinetics, pathways, and effect of reaction conditions. Environmental engineering science 23, 272-284.

Stewart, N.A., (2005) Reaction rates for the dehalogenation of trichloroethylene using various types of zero-valent iron. University of central florida.

Su, C., Puls, R.W. (2004) Nitrate reduction by zerovalent iron: effects of formate, oxalate, citrate, chloride, sulfate, borate, and phosphate. Environmental science & technology 38, 2715-2720.

Sun, S., Zeng, H., Robinson, D.B., Raoux, S., Rice, P.M., Wang, S.X., Li, G. (2004) Monodisperse mfe2o4 (m= fe, co, mn) nanoparticles. Journal of the American chemical society 126, 273-279.

Sun, Y.P., Li, X.Q., Cao, J., Zhang, W., Wang, H.P. (2006) Characterization of zero-valent iron nanoparticles. Advances in colloid and interface science 120, 47-56.

Sun, Y.P., Li, X.Q., Zhang, W.X., Wang, H.P. (2007) A method for the preparation of stable dispersion of zero-valent iron nanoparticles. Colloids and surfaces A: Physicochemical and engineering aspects 308, 60-66.

Syrbe, A., Bauer, W., Klostermeyer, H. (1998) Polymer science concepts in dairy systems—an overview of milk protein and food hydrocolloid interaction. International dairy journal 8, 179-193.

Tepper, H.L., Voth, G.A. (2006) Mechanisms of passive ion permeation through lipid bilayers: insights from simulations. The journal of physical chemistry B 110, 21327-21337.

Tiraferri, A., Chen, K.L., Sethi, R., Elimelech, M. (2008) Reduced aggregation and sedimentation of zero-valent iron nanoparticles in the presence of guar gum. Journal of colloid and interface science 324, 71-79.

Tratnyek, P.G., Johnson, R.L. (2006) Nanotechnologies for environmental cleanup. Nano today 1, 44-48.

Tratnyek, P.G., Salter-Blanc, A.J., Nurmi, J.T., Amonette, J.E., Liu, J., Wang, C., Dohnalkova, A., Baer, D.R., (2011) Reactivity of zerovalent metals in aquatic media: Effects of organic surface coatings, Aquatic redox chemistry. ACS Publications, pp. 381-406.

Tratnyek, P.G., Scherer, M.M., Deng, B., Hu, S. (2001) Effects of natural organic matter, anthropogenic surfactants, and model quinones on the reduction of contaminants by zero-valent iron. Water research 35, 4435-4443.

Tufenkji, N., Elimelech, M. (2004) Correlation equation for predicting single-collector efficiency in physicochemical filtration in saturated porous media. Environmental science & technology 38, 529-536.

Uegami, M., Kawano, J., Okita, T., Fujii, Y., Okinaka, K., Kakuya, K., Yatagi, S., (2006) Iron particles for purifying contaminated soil or ground water. US. Patent.

Ullrich, A., Hohenberger, S., Özden, A., Horn, S. (2014) Synthesis of iron oxide/manganese oxide composite particles and their magnetic properties. Journal of nanoparticle research 16, 2580.

Vecchia, E.D., Luna, M., Sethi, R. (2009) Transport in porous media of highly concentrated iron micro-and nanoparticles in the presence of xanthan gum. Environmental science & technology 43, 8942-8947.

Vindedahl, A.M., Stemig, M.S., Arnold, W.A., Penn, R.L. (2016) Character of humic substances as a predictor for goethite nanoparticle reactivity and aggregation. Environmental science & technology 50, 1200-1208.

Vogan, J., Focht, R., Clark, D., Graham, S. (1999) Performance evaluation of a permeable reactive barrier for remediation of dissolved chlorinated solvents in groundwater. Journal of hazardous materials 68, 97-108.

Vogel, T.M., Criddle, C.S., McCarty, P.L. (1987) ES&T critical reviews: transformations of halogenated aliphatic compounds. Environmental science & technology 21, 722-736.

Wang, C.-B., Zhang, W.-X. (1997) Synthesizing nanoscale iron particles for rapid and complete dechlorination of TCE and PCBs. Environmental science & technology 31, 2154-2156.

Wang, Z., Lam, A., Acosta, E. (2013) Suspensions of iron oxide nanoparticles stabilized by anionic surfactants. Journal of Surfactants and Detergents 16, 397-407.

Xiang, T.-X., Xu, Y.-H., Anderson, B. (1998) The barrier domain for solute permeation varies with lipid bilayer phase structure. Journal of membrane biology 165, 77-90.

Xiong, Z., Zhao, D., Pan, G. (2009) Rapid and controlled transformation of nitrate in water and brine by stabilized iron nanoparticles. Journal of nanoparticle research 11, 807-819.

Xu, X., Yu, Z., Zhu, Y., Wang, B. (2005) Effect of sodium oleate adsorption on the colloidal stability and zeta potential of detonation synthesized diamond particles in aqueous solutions. Diamond and related materials 14, 206-212.

Xu, Y., Zhao, D. (2007) Reductive immobilization of chromate in water and soil using stabilized iron nanoparticles. Water research 41, 2101-2108.

Yan, W., Lien, H.-L., Koel, B.E., Zhang, W.-x. (2013) Iron nanoparticles for environmental clean-up: recent developments and future outlook. Environmental science: Processes & impacts 15, 63-77.

Yandrapati, R.K. (2012) Effect of lipid composition on the physical properties of liposomes: a light scattering study.

Yang, K., Peng, H., Wen, Y., Li, N. (2010) Re-examination of characteristic FTIR spectrum of secondary layer in bilayer oleic acid-coated Fe_3O_4 nanoparticles. Applied surface science 256, 3093-3097.

Yao, K.-M., Habibian, M.T., O'Melia, C.R. (1971) Water and waste water filtration. Concepts and applications. Environmental science & technology 5, 1105-1112.

Yu, H., Kotsmar, C., Yoon, K.Y., Ingram, D.R., Johnston, K.P., Bryant, S.L., Huh, C., (2010) Transport and retention of aqueous dispersions of paramagnetic nanoparticles in reservoir rocks, SPE improved oil recovery symposium. Society of petroleum engineers.

Yu, W.W., Falkner, J.C., Yavuz, C.T., Colvin, V.L. (2004) Synthesis of monodisperse iron oxide nanocrystals by thermal decomposition of iron carboxylate salts. Chemical communications, 2306-2307.

Zhang, L., He, R., Gu, H.-C. (2006) Oleic acid coating on the monodisperse magnetite nanoparticles. Applied surface science 253, 2611-2617.

Zhang, M., He, F., Zhao, D., Hao, X. (2011) Degradation of soil-sorbed trichloroethylene by stabilized zero valent iron nanoparticles: effects of sorption, surfactants, and natural organic matter. Water research 45, 2401-2414.

Zhang, W. (2003) Nanoscale iron particles for environmental remediation: An overview. Journal of nanoparticle research 5, 323-332.

Zhao, X., Liu, W., Cai, Z., Han, B., Qian, T., Zhao, D. (2016) An overview of preparation and applications of stabilized zero-valent iron nanoparticles for soil and groundwater remediation. Water research 100, 245-266.

Zhou, Q., Li, J., Wang, M., Zhao, D. (2016) Iron-based magnetic nanomaterials and their environmental applications. Critical reviews in environmental science and technology 46, 783-826.

국문초록

지중환경오염물질로 주로 발견되는 트리클로로에틸렌, 사염화탄소 등의 유기용제류의 염화유기화합물은 물 보다 비중이 크고 용해도가 낮으며 난분해성인 특성을 가지고 있어 위의 물질로 오염된 지하수 및 토양을 정화하기 위해 지상처리공법을 적용하는 것은 효율적이지 않다. 환원조건에서 염화유기화합물을 분해할 수 있는 나노크기 철 입자를 오염된 지중환경에 직접 주입해 오염원 및 오염원을 정화하는 지중처리공법이 효과적인 대안으로 떠오르고 있으나, 몇 가지의 문제점이 지적되고 있다. 나노크기 철 입자는 입자 간 강한 상호인력을 가지고 있어 주입된 철 입자가 쉽게 뭉쳐져 지중환경에서 이동성을 잃고 침전되는 것으로 알려져 있다. 또한, 나노크기 철 입자의 강한 반응성이 지하수에 용존된 유무기물에 의해 감소될 수 있다. 대수층 불투수층까지 이동한 오염원과 오염원의 이동 중 형성된 오염운을 반응성 나노입자를 이용한 지중처리공법으로 제거하기 위해서는 입자의 지중 내 안정적인 이동성과 반응성이 확보되어야 하므로 기존 나노크기 철 입자를 이용한 지중처리공법의 개선은 필수적이라 할 수 있다.

본 연구에서는 세포벽을 구성하는 지질이중층을 모사하여 지방산 이중층을 나노크기 철 입자에 결합시켜 안정적인 지중 내 이동성과 반응성을 확보하고자 하였다. 이를 위해, 올레익산을 지방산 이중층의 기본 구성 요소로 사용하고 올레이트를 이용해 수중 분산성을 확보하는 나노크기 철 입자의 지방산 이중층 조성 방안을 개발하였다. 개발된 지방산 이중층

안정화 나노크기 철 입자는 전체 무게의 약 50%에 해당하는 지방산 이중층을 가지고 있으며 −100 mV 이상의 큰 음의 표면전위를 가져 정전기적 반발력(electrostatic repulsion)과 입체 안정화 반발력(steric repulsion)을 통해 수중에서 안정적으로 분산성을 유지할 수 있었다.
지방산 이중층 안정화 나노크기 철 입자를 이용한 일차원 주상실험에서도 침전 및 정착현상(deposit)이 나타나지 않았으며 기존의 개발된 안정화 방법으로 안정화시킨 나노크기 철 입자에 비해 높은 이동성이 나타났다. 안정화되지 않은 나노크기 철 입자 및 기존 안정화 물질로 안정화된 나노크기 철 입자는 사염화탄소에 대해 높은 환원분해 반응성을 보였지만 질산염, 중탄산염 등의 지하수 용존무기이온 및 용존유기물이 존재하는 경우 반응성이 최대 95% 감소됐다. 반면, 지방산 이중층 안정화 나노크기 철 입자는 용존유무기물에 의해 사염화탄소에 의한 반응성이 감소되지 않았다. 이는 표면에 결합된 지방산 이중층이 용존유무기물의 침투를 막고 소수성 오염물질만 선택적으로 통과시켜 나타난 결과로 해석할 수 있다.
본 연구에서 개발된 지방산 이중층 안정화 나노크기 철 입자는 주입정과 오염원의 거리가 멀어 높은 이동성과 장기간의 반응성 유지가 가능한 반응성 소재가 필요한 부지의 정화에 효율적으로 사용될 수 있을 것으로 판단된다.

주요어 : 나노크기 철 입자, 지방산, 이중층, 응집, 안정화, 이동성, 선택적 반응성, 염화유기화합물, 환원분해

학 번 : 2008−21041